THE ROLE OF MITOTIC KINESINS AND CROSSLINKERS NUMA AND PRC1 IN THE MICROTUBULE POLEWARD FLUX REGULATION DURING PROMETAPHASE

Martinčić, Jelena

Sveučilište u Zagrebu

PRIRODOSLOVNO-MATEMATIČKI FAKULTET

BIOLOŠKI ODSJEK

Jelena Martinčić

ULOGA MITOTSKIH KINEZINA I VEZNIH PROTEINA NUMA I PRC1 U REGULACIJI TOKA MIKROTUBULA U PROMETAFAZI

DOKTORSKI RAD

Zagreb, 2023

University of Zagreb

FACULTY OF SCIENCE

DEPARTMENT OF BIOLOGY

Jelena Martinčić

THE ROLE OF MITOTIC KINESINS AND CROSSLINKERS NUMA AND PRC1 IN THE MICROTUBULE POLEWARD FLUX REGULATION DURING PROMETAPHASE

DOCTORAL THESIS

Zagreb, 2023

This work was done in the Laboratory of Cell Biophisics at Ruđer Bošković Institute, Zagreb, under supervision of Iva M. Tolić, PhD, Senior Research Group Leader. As a part of Postgraduate doctoral programme of Biology, this thesis is submitted for review to Department of Biology at Faculty of Science, University of Zagreb in order to achieve the academic degree Doctor of Biology.

Supervisor biography

Professor Iva M. Tolić was born in Zagreb, Croatia. She graduated Molecular biology at Faculty of Science, University of Zagreb, Croatia in 1996. During graduate studies, Prof Tolić worked as research assistant in the group of Prof Nenad Trinajstić at Ruđer Bošković Institute. Her PhD work was done with Prof Ning Wang at Harvard School of Public Health, Boston, MA, USA. She achieved the academic degree Doctor of biology at University of Zagreb in 2002. After this, she worked as a postdoctoral fellow with Prof Kirstine Berg-Sørensen at Niels Bohr Institute, Copenhagen, Denmark, and later with Prof Francesco Pavone at European Laboratory for Non- Linear Spectroscopy, Florence, Italy. From 2005 to 2014, Prof Tolić worked as a research group leader at Max Planck Institute of Molecular Cell Biology and Genetics in Dresden, Germany. Her research areas are mitosis, mitotic spindle mechanics, microtubules, motor proteins and aneuploidy. Currently she is a Senior Research Group Leader with tenure at Ruđer Bošković Institute (RBI) in Zagreb. Professor Tolić has received 16 research grants including prestigious projects funded by the European Research Council (ERC), Consolidator and Synergy. She has published more than 100 papers in peer-reviewed journals including Nature, Science, Cell, and Nature Cell Biology, cited more than 4500 times, and served as a reviewer for these and various other journals. To this date, she has mentored 12 PhD and 23 Master theses. Professor Tolić has been elected member of Academia Europaea (since 2022), an elected associate member of the Croatian Academy of Sciences and Arts – HAZU (since 2020) and an elected member of the European Molecular Biology Organization – EMBO (since 2018). She received numerous awards such as the Ignaz Lieben Award of the Austrian Academy of Sciences, the European Biophysical Societies Association (EBSA) Young Investigators' Medal and Prize, the Outstanding Paper Award of the European Microscopy Society in the category Life Sciences and National Science Award of the Republic of Croatia. As an invited speaker, she has participated in more than 150 conferences and research seminars worldwide. She organized several scientific meetings including the EMBO Conference on Meiosis (2017) and Mitotic spindle: From living and synthetic systems to theory (2019, 2021 and 2023).

University of Zagreb
Faculty of Science
Department of Biology

Doctoral thesis

THE ROLE OF MITOTIC KINESINS AND CROSSLINKERS NUMA AND PRC1 IN THE MICROTUBULE POLEWARD FLUX REGULATION DURING PROMETAPHASE

JELENA MARTINČIĆ

Ruđer Bošković Institute

Microtubule poleward flux is a fascinating phenomenon that occurs throughout mitosis, including prometaphase. Studying the involvement of different proteins in prometaphase flux regulation is challenging because of high dynamics of microtubule and chromosome movements in this phase. Here I show that the prometaphase spindle consists of k-fibers and bridging fibers, and their poleward flux velocities are similar as in metaphase. By using tubulin photoactivation and speckle microscopy experiments I defined the role of mitotic kinesins and passive crosslinkers in the flux regulation. CENP-E and HSET are generating flux at the antiparallel fibers and this force is transmitted to the k-fibers via HSET and NuMA. The congressing kinetochores are asymmetrically bioriented with more microtubules on the side of the closer pole, and interkinetochore distance close to the metaphase values. I demonstrated that kinetochores congress on long antiparallel overlaps, and the flux is generating forces that help the congression.

(123 pages, 54 figures, 1 table, 162 references, original in English)

Keywords: mitosis, prometaphase, mitotic spindle, microtubule poleward flux, kinesins, congression

Supervisor: Iva M. Tolić, PhD, Full Professor and Senior Research Group Leader

Reviewers: Maja Matulić, PhD, Associate Professor

Marin Barišić, PhD, Associate Professor, Group Leader

Andreja Ambriović Ristov,PhD, Full Professor and Senior Research Group Leader

Sveučilište u Zagrebu Doktorski rad

Prirodoslovno-matematički fakultet

Biološki odsjek

ULOGA MITOTSKIH KINEZINA I VEZNIH PROTEINA NUMA I PRC1 U REGULACIJI TOKA MIKROTUBULA U PROMETAFAZI

JELENA MARTINČIĆ

Institut Ruđer Bošković

Tok mikrotubula prema polu je fascinantan fenomen koji se događa tijekom mitoze, uključujući i prometafazu. Proučavanje uloge različitih proteina u regulaciji toka mikrotubula je izazovno zbog velike dinamike u kretnji mikrotubula i kinetohora u toj fazi mitoze. Ovdje sam pokazala da se prometafazno vreteno sastoji od kinetohornih i premošćujućih vlakana kojima su brzine toka mikrotubula slične kao u metafazi. Koristeći metode fotoaktivacije i "speckle" mikroskopije definirala sam ulogu mitotskih kinezina i pasivnih veznika u regulaciji toka mikrotubula. CENP-E i HSET pokreću tok mikrotubula u antiparalelnim vlaknima, a ta sila se prenosi na k-vlakna pomoću proteina HSET i NuMA. Kinetohore su tijekom kongresije asimetrično biorijentirane s više mikrotubula na strani prema bližem polu, a interkinetohornom udaljenošću blizu vrijednosti u metafazi. Pokazala sam da se kongresija događa na dugim antiparalelnim snopovima, a tok mikrotubula proizvodi sile koje pomažu u kongresiji.

(123 stranice, 54 slike, 1 tablica, 162 literaturna navoda, jezik izvornika engleski)

Ključne riječi: mitoza, prometafaza, mitotsko vreteno, tok mikrotubula prema polu, kinezini, kongresija

Mentor: prof. dr. sc. Iva M. Tolić, Znanstvena savjetnica u trajnom izboru

Ocjenjivači: izv. prof. dr. sc. Maja Matulić

izv. prof. dr. sc. Marin Barišić

prof. dr. sc. Andreja Ambriović Ristov, Znanstvena savjetnica u trajnom izboru

Table of Contents

1. INTRODUCTION

Eukaryotic cells undergo cell cycle with main goal to duplicate genetic material, and to correctly divide it into daughter cells. Mitosis can be divided in the few dynamic phases. In prophase, before the nuclear envelope breakdown (NEBD), the chromosomes become condensed and interphase microtubules become more dynamic and restructure. Prometaphase begins with NEBD and formation of the mitotic spindle. The chromosomes are incorporated into the spindle and congress to the future equatorial plane (Maiato et al., 2017). In metaphase, the chromosomes are tightly arranged in the metaphase plate at the spindle equator and the amphitelic attachments are formed. If the sister chromatids of the duplicated chromosomes attach properly to the opposite spindle poles, anaphase initiates sister chromatids segregation towards the opposite poles. In telophase, the chromosomes arrive at the spindle poles, they decondense and the new envelope around each set forms (Alberts et al., 2014).

Central component of mitosis is the mitotic spindle, a dynamic structure made of microtubules and other proteins necessary to correctly divide the chromosomes into the new daughter cells (Pavin & Tolić, 2016). In the mitotic spindle, microtubules can form three main classes of microtubules. Kinetochore fibers (k-fibers) consist of microtubules joined in a parallel conformation. They grow from the same spindle pole and attach to the kinetochores, protein complexes on the chromosomes (Musacchio & Desai, 2017). Interpolar fibers consist of microtubules that nucleate from the opposite poles and overlap at the equatorial plane of the mitotic spindle (Mastronarde et al., 1993). Astral microtubules grow individually from the poles towards the cell membrane and participate in positioning of the spindle (Dumont & Mitchison, 2009).

Beside the microtubules, another important component in spindle microtubules organization, function and dynamics are the microtubule associated proteins. They can be divided into four groups. Motor proteins can convert chemical energy into mechanical work by ATP hydrolysis which enables them to move on the microtubule surface. Members of this group are kinesin motor proteins which can move towards plus or minus-end of the microtubules, depending on the type, and dynein which moves towards the minus-end. Second group consists of plus-end associated proteins which influence the plus-end dynamics, and the third are microtubule

destabilizing proteins. Fourth group consists of proteins that can't move, but passively crosslink microtubules in parallel or antiparallel configuration (Lodish et al., 2008).

Microtubules are protein tubes made by the polymerization of α- and β-tubulin heterodimers joint together by non-covalent bonds. They merge into 13 parallel protofilaments, making a hallow cylindrical structure. Microtubules have structural polarity with α- tubulin on the minus and β- tubulin on the plus end. The exchange between the period of growth and shrinkage by constant monomer concentration is called microtubule dynamic instability (Alberts et al., 2014).

In the late 80's of the last century, it was discovered that the new tubulin subunits preferentially incorporate into the microtubules at the plus-end. At the same time, tubulin dissociates from the end facing the poles of the mitotic spindle (minus-end). As the consequence of this behavior, the tubulin inside the spindle microtubules fluxes towards the spindle poles (Mitchison, 1989; Mitchison et al., 1986). In that way, the size and shape of the metaphase spindle stay constant with tubulin being constantly recycled. Microtubule poleward flux is evolutionary conserved, but the velocity differs between different organisms (Rogers et al., 2005) and different phases of mitosis (Cimini et al., 2006).

Microtubule poleward flux and dynamics can be investigated by marking the targeted tubulin population separately inside the microtubule bundles. It can be done with fluorescence microscopy using photoactivatable GFP bound to tubulin (Mitchison, 1989; Patterson & Lippincott-Schwartz, 2002). This protein can be photoactivated by using UV laser beam and targeted tubulin population can then be tracked inside the mitotic spindle microtubules (He & Cimini, 2016; Steblyanko et al., 2020; Tulu & Ferenz, 2010; Vukušić et al., 2017). Tubulin photoactivation technology can give insight in the poleward flux velocity, but it is hard to distinguish between the movement of the different classes of microtubules. Recently developed permeable dye-based fluorescent speckle microscopy assay (Risteski, 2023; Risteski et al., 2022) enables to distinguish between different classes of microtubules in human cells, kinetochore and bridging fibers, and to define their microtubule poleward flux movements.

Since the discovery of the poleward flux few decades ago, the proteins responsible for that phenomenon are not yet fully revealed. Motor proteins that can slide antiparallel microtubule bundles apart can use this motion as the driving force for poleward flux. The main candidate in this theory is kinesin-5 (Eg-5) (Kapitein et al., 2005; Miyamoto et al., 2004). In *Xenopus,*

the loss of its function causes formation of monopolar spindles which do not flux. However, in mammalian cells, monopolar spindles do flux, although at a slightly reduced rate (Cameron et al., 2006; Steblyanko et al., 2020), meaning that Eg-5 dependent antiparallel sliding of microtubules plays a significant, although probably not essential, role in driving mammalian metaphase poleward flux. Similar role as Eg-5 has Kif-15, a protein from the kinesin-12 family (Steblyanko et al., 2020; Tanenbaum et al., 2009) and their role in powering the poleward flux has been recently proposed (Steblyanko et al., 2020).

The disassembly of microtubules at their minus ends may reel in microtubules to drive flux. Kinesin-13 family members: Kif2A, Kif2B and Kif2C/MCAK are responsible for regulation of microtubule ends dynamic (Manning et al., 2007). Simultaneous depletion of Kif2A and Kif2C in mammalian cells results in normal metaphase spindles without poleward flux (Ganem et al., 2005). The generation of pushing force by microtubule polymerization at plus ends could also potentially drive poleward flux. This is supported by a study in which plus-end tracking protein CLASP is depleted, which causes cessation of poleward flux in S2 cells (Maiato et al., 2005). Also, it is known that CENP-E protein (kinesin-7) and chromokinesins (kinesin-4 family) participate in translocation of kinetochore and non-kinetochore microtubules towards the spindle pole (Steblyanko et al., 2020). Possible additional role in microtubule poleward flux regulation could have passive crosslinkers, like PRC1 (Kajtez et al., 2016; Polak et al., 2017), NuMA (Elting et al., 2017; Steblyanko et al., 2020) and HSET (Cai et al., 2009). The most recent research proposes that the flux is driven by the coordinated action of four kinesins: CENP-E, Kif4A, kinesin-5 and kinesin-12 and the force is transmitted from the non-kinetochore to the kinetochore microtubules by the crosslinkers HSET and NuMA (Steblyanko et al., 2020).

Most of the research of microtubule poleward flux was conducted in metaphase because it is well defined and the spindle has relative constant shape. In prometaphase, non-kinetochore microtubules make about 70% of spindle microtubules with very fast microtubule half-life. In addition, half-life for kinetochore microtubules is about two times slower in metaphase than in prometaphase (Cimini et al., 2006). Not so precisely defined shape of prometaphase spindle and fast microtubule dynamic are the main reasons why precise organization of microtubule bundles and poleward microtubule flux are in that mitotic phase less explored.

The hypothesis of this study is that mitotic kinesins play a role in regulating the microtubule poleward flux dynamics in prometaphase of human cells. They push the interpolar microtubules in the antiparallel region of the mitotic spindle and thus start the flow of

microtubules towards pole, which is followed by depolymerization of microtubules at the poles. Furthermore, the hypothesis is that crosslinking proteins transmit the sliding force from interpolar to kinetochore fibers, and therefore make the role of the length of the overlapping region also important. The aim of the research is to experimentally examine the possible roles of protein candidates in prometaphase microtubule poleward flux of osteosarcoma U2OS and non-cancer immortalized RPE1 cell lines. The goal is to discover their role using tubulin photoactivation assay and speckle microscopy assay by using various techniques of protein inhibition or depletion. Main conceptual advance of this work is potential definition of new and more precise explanation of current mechanisms which contribute to the poleward flux of k-fibers and bridging fibers in prometaphase. Moreover, precise examination of prometaphase spindle architecture during the chromosome congression will be carried out by using fast live cell confocal microscopy. Finally, the impact of prometaphase poleward flux on chromosome congression will be defined.

2. RESEARCH OVERVIEW

2.1 Cell cycle

Cell division is a fundament of life. It is a process in which a cell duplicates and then segregates its genetic material, producing two genetically identical daughter cells. The whole cycle is highly organized and temporally controlled, consisting of four main phases: G1 (gap one), S (synthesis) and G2 (gap 2), together called the interphase, and M (mitosis) (**Figure 1)**. During G1 phase the cell grows, synthesizes molecules needed for DNA replication, and goes through restriction point as the gate to the S phase. The S phase is the period when all genetic material is being duplicated. Next, G2 phase, serves as the preparation for the M phase where the genetic material is finally getting divided (mitosis) and then the cell itself divides in two (cytokinesis) (Alberts et al., 2014).

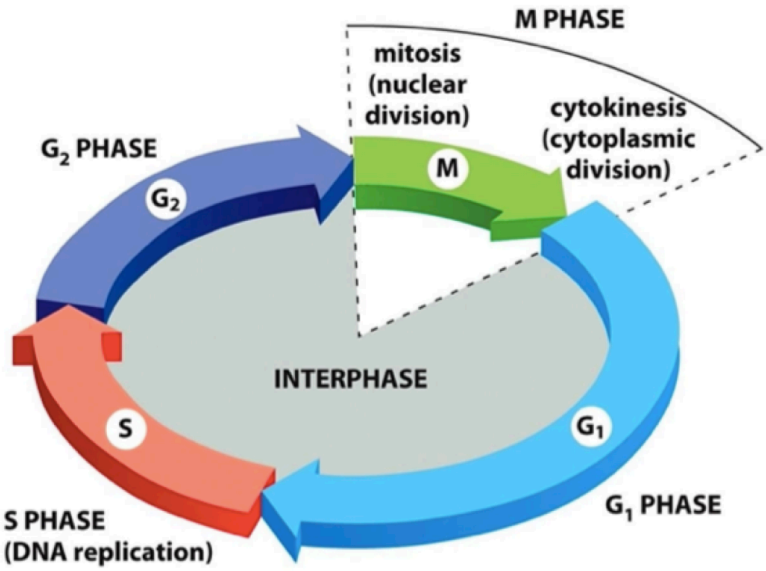

Figure 1. The phases of the cell cycle. Interphase consists of three phases: S phase which includes DNA replication, G1 phase as the gap between M phase and S phase and G2 phase as the gap between S phase and M phase. The M phase consists of mitosis and cytokinesis (Alberts et al., 2014).

2.2 Mitosis

At the onset of mitosis, the cell assembles the mitotic spindle, a fascinating and complex micromachine made of chromosomes and microtubules whose main task is to faithfully segregate duplicated genetic material. Although mitosis is a continuous process, we can distinguish five phases which differ in chromosome behavior and spindle morphology: prophase, prometaphase, metaphase, anaphase and telophase (Lodish et al., 2008) (**Figure 2**).

In prophase the chromosomes are becoming condensed and the microtubules become more dynamic (Saxton et al., 1984) with the interphase microtubule array getting dramatically rearranged. Increased microtubule nucleation at the centrosomes can be seen (Kuriyama & Borisy, 1981), as they form two future spindle poles. Each sister chromatid builds the kinetochore- a multiple protein complex which enables the connection of the microtubules to the chromosomes (Musacchio & Desai, 2017). Prometaphase starts with the nuclear envelope breakdown (NEBD) and the first microtubule-kinetochore connections can be achieved and spindle assembly occurs. The chromosomes congress towards the future spindle equator and align between the spindle poles. When all the chromosomes align at the spindle equator, the next phase, metaphase, begins. If all the chromosomes are attached properly to the opposite spindle poles, cohesion between sister chromatids is destroyed and the cell enters anaphase. This phase is additionally divided into anaphase A, characterized by the poleward movement of daughter chromosomes, and anaphase B, where poles separation occurs. The last phase, telophase, is characterized by the decondensation of the chromosomes and the reformation of the nuclear envelope. Finally, during cytokinesis, the cell cytoplasm divides between the two newly formed daughter cells (Walczak et al., 2010).

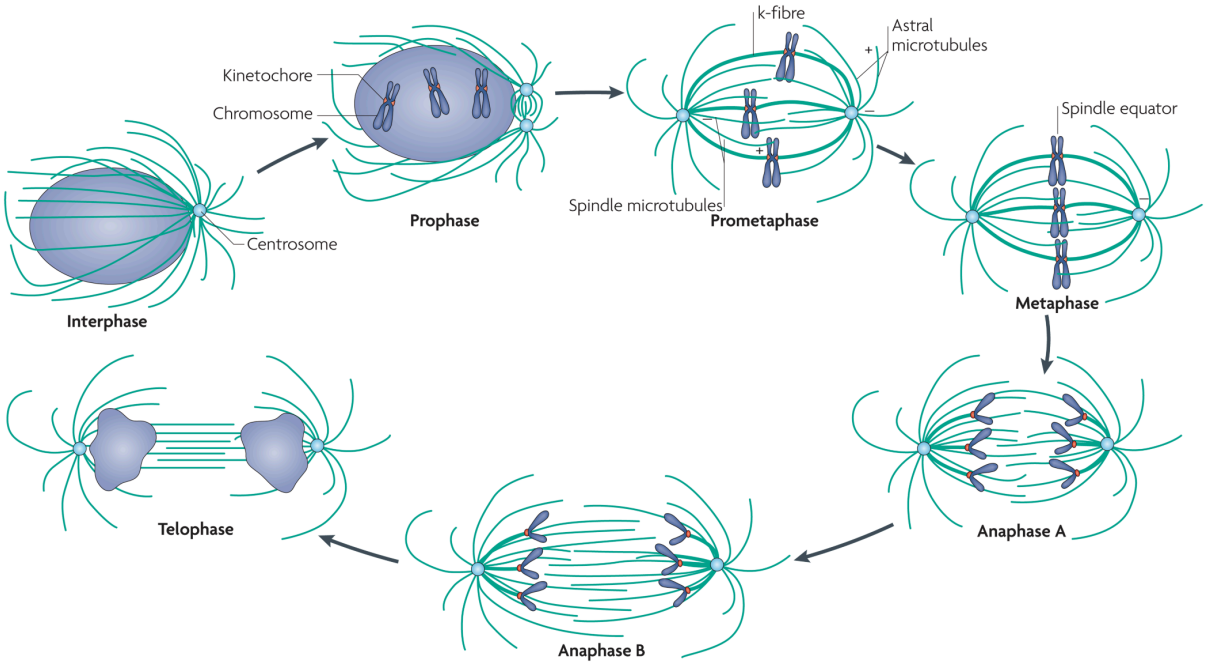

Figure 2. The phases of mitosis. Mitosis is separated into phases. Before the mitosis, in interphase, the chromosomes are duplicated. In prophase the chromosomes condense and kinetochores appear. After NEBD, during prometaphase the bipolar spindle appears and first microtubule-kinetochore attachments occurre so the chromosomes can congress to the metaphase plate. During anaphase the chromosome segregate (anaphase A) ant the poles separate (anaphase B). In telophase the DNA decondenses and the nuclear envelope reappears (Walczak et al., 2010).

2.3. Spindle architecture and chromosome behavior in prometaphase

The main focus of this thesis is prometaphase, so it is necessary to address the complexity of this phase in more detail. Prometaphase is the longest phase of mitosis, which lasts from NEBD until metaphase, when all the chromosomes become aligned at the metaphase plate. In short, the main events during this period are the assembly of the bipolar spindle, microtubule attachment to chromosomes and the congression of those chromosomes to the cell equator whilst the spindle assembly checkpoint (SAC) simultaneously monitors the proper kinetochore-microtubule connection to prevent chromosome missegregation (Ferreira & Maiato, 2021).

2.3.1. Mechanisms of microtubule nucleation

At the onset of mitosis, the interphase microtubule array is reorganized and recycled into the bipolar mitotic spindle. The microtubules from the centrosomes become more dynamic and the breakdown of the nuclear envelope allows them to start exploring the former nuclear area (Kuriyama & Borisy, 1981; Saxton et al., 1984). They start to probe the anterior nuclear space for chromosomes, to connect to them via the kinetochores.

In most mammalian cell types, the centrosome microtubule nucleation and organization is the major mechanism that assures efficient and accurate spindle assembly. The centrosomes consist of centrioles and the pericentriolar matrix, enriched in γ-tubulin, as the main microtubule nucleator. The microtubule nucleation is initiated from the γ-tubulin ring complexes (γTuRCs) (Lüders et al., 2006). Microtubules nucleated at the centrosomes search the cell space in order to capture the chromosomes. This "search-and-capture" model was the first experimentally proven mechanism for the spindle assembly in animal cells (Kirschner & Mitchison, 1986). But, the mathematical modelling of the spindle assembly showed that such model alone could not provide enough time for all the sister kinetochores to attach stably to the microtubule bundles (Wollman et al., 2005). The necessary time of mitosis would be exceeded multiple times so it implies the existence of additional mechanisms that cooperate to facilitate the spindle assembly. Some of them are the prometaphase rosette spatial organization of chromosomes around the spindle microtubules which helps the capture (Magidson et al., 2011). Also, the kinetochore architecture changes in the way that at the onset of prometaphase it expands to almost encircle the centromere and later, after the formation of end-on attachments, it shrinks to suppress the possibility of erroneous attachments (Magidson et al., 2015). Moreover, there are several acentrosomal mechanisms that facilitate the spindle assembly, that involve chromosomal and kinetochore- driven microtubule nucleation, and the nucleation from the pre-existing microtubules (Prosser & Pelletier, 2017) (**Figure 3**).

Chromosomes are not just passive observers, but creators of an environment favorable for spindle assembly. The small GTPase RAN is the main driver of the chromatin dependent microtubule nucleation, independent of centrosome (Carazo-Salas et al., 1999). RAN activates various factors around the chromosomes necessary for the spindle assembly. Its activity is regulated by Regulator of chromosome condensation 1 (RCC1) and RAN GTPase-activating protein 1 (RANGAP1). RCC1 is enriched around the chromosomes where it

stimulates the exchange of GDP with GTP on RAN, whereas RANGAP1 stimulates RAN GTPase activity and is localized in the cytoplasm. In that way the RAN-GTP gradient arises and ensures that RAN is active only in the vicinity of chromosomes. There, it binds to importin-β and causes the dissociation of its inhibitory interaction with the cargo. These proteins, like TPX2 promote the microtubule nucleation and stabilization near the chromosomes.

There is a second mechanism of chromosomal microtubule nucleation, independent of RAN-GTP gradient. It is called chromosome passenger complex (CPC), made of Aurora B kinase, Survivin, Borealin and Inner Centromere Protein (INCENP) (Maresca et al., 2009; Sampath et al., 2004). CPC participates in microtubule stabilization near the chromosomes by inhibiting the microtubule destabilizing proteins, such as the mitotic centromere-associated protein (MCAK) and stathmin (STMN1) (Klein et al., 2006).

Microtubule nucleation is facilitated also in the vicinity of kinetochores (Renda et al., 2022; Telzer et al., 1975). As for chromosomes, the kinetochores rely on the existence of RAN-GTP and CPC gradient (Tulu et al., 2006). Increased density of microtubules near the kinetochores facilitates their nucleation, growth and incorporation into the microtubule bundles. It was shown that the short near-kinetochore-nucleated microtubules are sorted and end-on attached by CENP-E at the fibrous corona (Sikirzhytski et al., 2018).

Furthermore, an important mechanism of acentrosomal microtubule nucleation is from the pre-existing microtubules. It is carried out by augmin, an octameric protein complex (David et al., 2019; Goshima et al., 2008; Kamasaki et al., 2013). It binds to the pre-existing microtubules and mediates the recruitment of γTuRCs to the microtubules, thereby promoting the microtubule nucleation. In humans, of the eight proteins in the complex, HAUS6 interacts directly with a γ-TuRC adapter protein NEDD1, whereas HAUS8 interacts directly with microtubules (Song et al., 2018; Uehara et al., 2009). This mechanism is not essential for the spindle formation, but its depletion causes less microtubules in the spindle, especially in the inner part, reduced interkinetochore distance and altered rate of segregation errors (Štimac et al., 2022).

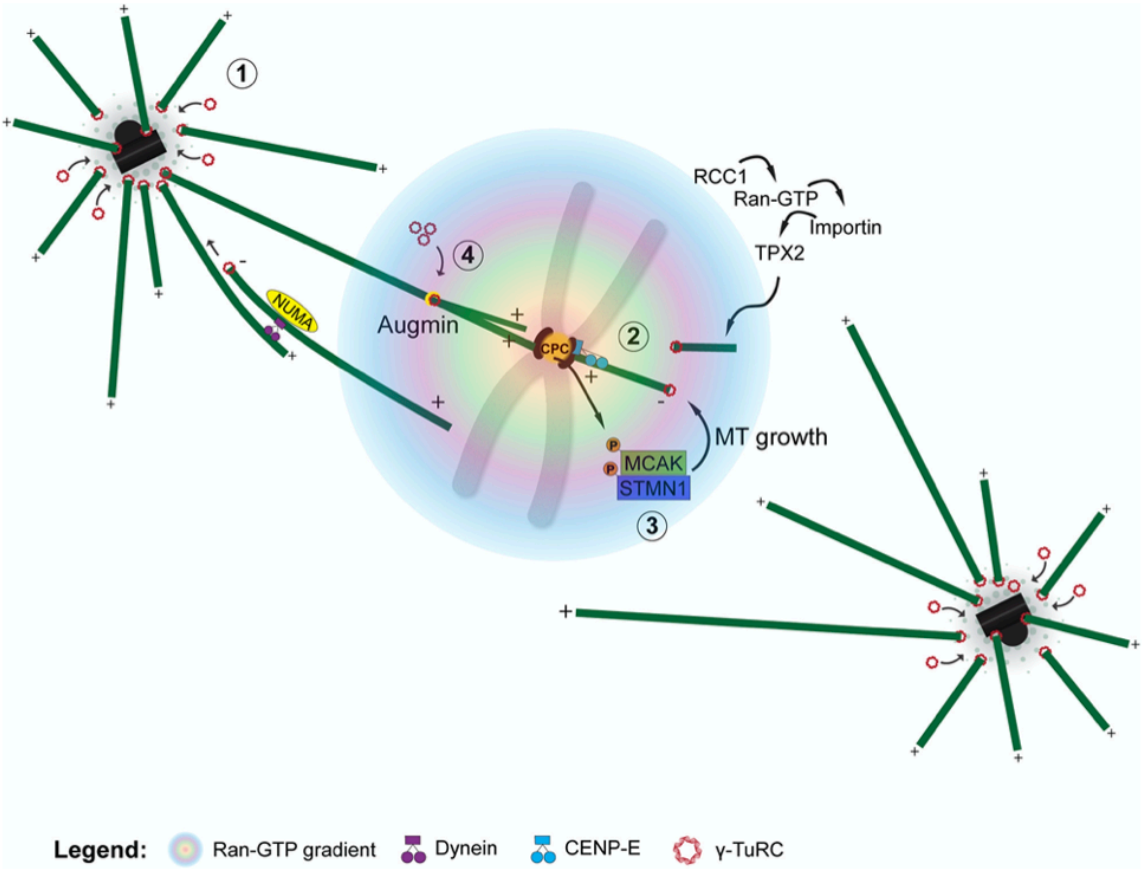

Figure 3. Mechanisms of microtubule nucleation in prometaphase. During prometaphase, the bipolar spindle assembles via centrosomal (1) and acentrosomal (2,3,4) pathways. Microtubules nucleate from the γTuRC at the centrosomes, search for the kinetochores and then stabilize the attachment. Nucleation at the chromosomes (2) is dependent of the RAN-GTP gradient, leading to the activation of the factors important for the spindle assembly. The CPC-dependent nucleation (3) induces microtubule growth around the kinetochores by inhibiting the microtubule- destabilizing factors. Augmin recruits γTuRC to the microtubules promoting the nucleation from the pre-existing microtubules (4) (Ferreira & Maiato, 2021).

2.3.2. Microtubule bundle organization in the prometaphase spindle

The mitotic spindle consists of several different classes of microtubules (**Figure 4**). During prometaphase, the majority of the microtubule bundles is not connected to the kinetochores. They nucleate from the opposite poles and are called interpolar or overlap when joined together in the antiparallel manner at the spindle center (Mastronarde et al., 1993; Tolić, 2018). They regulate spindle length throughout mitosis and help to separate the spindle poles

during anaphase via sliding inside their antiparallel regions (Kajtez et al., 2016; Vukušić et al., 2017). Furthermore, non-kinetochore fibers that have free ends are often called polar (McIntosh & Landis, 1971). The fibers that nucleate at the same pole often join together in the parallel manner. The most important parallel bundles are kinetochore fibers (k-fibers), whose name implies that they are connected to the kinetochores (McDonald et al., 1992). They exert forces on the kinetochores that help them to congress, align and segregate. Finally, astral microtubules nucleate at the poles towards the cell cortex and help to position the spindle within the cell (Dumont & Mitchison, 2009). Mitotic spindle could not exist without the help of numerous motor proteins and passive crosslinkers, and their role will be described later in the text.

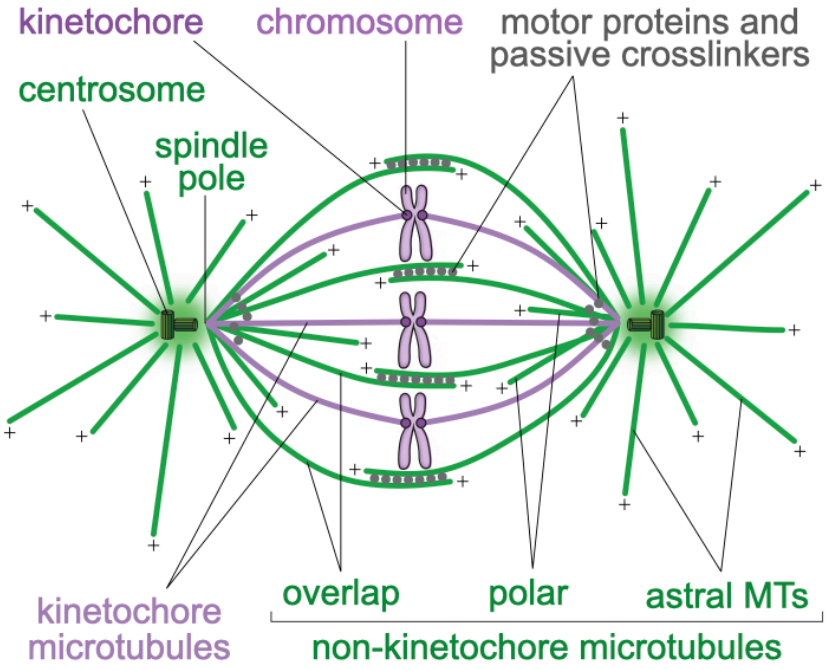

Figure 4. Types of microtubule bundles. Kinetochore microtubules (magenta) are attached to kinetochores whilst non-kinetochore (green) are not. Non-kinetochore microtubules are further divided into overlap, polar and astral (Tolić, 2018).

While the cell progresses through prometaphase, the spindle changes in size and shape. The unorganized interphase microtubule array dramatically changes and organizes into distinct bundles that overlap at the spindle middle (**Figure 5**). Protein regulator of cytokinesis 1 (PRC1) is a passive crosslinker that binds antiparallel microtubules. In the mature spindle it is located in the antiparallel bundles that link sister k-fibers, known as the bridging fibers. It was shown that the transition from the loose microtubule array into PRC1-enriched bundles during prometaphase is driven by the kinetochores and chromosomes. The kinetochores bind

laterally to the microtubules by CENP-E/kinesin-7 and help to bundle them. At the spindle midplane the steric interactions between the chromosomes causes the widening of the spindle by driving the bundle separation (Matković et al., 2022).

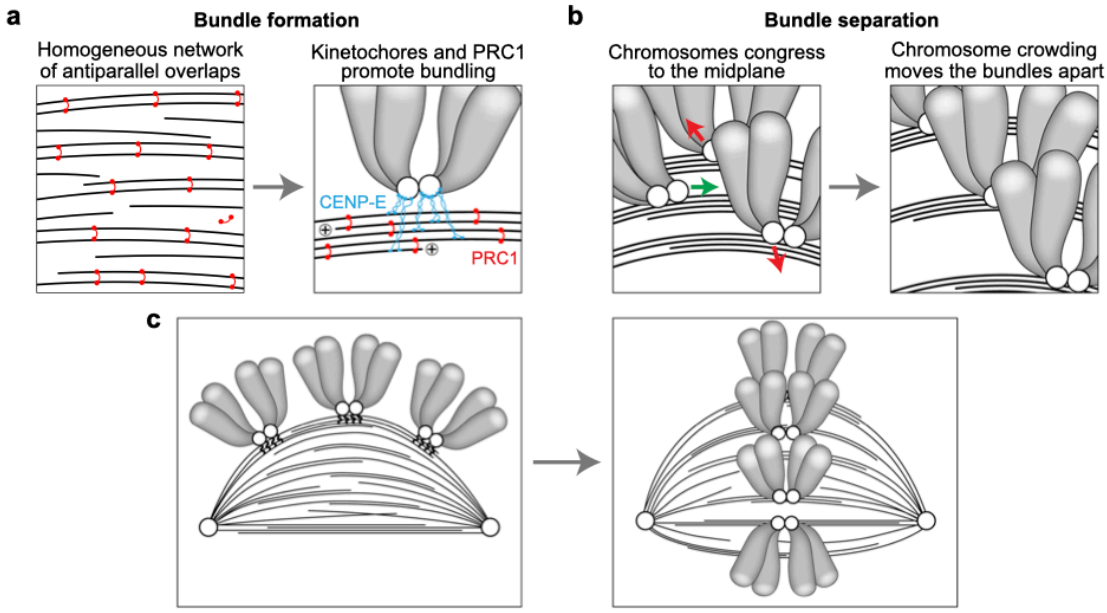

Figure 5. Kinetochore- driven antiparallel bundle formation. A) Homogenous microtubule network connected with PRC1 (red) is organized into bundles via CENP-E (blue) at the kinetochores. B) The chromosome congression causes the moving of the bundles apart. C) The processes from A and B drive the formation of the mature spindle (Matković et al., 2022).

2.3.3. Kinetochore-microtubule attachments and spindle assembly checkpoint

The purpose of mitosis is to faithfully segregate all chromosomes, but firstly before segregation, they have to be properly attached to the spindle microtubules. The centromere is a region on the chromosomes that acts as the area of recognition for the microtubules. Histone H3 variant centromere protein A (CENPA) defines the centromere in vertebrates. The inner kinetochore containing constitutive centromere- associated network (CCAN) binds directly to CENPA (McKinley et al., 2015), and during mitosis the multiprotein complex outer kinetochore assembles onto the inner kinetochore. So, the inner kinetochore connects to the chromosome, and the outer serves as the microtubule recognition site to connect the

chromosome to them. The main component of the outer kinetochore is the KNL1-MIS12-NDC80 (KMN) complex, essential for the chromosome-microtubule connection and the assembly of the k-fiber (Cheeseman et al., 2006) (**Figure 6)**. K-fibers are the most stable fibers in the spindle (Brinkley & Cartwright Jr., 1975; Rieder, 1981) and are essential for the accurate chromosome movements (Rieder, 2005). In HeLa cells the average metaphase k-fiber consists of 17 microtubules (McEwen et al., 2001; Wendell et al., 1993). The number of microtubules inside the k-fiber increases throughout mitosis as the fiber matures (McEwen et al., 1997).

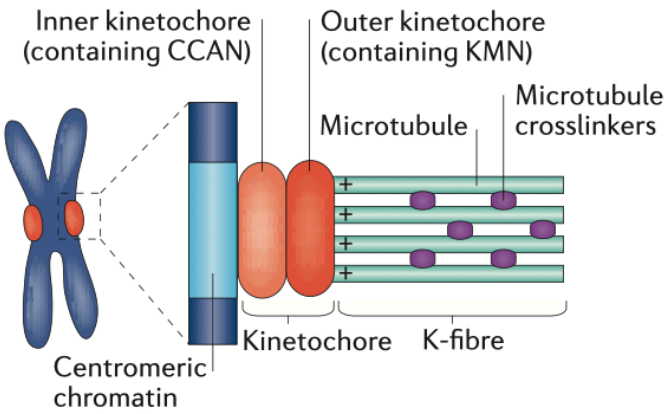

Figure 6. Kinetochore- microtubule attachment. At the centromere the kinetochore assembles. The inner kinetochore attaches to the chromosome whilst the outer enables the connection to the microtubules, making the k-fiber (Prosser & Pelletier, 2017).

The kinetochores contain the surveillance system which monitors and fixes erroneous microtubule attachments. Sister kinetochores have to be attached properly to the opposite spindle poles, i.e. bioriented, in the configuration named amphitelic attachment. The Aurora B kinase senses the tension on the centromere and removes erroneous microtubule attachments (Godek et al., 2015; Trivedi & Stukenberg, 2016). The wrong attachments can occur if only one kinetochore is attached to the microtubule (monotelic), if both kinetochores are attached to the microtubules from the same pole (syntelic), or if a single kinetochore is attached to the both poles (merotelic) (**Figure 7**).

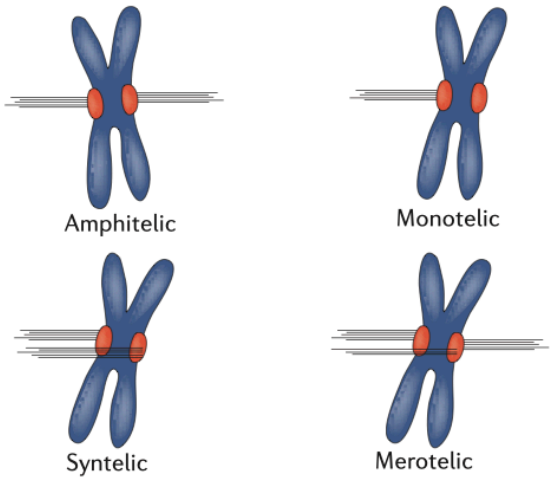

Figure 7. Types of kinetochore-microtubule attachments. Amphitellic: the correct configuration when sister kinetochores are attached to the opposite poles; Monotelic: only one kinetochore is attached; Syntelic: sister kinetochores are attached to the same pole; Merotelic: one kinetochore is attached to the both poles (Prosser & Pelletier, 2017).

If the kinetochore assembles an erroneous attachment, SAC is activated at the wrongly attached kinetochores and the progression throughout mitosis is stopped (Lara-Gonzalez et al., 2021). Single unattached kinetochore is sufficient to trigger the SAC activation (Rieder et al., 1995), but merotelic attachments can be unnoticed and thus be a major source of aneuploidy (Cimini et al., 2001). The SAC operates by inhibiting the activity of the anaphase-promoting complex/cyclosome (APC/C), an E3 ubiquitin ligase required for sister chromatid separation (Barford, 2020). The APC/C complex is activated by Cdc20 and ubiquitinates the anaphase inhibitors enabling the anaphase entry and mitotic exit (**Figure 8 A**). Unattached kinetochores block the activity of this complex by catalyze the formation of the mitotic Checkpoint Complex (MCC) composed of Mad2, Cdc20, BubR1 and Bub3 (Fang, 2002; Hardwick et al., 2000; Sudakin et al., 2001) (**Figure 8 B**). When the kinetochore-microtubule attachment is satisfied, it silences the SAC signaling by different means. Microtubules promote the stripping of the Mad1/Mad2 complex from the kinetochore by dynein (Griffis et al., 2007; Howell et al., 2001). Also, the kinetochore components like Ndc80 cause the displacement of the SAC components (Hiruma et al., 2015; Ji et al., 2015). Moreover, intrakinetochore stretching caused by the microtubule attachment satisfies the SAC (Maresca & Salmon, 2009; Uchida et al., 2009).

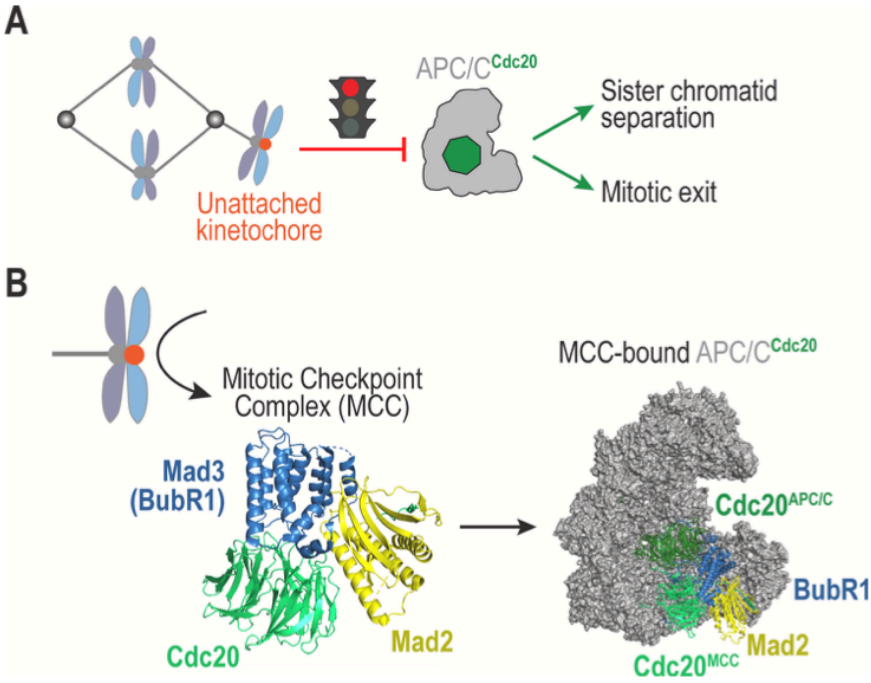

Figure 8. SAC-dependent control of mitosis progression. A) Unattached kinetochores activate SAC which inhibits the APC/C complex. Its activation enables the progression into anaphase and mitotic exit. B) Structure of the MCC complex (color) bound to the APC/C complex (gray) (Lara-Gonzalez et al., 2021).

2.3.4. Chromosome congression

The ultimate goal of prometaphase is to precisely translocate all chromosomes to the future metaphase plate and to correctly attach the sister kinetochores to the opposite poles. This chromosome translocation is called congression, and it is evolutionarily conserved and essential for the accurate chromosome segregation (Nicklas & Arana, 1992) (**Figure 9**).

The initial position of the chromosomes in relation to the poles during NEBD determines the mechanism of their translocation to the spindle equator. After NEBD, some chromosomes position in the middle of the spindle, between two poles. They are already “at the right place” to biorient and stabilize their attachments with the microtubules. On the other hand, some chromosomes are positioned around and/or behind the poles, far from the future metaphase plate so they need to be actively transported towards the spindle equator (Maiato et al., 2017). This is achieved by the synchronized actions of Dynein/Dynactin, CENP-E/kinesin-7 and chromokinesins (Kid/kinesin-10 and Kif4A/kinesin-4) (Barisic et al., 2014; Li et al., 2007;

Schaar et al., 1997; Wandke et al., 2012) that transport chromosomes along pre-existing spindle microtubules towards the spindle equator, independently of biorientation (Kapoor et al., 2006). Note that the experiments involving visible chromosomes in this thesis are focused on the chromosomes that use this kind of congression. First, the chromosomes are pulled towards the pole by dynein. At the poles the concentration of Aurora A is high and it phosphorylates CENPE thereby regulating its direction (Kim et al., 2010; Ye et al., 2015), whereas other centrosome kinases as Plk1 inactivates dynein (Whyte et al., 2008). CENPE "takes over" the congression of the chromosomes towards the spindle equator by laterally interacting with the existing microtubules. At the same time, chromokinesins at the chromosome arms cause polar ejection force (PEF) that pushes the chromosomes in the equatorial direction (Wandke et al., 2012) (**Figure 9**).

Moreover, it was shown that tubulin posttranslational modification act as a map to navigate the molecular motors in the right direction and help the congression. Astral microtubules are tyrosinated and favor the transport of chromosomes by dynein to the poles. More stable k-fibers and interpolar microtubules are detyrosinated and navigate CENP-E to carry the chromosomes towards the spindle equator (Barisic et al., 2015; Barisic & Maiato, 2016; McKenney et al., 2016). The approaching towards the spindle middle enhances the chance of the appropriate chromosome biorientation.

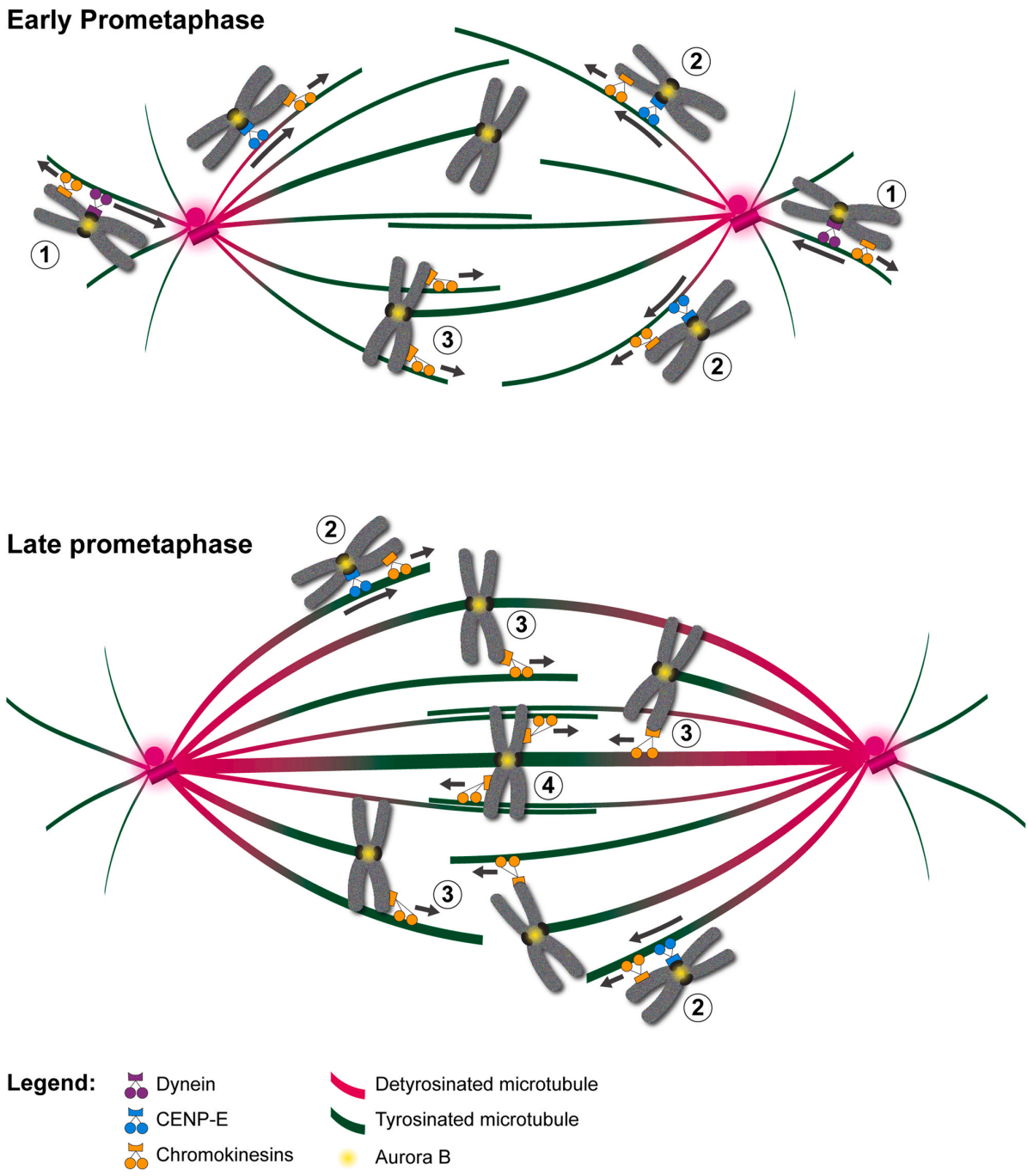

Figure 9. Current model of chromosome congression. The position of chromosomes during NEBD determines the mechanism of their congression. Peripheral chromosomes (1) are captured by dynein on tyrosinated microtubules (green) and pulled towards the poles, and then transported to the equator via CENP-E on the detyrosinated microtubules (red) (2). Poleward ejection force help the congression by pushing the chromosome arms towards the equator (3) and helping kinetochore-microtubule stabilization (4). (Maiato et al., 2017).

2.4. Microtubule-associated proteins

Cell cycle would be disturbed and the mitotic spindle couldn't self-assemble or fulfill any of the mitotic goals without the help of the hundreds of the microtubule associated proteins (MAPs) that have diverse activities throughout the cell cycle (**Figure 10**). Usually, they are divided into four groups: crosslinking proteins that stabilize and organize microtubules into specific assemblies; plus-end tracking proteins that regulate microtubule growth or connect them to the other structures; proteins that control microtubule destabilization; and motor proteins that move with respect to the microtubules powered by the ATP (Lodish et al., 2008). Note that the general overview of their roles is given in this chapter and their roles in the microtubule poleward flux will be discussed later in the text.

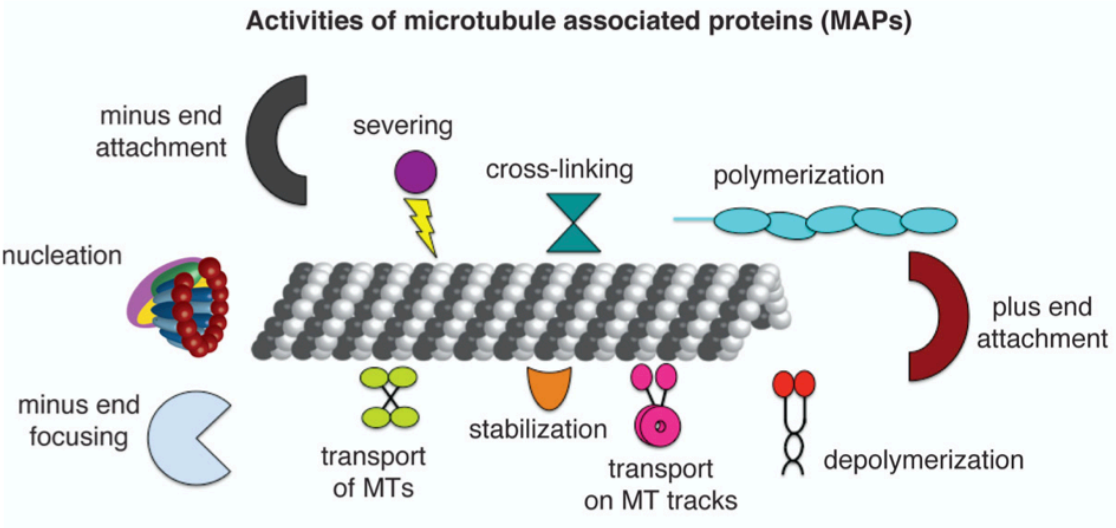

Figure 10. Activities of MAPs. Schematic representation of diverse MAP roles (Alfaro-Aco & Petry, 2015).

An important group of MAPs for this thesis is the motor protein group. In general, motor proteins are ATPases, meaning that they can bind ATP and hydrolyze it into ADP (Barton, 1996). The release of energy from this process causes conformational change in their motor domain enabling them to switch between bound and unbound state, i.e. to "walk" along microtubules. Motor proteins have preferable directionality of the movement with respect to the microtubule intrinsic polarity. Most motors move towards the plus-ends of microtubules, whereas some of them move towards the minus end (Lodish et al., 2008). The important motor proteins in mitosis are dynein and the kinesins, currently grouped in the 14 major

subfamilies (Lawrence et al., 2004) (**Table 1**). Also, for mammalian kinesins the kinesin family (KIF) nomenclature exists (Hirokawa et al., 2009). Kinesins are important throughout mitosis, including prometaphase where they help in microtubule organization into bipolar spindle by separating the poles, antiparallel microtubule sliding, self-organization, pole focusing, chromosome congression, poleward flux, etc. (**Figure 11; Table 1**).

Table 1. Motor proteins and their role in spindle assembly. Kinesins are separated into distinct groups with various roles in spindle assembly, taken and adjusted from (Prosser & Pelletier, 2017).

Protein family	Examples	Directionality and function	Role in spindle assembly	siRNA phenotype
Kinesin-3	KIF14	Plus end	Chromosome congression and alignment, bipolar spindle stabilization	ND
Kinesin-4	KIF4A, KIF4B	Plus end	Chromosome attachment to the spindle, anaphase spindle dynamics, spindle microtubule polymerization rates	Chromosome missegregation
Kinesin-5	EG5	Plus end bipolar tetramer, drives extensile sliding of antiparallel microtubules	Centrosome separation and establishment and/or maintenance of bipolarity	Monopolar spindles
Kinesin-6	MKLP1, MKLP2	Plus end, crosslinks and moves microtubules	Component of central spindle and essential for cytokinesis	Cytokinesis failure
Kinesin-7	CENPE	Bi-directional tracker of microtubule tips, slow processive motor	Mediates lateral kinetochore-microtubule attachments and chromosome congression	Prometaphase and/or metaphase block, failure of chromosomes to congress
Kinesin-8	KIF18A, KIF18B	Plus end, length-specific depolymerization	Regulates microtubule length and chromosome congression	Increased spindle length
Kinesin-10	KID	Plus end, microtubule- and DNA-binding	Polar ejection force, chromosome congression	ND
Kinesin-12	KIF15	Plus end tetramer, crosslinks and focuses plus ends	Maintenance of bipolarity	ND
Kinesin-13	KIF2B, KIF2A, MCAK	Plus and minus ends, microtubule depolymerization	Regulates microtubule length, rate of poleward flux and turnover of kinetochore microtubules, chromosome movements	Monopolar spindles, longer spindles after monastrol washout
Kinesin-14	HSET, ctk2, KifC1	Minus end, crosslinks and slides microtubules	Regulates spindle length and minus-end focusing, centrosome clustering and bipolar spindle formation	Reduced spindle length, multipolar spindles
Dynein		Minus end	Focuses spindle poles, transports K-fibre minus ends to the poles, spindle positioning	Mispositioned spindles, unfocused poles; congression problems

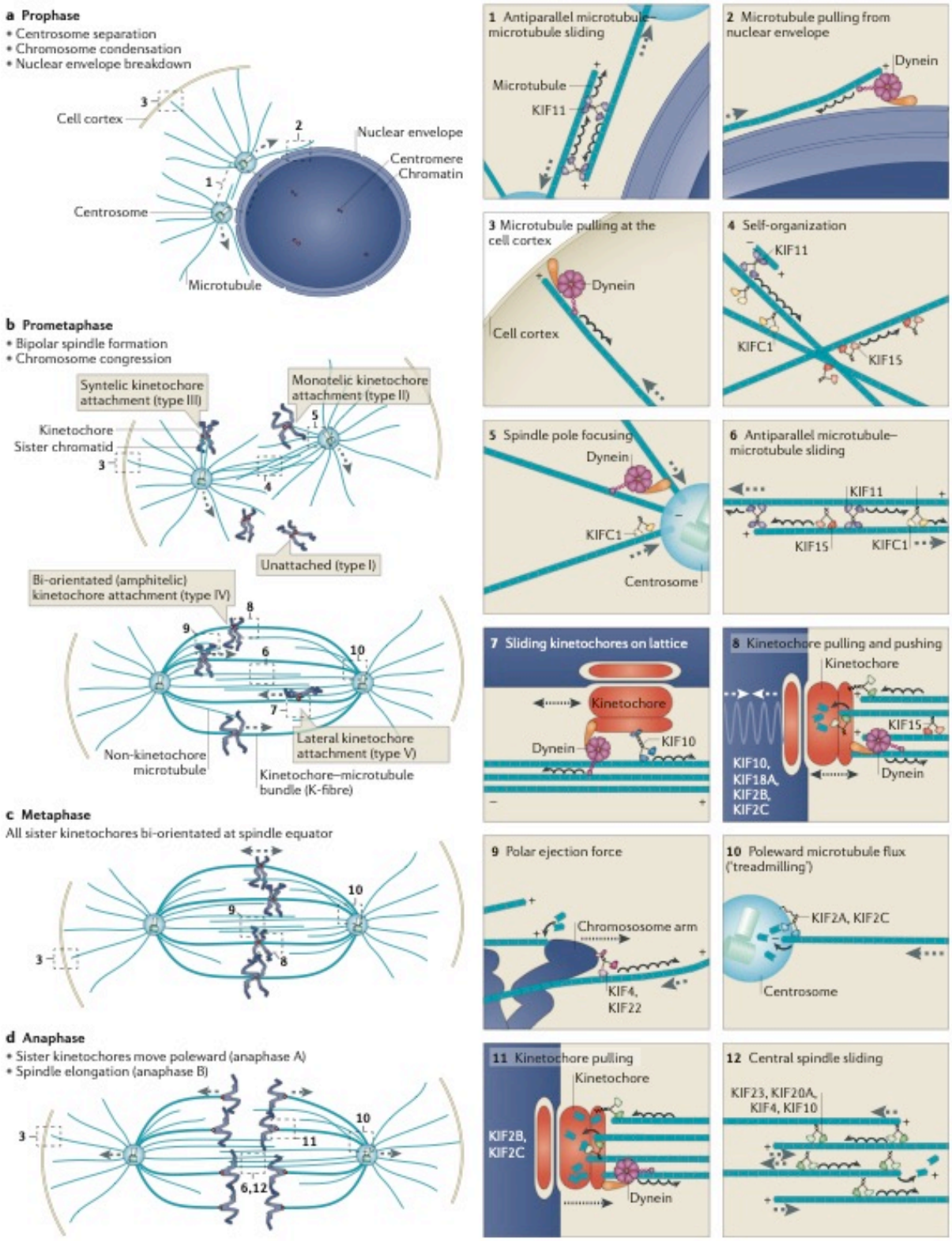

Figure 11. Motor proteins throughout mitosis. Left: mitotic stages with the important events and the roles of the various kinesins (right). See text for details. (Cross & McAinsh, 2014).

Kif11 (EG5) is a member of the kinesin-5 family and an important plus-end directed protein. It binds and crosslinks antiparallel bundles and slides them apart by walking towards the plus-ends (Waitzman & Rice, 2014). This kinesin is essential for the bipolar spindle assembly by centrosome separation, but it is not required for the maintenance of the bipolarity in all organisms. Namely, Kif15 is a kinesin-12 family member that has a redundant role with Eg5 in maintaining the bipolarity by crosslinking and sliding antiparallel microtubules apart (Drechsler et al., 2014; Reinemann et al., 2017; Tanenbaum et al., 2009).

The main antagonist of the above-mentioned kinesins is kinesin-14 (Kifc1/HSET in humans). It is a minus-end directed kinesin which slides the minus ends inside the antiparallel bundles towards each other and in that way plays an important role in prometaphase spindle assembly and spindle length regulation (Cai et al., 2009). This group of kinesins has additional roles in microtubule organization (She & Yang, 2017) because they can also bind parallel microtubules and cluster them, thereby being an important protagonist in pole focusing (**Figure 12**). Furthermore, they can bind to antiparallel microtubules and contribute to search and capture and help prometaphase spindle to self-organize (Cross & McAinsh, 2014).

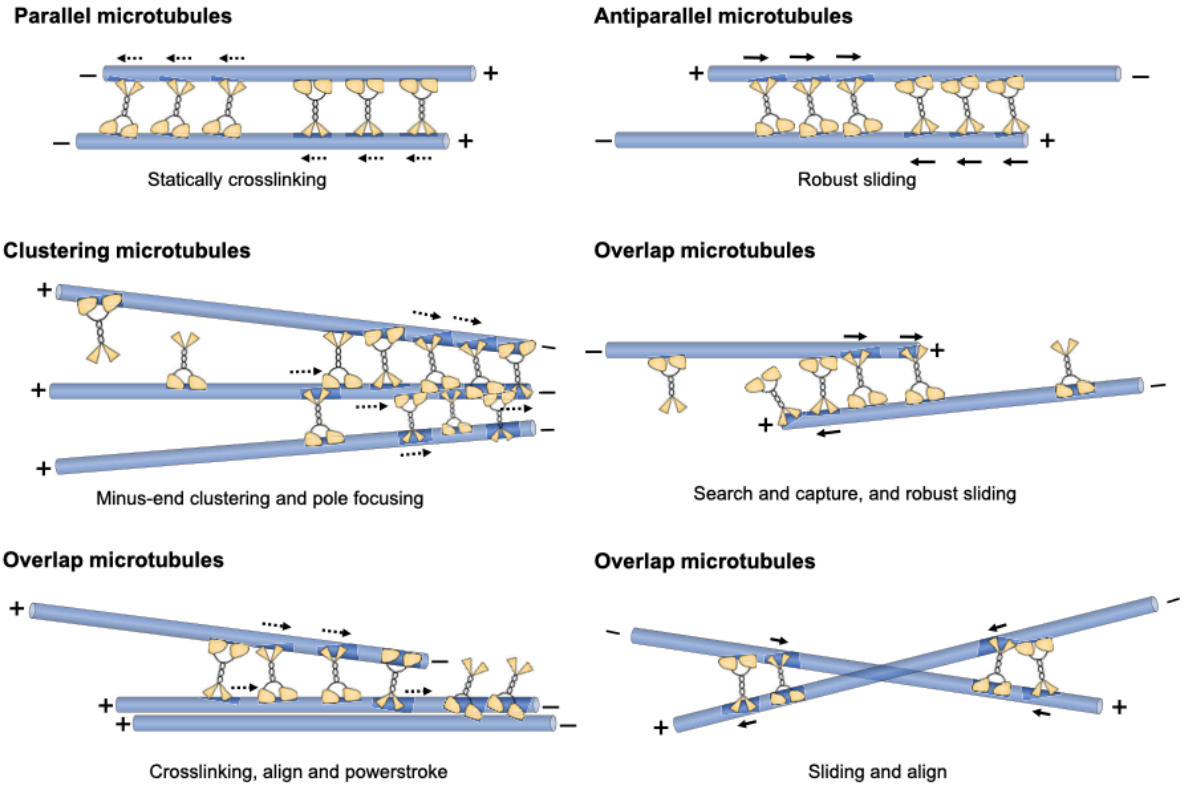

Figure 12. Roles of the kinesin-14 family. Kinesin-14 (yellow) can bind to antiparallel and parallel microtubules (blue) and thus have various functions in spindle assembly. Dashed or solid arrows show forces in the same or opposite direction, respectively (She & Yang, 2017).

The other important minus-end directed proteins is dynein. Its important role in chromosome congression was discussed above. Furthermore, it binds one microtubule as a cargo and carries it towards the minus end of the another microtubule, thereby focusing the microtubules into the poles (Civelekoglu-Scholey & Scholey, 2010). Also, it can bind different proteins important for the spindle maintenance at the minus ends of the microtubules to stabilize the structure of the poles (Goshima & Scholey, 2010).

Interesting group of kinesins are chromokinesins. As mentioned above, they are the main generators of poleward ejection forces (PEFs). They bind to the chromosome arms, and by walking towards the plus-ends of microtubules, push the chromosomes away from the poles. Important members are Kid/kinesin-10 and Kif4A/kinesin-4. Furthermore, Kif4A is known to regulate microtubule dynamics. It is a plus-end directed kinesin, which accumulates there and reduces the microtubule dynamic instability (Bringmann et al., 2004; Jagrić et al., 2021).

Another kinesin important for the regulation of microtubule dynamics is Kif18A from the kinesin-8 group. It is known to regulate the microtubule plus-end dynamics in a way that it accumulates at the plus-end in the length-dependent manner and causes microtubule depolymerization. In that way it regulates the k-fiber plus-end dynamics and chromosome alignment at the metaphase plate (Mayr et al., 2007; Stumpff et al., 2008, 2012).

Kinesin-13 family members, Kif2A and Kif2C (MCAK) are known microtubule depolymerases (Manning et al., 2007). They are nonmotile, but use the chemical energy to depolymerize microtubules (Desai et al., 1999). MCAK localizes to the spindle poles, midzone, kinetochores and the tips of the growing microtubules (Moore et al., 2005; Wordeman & Mitchison, 1995). It uses its depolymerizing activity to resolve erroneous kinetochore-microtubule attachments (Andrews et al., 2004; Knowlton et al., 2006). Kif2A is located at the spindle poles and is essential for the bipolar spindle assembly and chromosome movements by depolymerizing the minus ends of the microtubules (Ganem & Compton, 2004).

An important group of MAPs for this thesis are passive microtubule crosslinkers, with significant members: Nuclear Mitotic Apparatus (NuMA) and Protein Regulator of Cytokinesis1 (PRC1). As the name implies, they are immobile, and have the ability to crosslink parallel or antiparallel microtubules. NuMA locates at the microtubule minus ends near the spindle poles, associates with dynactin and accumulates dynein to tether the

microtubule minus ends into spindle poles (Hueschen et al., 2017) (**Figure 13**). Moreover, NuMA associates with leucine-glycine-asparagine repeat protein (LGN) to form a complex at the cell cortex important for the spindle positioning (Du & Macara, 2004).

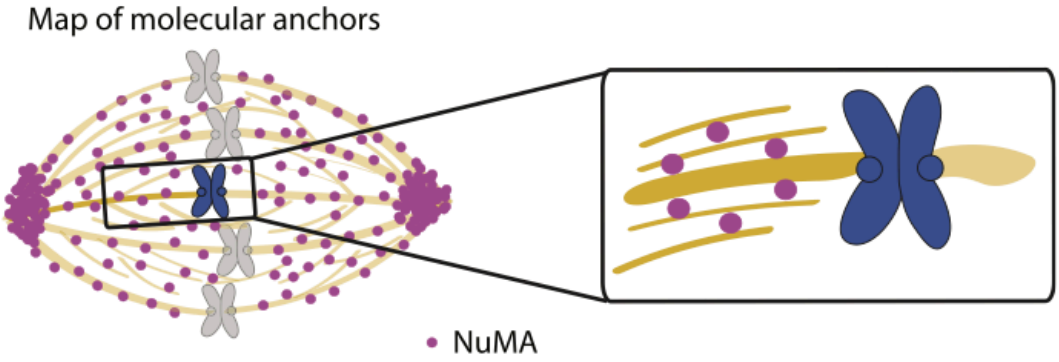

Figure 13. Localization of NuMA in the spindle. NuMA (purple circles) localizes throughout the spindle with the emphasis on the spindle pole region and provides local load-bearing (Elting et al., 2017).

PRC1 is a conserved MAP that has a preference for antiparallel microtubule bundles (Subramanian et al., 2010). As the majority of the antiparallel bundles appear at the spindle middle, its localization is enriched in that part of the spindle throughout mitosis (Kajtez et al., 2016; Matković et al., 2022; Polak et al., 2017) (**Figure 14, A**). In prometaphase and metaphase, it is known to be the main antiparallel crosslinker, forming the bridging fibers which balance the tension of the k-fibers (Jagrić et al., 2021; Kajtez et al., 2016; Matković et al., 2022) (**Figure 14, B**). Furthermore, it is essential for the formation of the central spindle during anaphase where it acts as a scaffold for the interaction with various proteins (Mollinari et al., 2002).

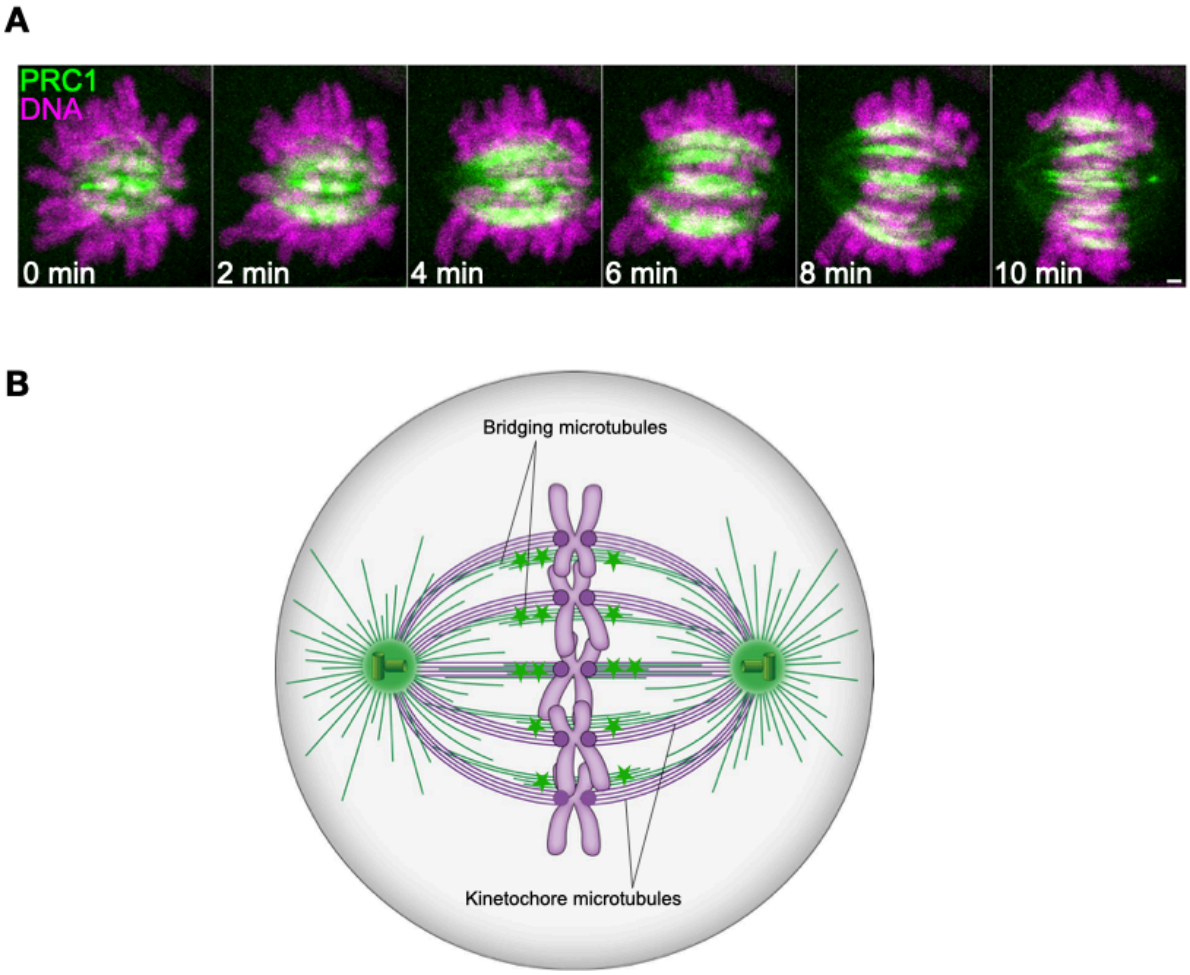

Figure 14. PRC1 localization in the spindle. A) localization of PRC1 (green) at the spindle from prometaphase to metaphase (Matković et al., 2022). B) schematic representation of PRC1 (green asters) localization in the bridging fibers of the metaphase spindle (Tolić, 2018).

Important group of MAPs that regulate the dynamics of the microtubule plus-ends throughout mitosis are +TIPs. The end binding (EB) proteins are very important members of this group. EB proteins bind selectively to the plus-ends of the growing microtubules throughout mitosis (**Figure 15**) (Maurer et al., 2012; Morrison et al., 1998; Yamashita et al., 2015), the feature that was also utilized in this thesis to track the comet-shaped plus-tips in time. In that way I was able to track the growth trajectory and see the range of the microtubule plus-ends in the prometaphase spindles. Also, they coordinate recruitment of a wide range of additional proteins that are important for microtubule dynamics regulation in a way that they are "hitchhiked" on EBs to the microtubule plus-ends (Mimori-Kiyosue et al., 2005; Nakamura et al., 2012).

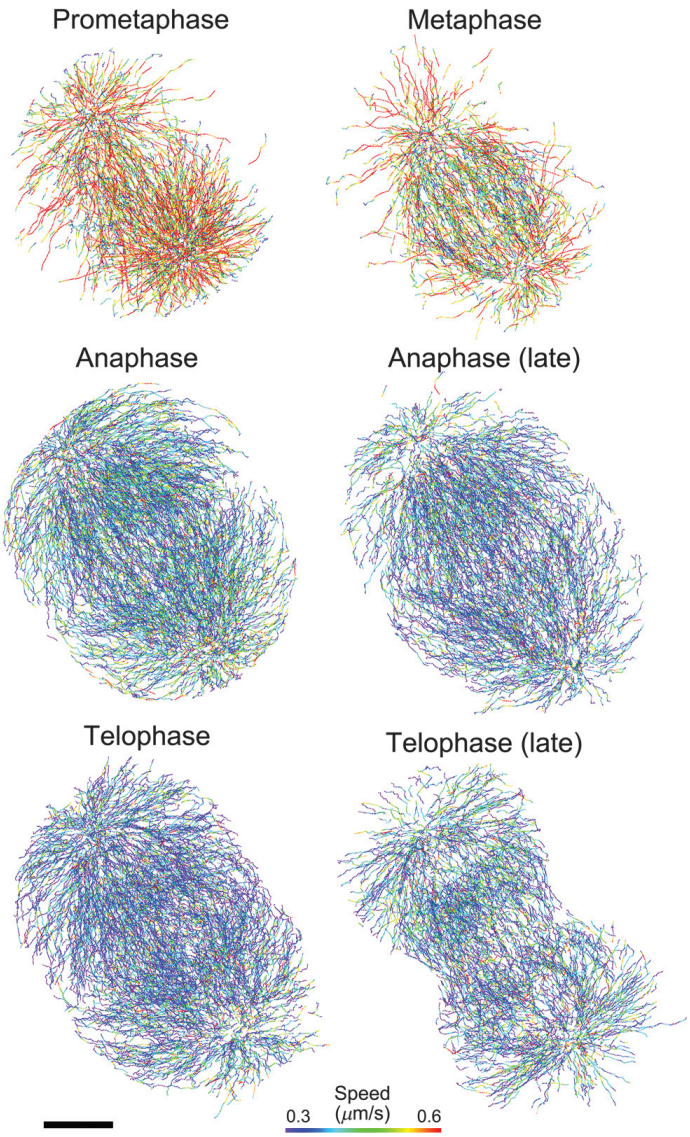

Figure 15. Localization of EB1 comets throughout mitosis. Representative images of EB1 trajectories in HeLa cells at different phases of mitosis. Color-code represents comet speed (Yamashita et al., 2015).

2.5. Microtubule structure and dynamic instability

The main topic of this thesis is the microtubule poleward flux, but before I introduce this complex microtubule behavior, it is important to have a closer look into the microtubule structure. Microtubules are protein tubes made by the polymerization of α- and β-tubulin heterodimers connected by non-covalent bonds (**Figure 16, A**). One microtubule consists of 13 protofilaments joint together in parallel configuration into hollow cylindrical structure (**Figure 16, B**). Protofilaments and microtubules have structural polarity with α- tubulin on

the minus and β- tubulin on the plus-end. Plus-end is more dynamic with higher constants of dissociation and association than the mins end. α-tubulin on the minus end is more prone to depolymerization whereas β-tubulin at the plus end polymerizes more often. α- and β-tubulin are enzymes. They can bound and β-tubulin can hydrolyze GTP. Hydrolysis of the GTP causes tubulin depolymerization and shortening of the protofilament. On the other hand, if the hydrolysis does not occur, protofilament growth will happen by incorporation of the new heterodimer. The exchange between the period of growth and shrinkage by constant monomer concentration is called microtubule dynamic instability (Akhmanova & Steinmetz, 2008) (**Figure 16, C**). The change from growth to shrinkage is called catastrophe, whereas growth is called rescue (Alberts et al., 2014).

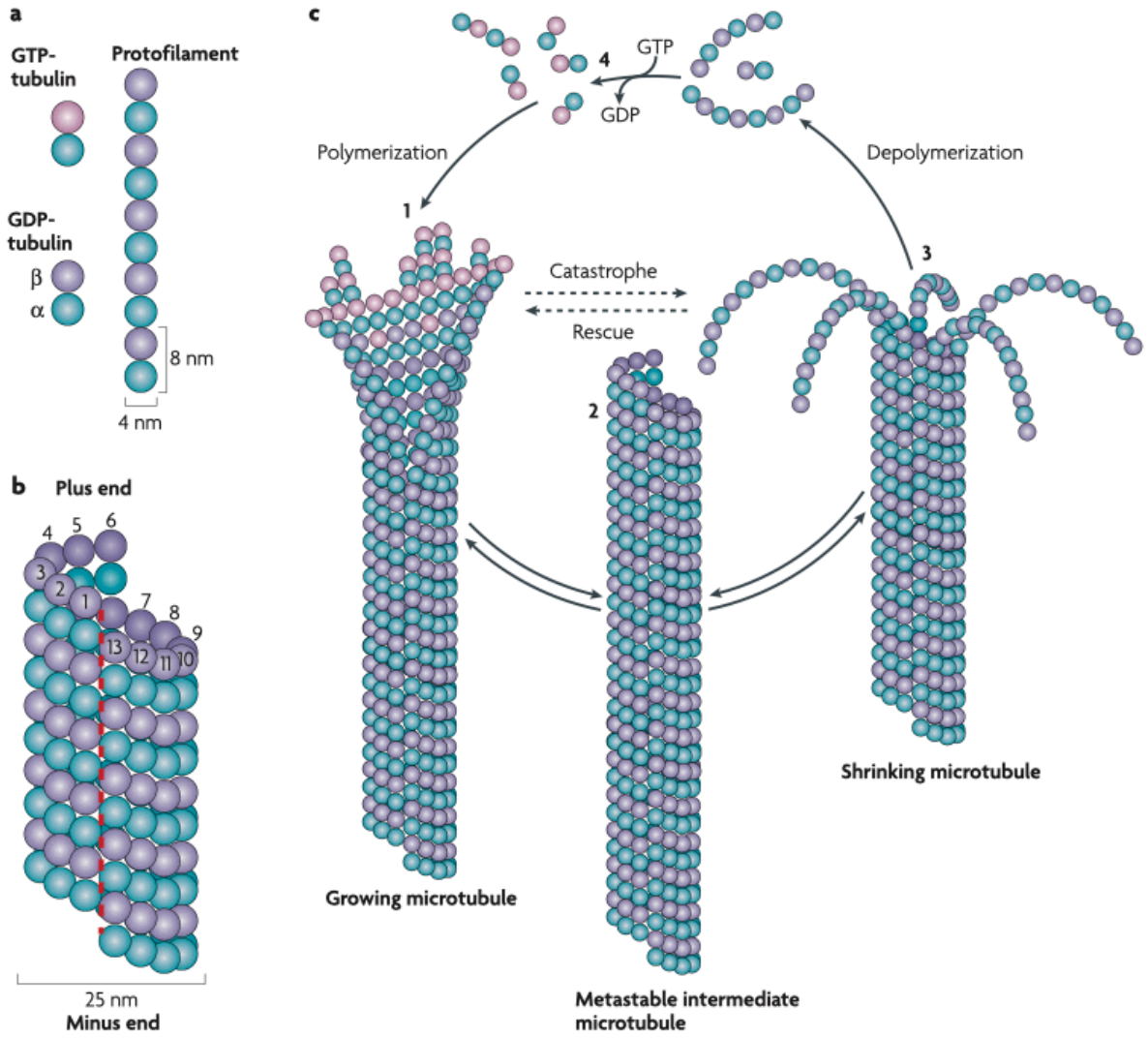

Figure 16. Microtubule structure and dynamic instability. Schematic representation of: A) αβ-tubulin heterodimers incorporation into protofilaments; B) 13 protofilaments connect laterally forming a tube with α-tubulin at the minus-end and β-tubulin at the plus-end; C) microtubules switch between the state of growth and shrinkage, termed dynamic instability lead by hydrolyzing the GTP-tubulin (Akhmanova & Steinmetz, 2008).

2.6. Microtubule poleward flux

New tubulin subunits preferentially incorporate at the microtubule plus-end, at the same time dissociating at the minus end at the spindle poles. In that way a continuous poleward motion of tubulin subunits inside the microtubule fiber arises, a phenomenon termed microtubule poleward flux (Mitchison, 1989). Thus, the tubulin inside the mitotic spindle is being constantly recycled. Poleward flux is evolutionary conserved, but the velocity differs between different organisms (Barisic et al., 2021; Rogers et al., 2005) and different phases of mitosis (Cimini et al., 2006).

2.6.1. Current methods to study poleward flux

Even before the 80's, when the poleward flux was experimentally proven, the researchers used various microscopy techniques to study the spindle dynamics during mitosis and meiosis in different organisms (Forer, 1965; Hiramoto & Izutsu, 1977; Inoué & Sato, 1967; Nicklas & Koch, 1972; Salmon, 1975). Later, as the fluorescence microscopy evolved, photobleaching experiments gave deeper insight into microtubule dynamics (Salmon et al., 1984; Saxton et al., 1984). Finally, Mitchison developed a photoactivation technique that generated fluorescent marks on the microtubule fibers and demonstrated microtubule poleward flux on k-fibers (Mitchison, 1989). Today, similar tubulin photoactivation methods are used. The mitotic spindle is marked with photoactivatable tubulin (**Figure 17, A**), a system that gives fluorescent signal after the irradiation with UV laser beam (Patterson & Lippincott-Schwartz, 2002; Tulu & Ferenz, 2010). With precise laser, a defined area on the microtubule can be irradiated and followed in time (**Figure 17, B**). In that way, the poleward flux of the subpopulation of tubulin within the spindle can be studied in different organisms and mitotic phases (Barisic et al., 2021; He & Cimini, 2016).

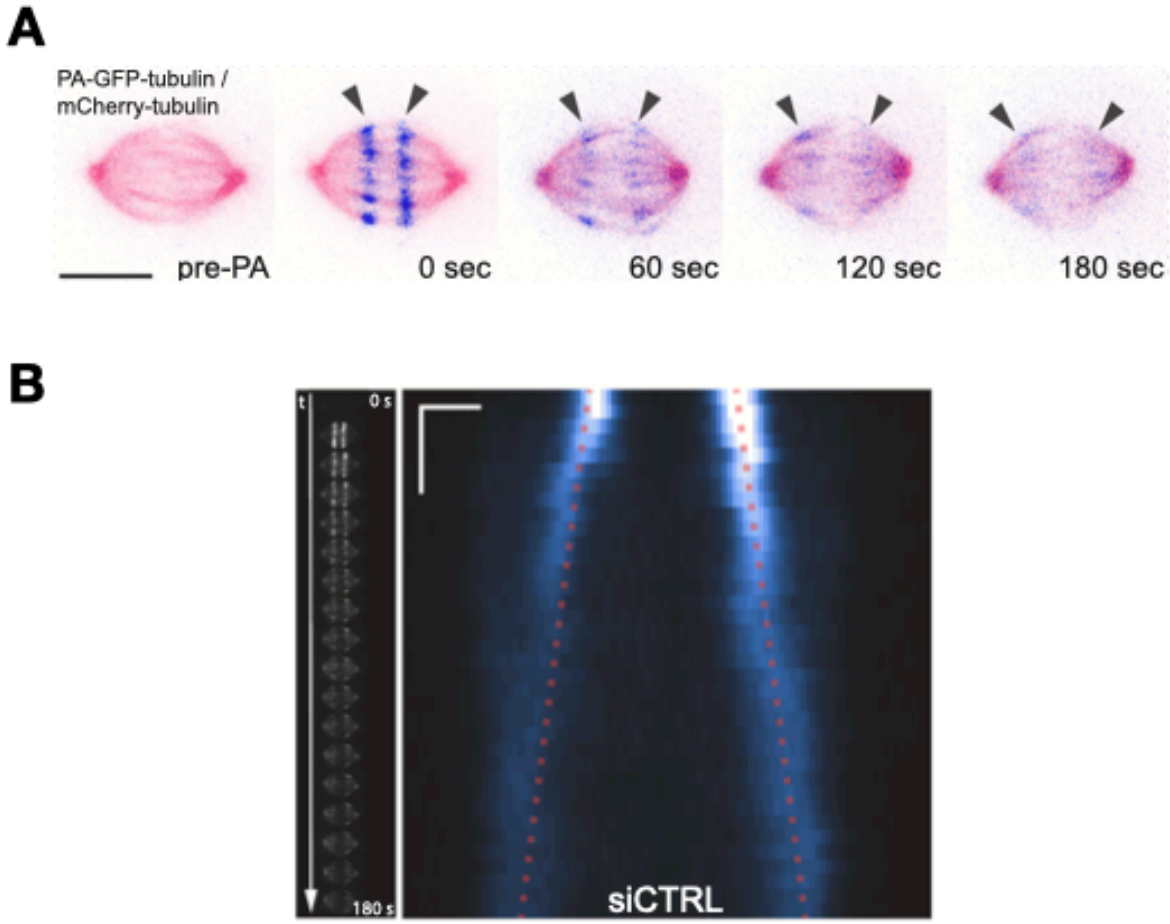

Figure 17. Poleward flux analysis using tubulin photoactivation assay. A) Metaphase spindle with the expression of photoactivatable-GFP-tubulin (blue) and mCherry-tubulin (red) before (first image) and after the photoactivation (arrowheads). B) irradiated signal can be traced in time and shown as a kymograph to calculate the poleward flux velocity (Barisic et al., 2021).

Tubulin photoactivation is a powerful tool to study poleward flux, but it can't distinguish the flux of the individual fibers because with this method all the microtubules inside the irradiated region are photoactivated. To get the more precise insight into prometaphase poleward flux and differentiate the movement of the bridging fibers and k-fibers, I used fluorescent speckle microscopy. This microscopy method was developed by injecting low doses of fluorescently-labelled tubulin into cells. The fluorescent tubulin incorporated stochastically into the microtubules among the unlabeled tubulin which gave a non-uniform speckle-like signal that could be tracked in time (Waterman-Storer et al., 1998) (**Figure 18**). Recently, an assay based on speckle microscopy was developed, which avoids microinjection or cell transfection (Risteski, 2023; Risteski et al., 2022). It is based on the simple application of 1 nM concentration of cell-permeable dye, silicon rhodamine (SiR)-tubulin (Lukinavičius et al.,

2014). It incorporates stochastically within the microtubule lattice and allows the labelling of individual fibers within multiple cells with high specificity and low background noise, a perfect condition to study poleward flux of individual fibers.

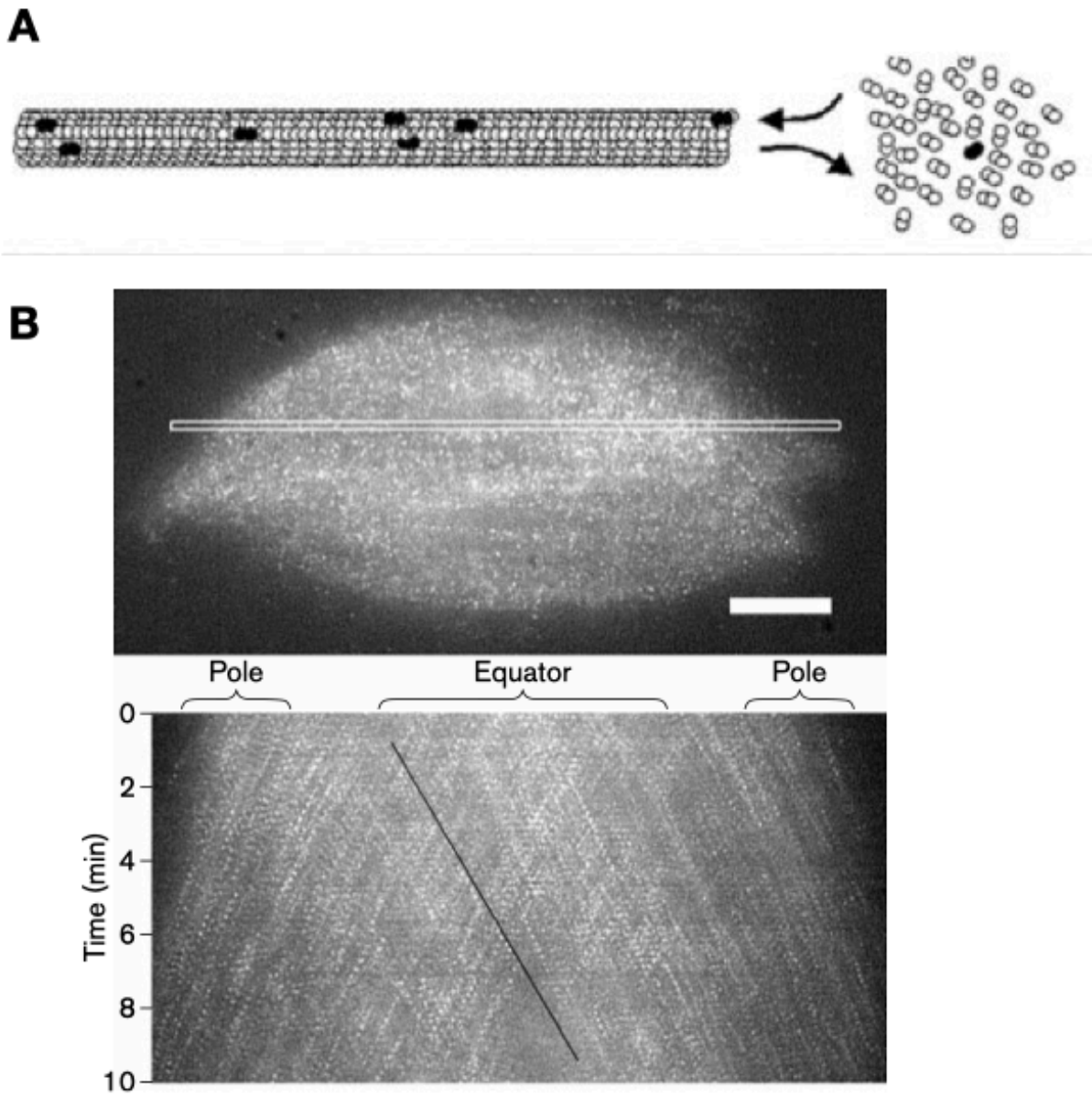

Figure 18. Fluorescent speckle microscopy assay. A) Schematic representation of stochastically incorporated fluorescently labelled tubulin (black) inside the unlabeled microtubule lattice (colorless). B) The boxed region in upper panel is used in time to produce kymograph (bottom panel). The slope of a black line gives poleward flux velocity (Waterman-Storer et al., 1998).

2.6.2. Models for poleward flux

Microtubule poleward flux is a complex and intriguing phenomenon that has been puzzling researches since its discovery. First photoactivation experiments on *Xenopus* egg extracts and *Drosophila* embryos and S2 cells indicated that the flux is driven by the sliding of the antiparallel fibers in the spindle middle (Brust-Mascher et al., 2009; Mitchison et al., 2004; Miyamoto et al., 2004). Functional inactivation of kinesin-5 severely reduced the flux speed in bipolar and monopolar spindle suggesting the kinesin-5 as the main flux driver. Thus, "slide and cluster" model suggested that a plus-end directed proteins inside the antiparallel fibers slides the microtubules toward the minus-ends and they are clustered by a minus-end directed protein (Burbank et al., 2007) (**Figure 19**). But, the spindles of the different organisms, although similar, vary in spindle organization and operate with different molecular participants (**Figure 20**). For instance, yeast (*Saccharomyces cerevisiae*) spindles do not flux and the microtubule dynamics is observed only at the plus-ends (Maddox et al., 1999, 2000). This complicates the search of the flux drivers. Namely, in mammalian cells kinesin-5 inhibition doesn't induce monopolar spindles in the cells that have established bipolar spindles and flux velocity is only slightly perturbed (Kapoor et al., 2000). Therefore, the "treadmilling model" was suggested stating that the poleward flux is generated by the depolymerization at the poles that "reels in" the microtubules to drive flux by simultaneous polymerization at the kinetochore (Cameron et al., 2006). Experiments on *Drosophila* embryos and human cells suggested Kif2A depolymerization at the poles as a major flux driver (Ganem et al., 2005; Rogers et al., 2004). This minus-end depolymerization was suggested to be coupled by the plus-end microtubule polymerization by CLASP. However, this concept was challenged and instead the "feeder-chipper" model was proposed: flux is driven by the antiparallel sliding and balanced by the plus-end polymerization and minus-end depolymerization (Gadde & Heald, 2004).

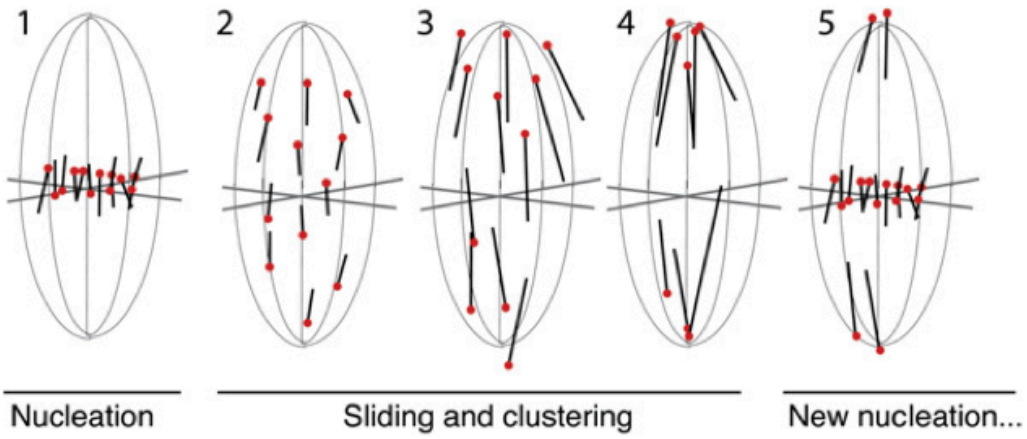

Figure 19. Slide and cluster model for poleward flux. Microtubules are nucleated in the spindle middle (1) and slide towards the minus ends where they cluster (2-4). New nucleation restocks the microtubule population in the middle (5) (Burbank et al., 2007).

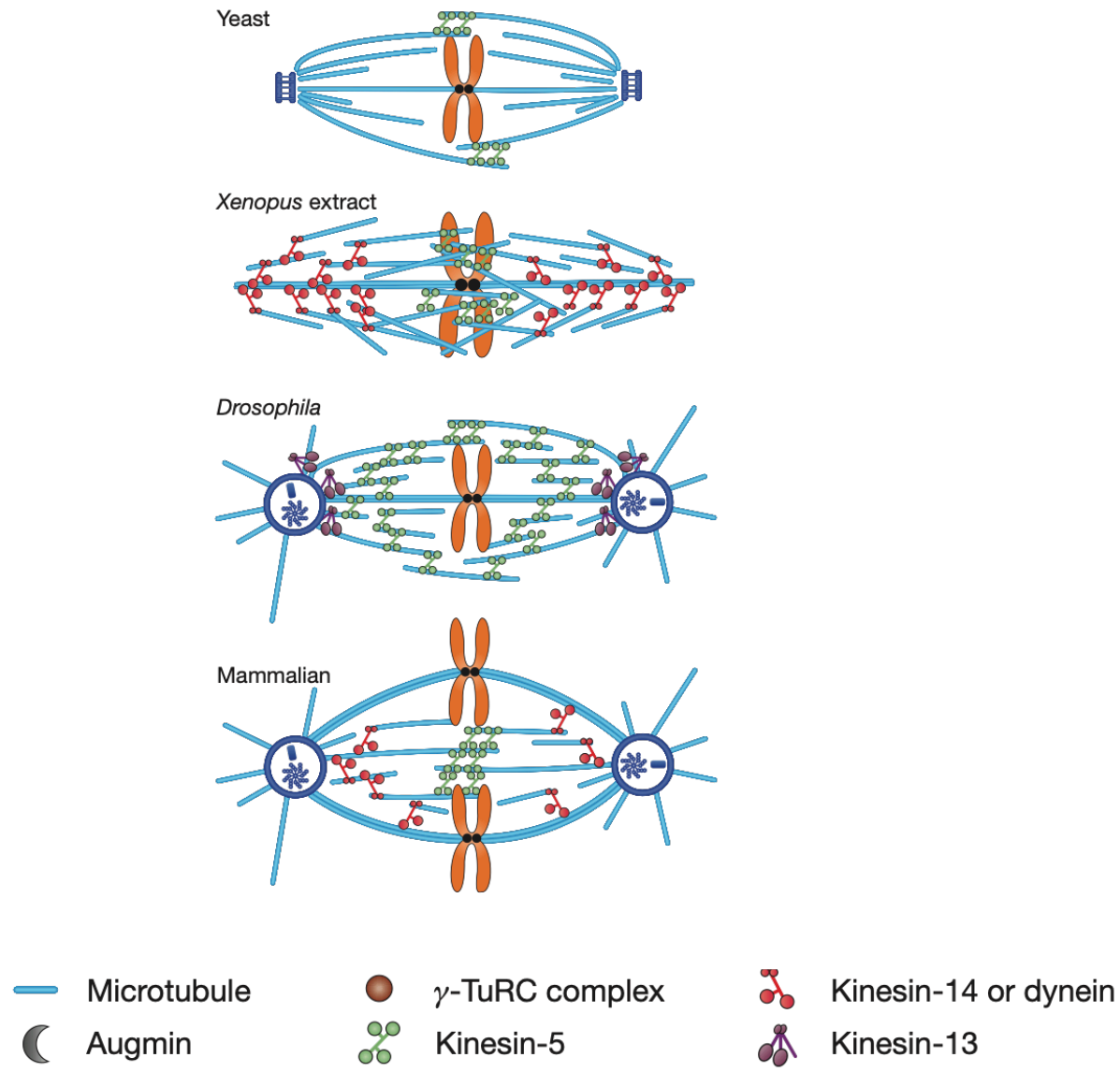

Figure 20. Variation in spindle organization. Spindle organization varies between different species (Wang et al., 2014).

Recent model on human cancer derived cells proposed that the flux is driven by the coordinated action of four kinesins (Steblyanko et al., 2020). The antiparallel sliding of Eg5 and Kif15 is supported by CENP-E at the kinetochores in prometaphase and Kif4A on chromosome arms in metaphase. This force is transmitted to the kinetochore fibers via the passive crosslinkers NuMA and HSET (**Figure 21**).

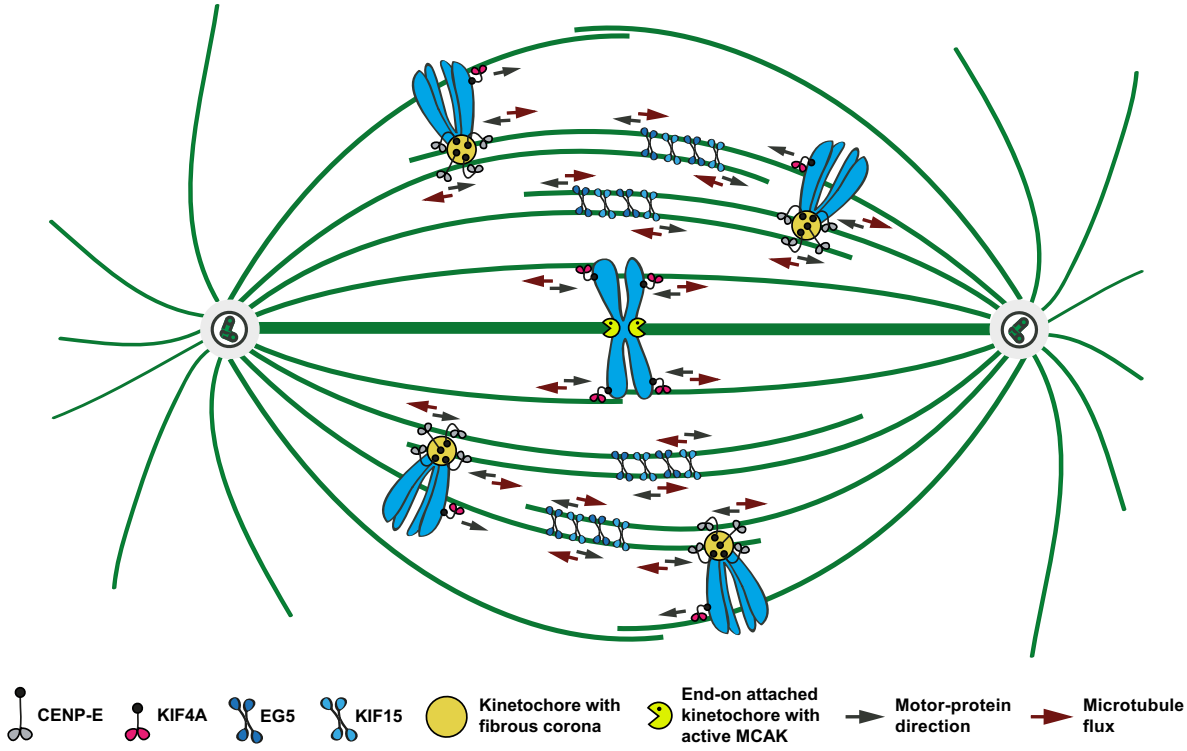

Figure 21. Poleward flux is driven by the coordinated action of the four kinesins. The sliding of the interpolar microtubules in the spindle middle is powered by the Eg5 and Kif15 and cooperated by CENP-E at kinetochores in prometaphase and Kif4A at chromosome arms in metaphase (Steblyanko et al., 2020).

My thesis is inspired by the work from Risteski et al. (2022) that demonstrated that the metaphase k-fiber flux is generated by the sliding in the bridging fibers which is transmitted to the k-fibers via the lateral interaction by the passive crosslinkers. Longer k-fibers flux faster that the shorter sister k-fibers and this length-dependent flux drives the metaphase chromosome alignment (**Figure 22**). It opened the questions about the flux mechanism in healthy human prometaphase cells and the potential impact of the flux on the chromosome congression.

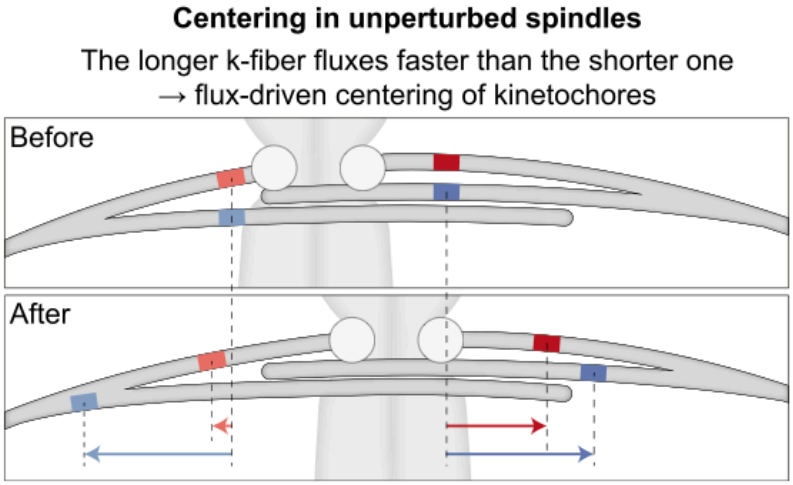

Figure 22. Poleward flux-generated kinetochore alignment. Longer k-fiber (right, red) fluxes faster than the sister k-fiber (left, red) because of the longer overlap with the bridging fiber (blue). It results in the movement of the displaced kinetochore (circles) towards the spindle middle (Risteski et al., 2022).

3. MATERIALS AND METHODS

3.1. Cell culture and maintenance

Untransformed hTERT-RPE-1 cell line (female) with a stable expression of CENP-A-GFP and centrin1-GFP was a gift from Alexey Khodjakov (Wadsworth Center, New York State Department of Health, Albany, NY, USA). RPE-1 cell line with a stable expression of Ruby-Mad2 and CENP-A-Cerulean was a gift from Jonathon Pines (The Institute of Cancer Research, London, UK). RPE-1 hTERT expressing EB3-GFP and H2B-mCherry were a gift from Patrick Meraldi (University of Geneva, Geneva, Switzerland). Osteosarcoma U2OS cell lines (female) expressing CENP-A-GFP and photoactivatable PA-GFP-a-tubulin; CENP-A-GFP, photoactivatable PA-GFP-a-tubulin and mCherry-a-tubulin were a gift from Marin Barišić (Danish Cancer Society Research Center, Copenhagen, Denmark) and Helder Maiato (Institute for Molecular Cell Biology, University of Porto, Portugal). U2OS cells expressing 2xGFP-EB3 and mCherry-CENP-A were a gift from Julie Welburn (University of Edinburgh, United Kingdom).

RPE-1 and U2OS cells were maintained in Dulbecco's Modified Eagle Medium (containing 4.5 g/L d-glucose, stable glutamine, sodium pyruvate; Capricorn Scientific) supplemented with 10% Fetal Bovine Serum (Sigma-Aldrich), 100 IU/mL penicillin and 100 mg/mL streptomycin (Lonza). For all U2OS cells and RPE-1 cells expressing EB3-GFP and H2B-mCherry 50 μg/mL geneticin (Life Technologies, Waltham, MA, USA) was added in the medium. All cells were grown at 37°C in a Galaxy 170 R humidified incubator (Eppendorf) with a 5% CO_2 atmosphere. Cells were routinely tested for mycoplasma by visual inspection using DAPI staining at the microscope. Cells were passaged for a maximum of 8–10 weeks (~10 passages).

3.2. Cell transfection

RPE-1 cell lines transfection was performed by lipofection method. One day before siRNA transfection, 120 000 cells were seeded on 35-mm glass coverslip dishes with 0.17-mm glass thickness (ibidi GmbH, Grafelfing, Germany). All siRNA constructs were diluted in Opti-

MEM Reduced Serum Medium (Gibco) and transfection was performed with Lipofectamine RNAiMAX Reagent (Invitrogen) by following manufacturer's protocol. Constructs and their final concentrations used were: 100 nM Kif4A siRNA (sc-60888; Santa Cruz Biotechnology), 100 nM Kid/Kif22 siRNA (4392420; Ambion), 100 nM CENP-E siRNA (L-003252-000010; Dharmacon), 20 nM Haus6 siRNA (L-018372-01-0005, Dharmacon), 300 nM PRC1 siRNA (L-019491-00-0010; Dharmacon), 100 nM NuMA siRNA (sc-43978; Santa Cruz Biotechnology), 100 nM Kif2A siRNA (sc-60884; Santa Cruz Biotechnology), 100 nM Kif2C siRNA (sc-105596, Santa Cruz Biotechnology). After 4 h of incubation with transfection mixture, the medium was replaced with regular cell culture medium. All experiments on siRNA-treated cells were performed 24 h after transfection, except for H6 and Kif2A siRNA-depleted cells, where silencing was done for 48 h.

3.3. Immunostaining

In experiments for determination of protein depletion level, the cells were fixed in ice-cold methanol (Sigma-Aldrich) for 1 min. After fixation, the cells were permeabilized for 15 min in 0.5% Triton X-100 (Sigma-Aldrich) in phosphate buffered saline (PBS, no Ca/Mg, Roth). Following permeabilization, cells were blocked with 1% normal goat serum (NGS, Invitrogen) in PBS for 1 h and incubated with primary antibodies at 4°C overnight. Primary antibodies were prepared in 1% NGS in PBS to 1:100 dilution (except for tubulin staining, with the dilution of 1:500). Following incubation with primary antibodies, cells were incubated with fluorescent-conjugated secondary antibodies at room temperature for 1 h. Secondary antibodies were prepared in 2% NGS in PBS to 1:250 dilution, or 1:1000 for tubulin staining. Additionally, when indicated, to visualize DNA, cells were stained with DAPI (1 μg/mL) for 10 min. After each step, cells were washed three times in PBS for five minutes.

Primary antibodies used were: mouse anti-Kif4A (sc-365144; Santa Cruz Biotechnology), mouse anti-Kid (sc-390640; Santa Cruz Biotechnology), rabbit anti-CENP-E (C7488; Sigma-Aldrich), mouse anti-PRC1 (sc-376983; Santa Cruz Biotechnology), mouse anti-NuMA (sc-365532; Santa Cruz Biotechnology), mouse anti-Kif2A (D-7, sc-271471; Santa Cruz Biotechnology), mouse anti-Kif2C (2488C3a, sc-81305), rabbit polyclonal anti-H6 (ab-150806, Abcam), rat anti-alpha tubulin (MA1-80017, Invitrogen). Secondary antibodies used

were: donkey anti- mouse IgG-Alexa 594 (Abcam, ab150112), donkey anti-rabbit IgG-Alexa 594 (Abcam, ab150064) and donkey anti-rat IgG-Alexa Fluor 647 (Abcam, ab150155).

For tubulin STED imaging, RPE-1 cells with a stable expression of CENP-AGFP, or Ruby-Mad2 and CENP-A-Cerulean were grown on 35-mm glass coverslip dishes with 0.17-mm glass thickness (ibidi GmbH, Grafelfing, Germany), cell medium was removed, and cytoskeleton extraction buffer (0.5% Triton X-100, 0.1 M 1.4-piperazinediethanesulfonic acid, 1mM EGTA, 1 mM magnesium chloride) was added for 20 s to extract the components of the cytoplasm. Following the extraction, the cells were fixed in a fixation solution (3% paraformaldehyde and 0.1% glutaraldehyde in 1x PBS) for 10 min. To reduce the background fluorescence, reduction solution (0.1 % sodium borohydride in PBS) was added for seven minutes, and after aspiration, quenching solution (100 mM glycine in PBS) for 10 min. To prevent the non-specific binding, cells were incubated in blocking/permeabilization buffer (2% normal goat serum and 0.5% Triton-X-100 in PBS) for 2 h at 4°C. Microtubules were then stained using a rat monoclonal anti-tubulin primary antibody (diluted 1:500 in blocking/permeabilization buffer, MA1-80017, Invitrogen) with a 4°C overnight incubation. The following day, the cells were washed three times with PBS for 5 minutes and a secondary antibody donkey anti-rat IgG-Alexa Fluor 568 (dilution 1:1000, Abcam, ab175475) was added and incubated for 1 h at room temperature and then washed three times with PBS.

3.4. Live cell imaging

3.4.1. Speckle microscopy

RPE1 cells expressing CENP-A-GFP and centrin1-GFP grown in glass coverslip dishes were stained with 1 nM SiR-tubulin dye (Spirochrome AG) that was added in the existing cell medium. After 15 min of staining, confocal live imaging was performed on a Dragonfly spinning disk confocal microscope system (Andor Technology) using 63x/1.47 HC PL APO oil objective (Leica) with Sona 4.2P scientific complementary metal oxide semiconductor camera (Andor Technology); and on Expert Line easy3D STED microscope system (Abberior Instruments) using 60x/1.2 UPLSAPO 60XW water objective (Olympus) and avalanche photodiode detector. Images were acquired using Fusion software for Dragonfly and Imspector software for STED microscopy system. During imaging, cells were maintained at

37°C and 5% CO_2 within heating chamber (Okolab). For live imaging of RPE1 cells expressing CENP-A-GFP and centrin1-GFP, and stained with SiR-tubulin, 488-nm and 640-nm laser lines for Dragonfly microscope system, and 485-nm and 640-nm for STED microscope system were used for excitation of GFP, and SiR, respectively. In order to visualize SiR-tubulin speckles, images were acquired with 80% laser power and exposure of one s for both microscopy systems. Image acquisition was done on one focal plane every 5 s. The imaging was carried out up to an hour after the dye was added, when individual speckles could be distinguished from the neighboring signal. The same movies were used to determine the positions of the kinetochores to determine the interkinetochore distance and KC tilt.

3.4.2. Photoactivation assay

For photoactivation experiments, helios one-line 405-nm solid state laser (Obis lasers, Coherent), mounted on Bruker Opterra Multi- point Scanning Confocal Microscope was used to photoactivate microtubules in U2OS cells with stable co-expression of photoactivatable-GFP-a-tubulin, CENP-A-GFP and mCherry-a-tubulin; or on U2OS cells with stable co-expression of photoactivatable-GFP-a-tubulin and mCherry-a-tubulin. Photoactivation experiments were performed in Live/Ablation mode, at 80% 405 nm laser power, by using Prairie View software (Prairie Technologies). In order to visualize GFP and mCherry, 488-nm and 561-nm laser lights were used, respectively, together with 250 ms exposure time. Images were acquired at one focal plane with a time interval of 10 or 15 s for prometaphase cells and 30 s for metaphase cells.

3.4.3. Imaging of EB3 comets to determine the antiparallel overlap length

To determine the antiparallel overlap length in RPE1 cells that stably express EB3-GFP and H2B-mCherry, whole spindle was imaged in one frame with both channels on one z-plain to determine the phase of mitosis. Then, the smaller area of the central part of the spindle was imaged every 1.3 s to precisely visualize the EB3 comets. Imaging was performed in confocal mode on Expert Line easy3D STED microscope system (Abberior Instruments) using 60x/1.2 UPLSAPO 60XW water objective (Olympus) and avalanche photodiode detector using the Imspector software.

3.4.4. Imaging of EB3 comets to determine the kinetochore occupancy

To explore the probability of microtubule end-on attachments on the kinetochores during the congression, live cell imaging of the U2OS cells with stable expression of GFP-EB3 and mCherry-CENP-A was used. It was inspected if EB3 comets can reach from both poles to both kinetochores during the congression. First, one image of the whole spindle was made to see that it is in prometaphase, and then fast live cell imaging of the small area of the spindle was obtained to precisely visualize the movements of EB3 comets and congressing kinetochores in 1.3 s interval in one z-plane. The images were taken in confocal mode on Expert Line easy3D STED microscope system (Abberior Instruments) using 60x/1.2 UPLSAPO 60XW water objective (Olympus) and avalanche photodiode detector using the Imspector software.

3.5. Imaging of fixed cells

3.5.1. Determination of protein depletion and PRC1 length

For determination of protein depletion or the length of the PRC1 signal, immunostained cells were imaged using Bruker Opterra Multipoint Scanning Confocal Microscope (Bruker Nano Surfaces) with a Nikon CFI Plan Apo VC 100x/1.4 numerical aperture oil objective (Nikon). 405/488/561/640-nm laser lights were used with following emission filters: BL HC 525/30, BL HC 600/37 and BL HC 673/11 (Semrock). Images were captured with an Evolve 512 Delta Electron Multiplying Charge Coupled Device Camera (Photometrics) using a 200 ms exposure time.

For tubulin STED imaging, Expert Line easy3D STED microscope system (Abberior Instruments) with 100 x/1.4NA UPLSAPO100x oil objective (Olympus, Tokio, Japan) and avalanche photodiode detector was used. Images were acquired using Imspector software. The 488 nm line was used for the excitation of GFP, and the 561 nm line was used for visualization of tubulin, with the 775 nm laser line for depletion. The xy pixel size was 20 nm with 500 nm distance between planes.

3.6. Image analysis

All measurements were performed in Fiji/ImageJ (National Institutes of Health). Quantification and data analysis were performed in MATLAB (MathWorks). Figures and schemes were assembled in Adobe Illustrator CC (Adobe Systems). Statistical analysis was performed using Student's t-test and Mann-Whitney test.

3.6.1. Microtubule poleward flux velocity measurement from speckle microscopy assay

The measurements of speckle velocities, kinetochore and pole positions were carried out similarly as in (Risteski et al., 2022). Upon inspection of tubulin speckle movement within the spindle, speckles which could be followed for at least 15 s (four time-frames) were taken into account. For every tubulin speckle position, corresponding CENP-A and centrin positions, representing the location of sister kinetochores and spindle poles, respectively, were also tracked. Tracking was done manually by using the *Multi-point tool* in Fiji. Speckles which started at a kinetochore were categorized as a part of k-fiber, whilst speckles which started between sister kinetochores and passed through sister kinetochore area were categorized as a part of the bridging fiber. Speckle-pole velocity was calculated by fitting linear regression on distances between the tubulin speckle and the associated spindle pole during first 15 s of their trajectories.

3.6.2. Microtubule poleward flux velocity measurement from photoactivation assay

Poleward flux in photoactivation experiments was analyzed by using 5-pixel-thick *Segmented line tool* in Fiji to obtain GFP and mCherry intensity profiles along the contour of the photoactivated microtubule bundle, taken from pole to pole. *Spline fit* option in Fiji enabled a more accurate tracking of the photoactivated bundles. Also, some images were smoothed with 0.5 pixel-sigma Gaussian blur filter to obtain better defined intensity maxima. The positions of the photoactivated tubulin intensity maxima and the poles were recorded. The distance between photoactivated spot intensity peak and the pole was calculated over time and linear regression was fitted on those tracks giving the velocity of the poleward movement of

photoactivated spot. Poleward flux velocity was measured during at least four time-frames of photoactivated spot movement.

3.6.3. Defining the antiparallel overlap length

To determine the antiparallel overlap length in RPE1 cells immunostained for PRC1, a 5-pixel-wide segmented line was used to track the pole-to-pole contour of individual PRC1-labelled overlap regions. The pole-to-pole tracking was performed similarly as in (Polak et al., 2017). The mean value of the cytoplasm was subtracted from the retrieved intensity profiles obtained on single z-planes. The overlap length of individual PRC1-labeled overlap regions was determined as the width of the peak of the signal intensity in the central part of the contour in SciDavis (Free Software Foundation Inc.). The width of the peak was measured at the base of the PRC1 intensity peak where the PRC1 signal is roughly equal to the mean value of the PRC1 signal along the contour on either side of the peak. The bundles that disappeared in the z-direction were not taken into account. Also, the spindles that appeared aslope were not tracked.

To determine the antiparallel overlap length in RPE1 cells that stably express EB3-GFP and H2B-mCherry, *Multipoint tool* in Fiji was used to obtain the xy coordinates of the EB3 comets and the poles. The tracking was done until the frame when the position of the comet was last visible or was no longer clearly distinguishable from its neighbors. The spindle equator was defined as half the distance between two poles. Half-overlap length was measured as the distance between the last location where a tracked EB3 spot was visible and the spindle equator.

3.6.4. Determination of protein depletion level

To define the percentage of protein depletion, sum intensity profiles of the corresponding spindle protein intensity was measured by encompassing the area of the spindle with the *Polygon selection tool* in Fiji. Mean background intensity in the cytoplasm, measured using a 1 x 1 μm rectangle, was subtracted from the sum spindle intensity. The intensity of Kif4A and kid on chromosome arms was measured in the corresponding protein channel on sum-

intensity projections of all z-planes using *Polygon selection tool* in Fiji by encompassing chromosomes in the DAPI channel.

3.6.5. Determination of kinetochore microtubule occupancy level

To count the possible tubulin end-on attachments on the kinetochores during the congression, the movement of the EB3 comets in the area of the congressing kinetochores was followed visually. It was counted how many times the comet hit the kinetochore facing the closer or the further pole. The average number of EB3 comet-kinetochore hit per minute was calculated by dividing the number of the hits by the total duration during which the visual inspection was taken.

To measure the tubulin intensity of the k-fibers on sister kinetochores in STED-images, the 24x24 pixels squared area (*Square tool*, Fiji) was used. The square was positioned on the microtubules next to the kinetochores, on the pole-side. The background intensity was measured with the same method within the spindle in the area without the microtubules. It was subtracted from the k-fiber intensities. All measurements were obtained only on the sister kinetochores in the same z-plane.

3.6.6. Measuring the Mad2 level at the kinetochores

The Mad2 signal on the cells with a stable expression of Ruby-Mad2 and CENP-A-Cerulean, and immunostained tubulin was measured with *Oval-tool* in Fiji. In Mad2 signal channel the kinetochore area was covered and Mad2 signal intensity was obtained for both sister kinetochores. Also, the xy coordinates of the spindle poles and sister kinetochores were obtained using the *Multi-point tool* in Fiji. The signal intensity analysis was made on the individual z-planes or on sum of multiple z-planes and divided by the number of the planes.

3.6.7. Determination of kinetochore congression parameters

For determination of kinetochore congression parameters (interkinetochore distance and KC Tilt), all kinetochores that were on the spindle body during the prometaphase were included

into analysis. *Multipoint tool* in Fiji was used to manually obtain the xy coordinates of kinetochores and spindle poles in time to calculate the interkinetochore distance and the angle of sister kinetochore pairs during the congression. KC tilt is calculated as the angle between the line connecting sister kinetochores and the line connecting the spindle poles (i.e., spindle long axis).

4. RESULTS

4.1. Investigating the spindle microtubule dynamics by using the tubulin photoactivation assay

4.1.1. Microtubule poleward flux velocity measured by tubulin photoactivation is faster in prometaphase than in metaphase

To investigate the poleward flux velocity of prometaphase spindles, I have utilized tubulin photoactivation assay. I have used U2OS cells expressing mCherry-tubulin and photoactivatable GFP-tubulin and imaged them live during prometaphase, about five minutes after nuclear envelope breakdown (**Figure 23, A**). Before the photoactivation, only the mCherry-tubulin signal could be seen. By using the 405 nm laser, I have photoactivated the defined area on the microtubule bundle of the prometaphase spindle and the photoactivated GFP-tubulin signal appeared in this defined position. After the photoactivation, I have followed the movement of the photoactivated spot towards the pole by imaging the spindle every ten s (**Figure 23, A**).

I performed intensity profile analysis of the photoactivated tubulin using a line from the pole along the photoactivated bundle to the other pole (**Figure 23, B**). I have tracked the position of the photoactivated tubulin maxima and its distance from the pole over time (**Figure 23, C, D**). The approaching of the photoactivated tubulin towards the pole is interpreted as the microtubule poleward flux. I have calculated the slope of the linear fit of the distance in time positions and in that way calculated the microtubule poleward flux velocity.

I have imaged the metaphase spindles in the same way and calculated their microtubule poleward flux velocity from the obtained movies (**Figure 23, E, F**). Interestingly, with this method prometaphase poleward flux velocity is 1.264 ± 0.103 μm/min (25 photoactivated spots from 22 cells), and in metaphase 0.6 ± 0.037 μm/min (29 photoactivated spots from 21 cells, $p < 0.0001$) (**Figure 23, G**). Faster flux in prometaphase was observed previously with the same method (Steblyanko et al., 2020). This difference in flux velocities in different phases of mitosis can be explained by the different spindle architecture between prometaphase and metaphase. Namely, prometaphase spindles contain less kinetochore fibers which in metaphase have slower flux than bridging fibers (Risteski et al., 2022), so the majority of the

photoactivated signal arises from non-kinetochore fibers which flux faster. I tested this hypothesis later with the speckle microscopy method.

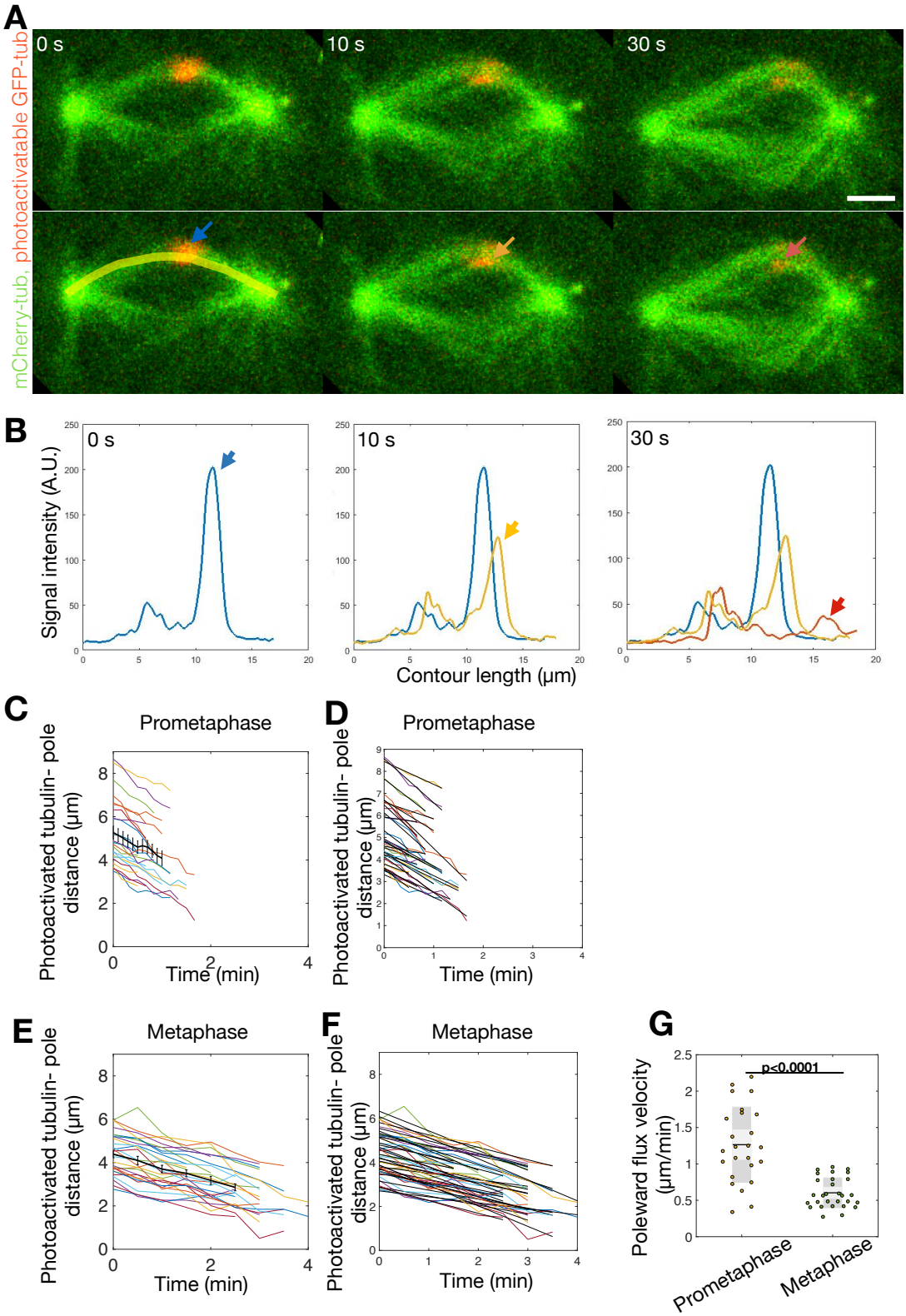

Figure 23. Tubulin photoactivation assay can be used to investigate the microtubule poleward flux velocity. A) Prometaphase spindle of U2OS cell expressing mCherry-tubulin

(green) and photoactivatable GFP-tubulin (red) imaged live during prometaphase (top). The red dot represents the photoactivated tubulin on the prometaphase spindle with the arrows pointing to the moving photoactivated spots (bottom). Yellow line represents the pole to pole contour along which the photoactivated signal intensity analysis was obtained (bottom). Scalebar represents 2 μm. B) Signal intensity profiles of photoactivated tubulin taken from the line along the contour of the photoactivated tubulin bundle. Arrows point to the signal intensity maxima measured at corresponding time points C-F) Distance between photoactivated signal maxima and the closer pole representing the microtubule poleward flux velocity in prometaphase (C, D) and metaphase (E, F). Colored lines represent individual tracks, black lines represent mean value and standard error of the mean. G) Average microtubule poleward flux velocity in prometaphase and metaphase spindles.

4.1.2. Prometaphase spindles undergo dynamic microtubule rearrangements

Occasionally, when I photoactivated thicker microtubule bundles in prometaphase spindles, photoactivated signal split laterally in two (**Figure 24, A**). I obtained intensity profiles of tubulin and photoactivated tubulin signals by drawing a line perpendicular to the photoactivated microtubule bundle (**Figure 24, B**). Both in photoactivated tubulin signal and in tubulin signal lateral splitting of the intensity maxima can be seen (**Figure 24, C**). It demonstrates that during prometaphase the microtubules are being split laterally or becoming better defined, as indicated previously (Matković et al., 2022) (**Figure 24, D**).

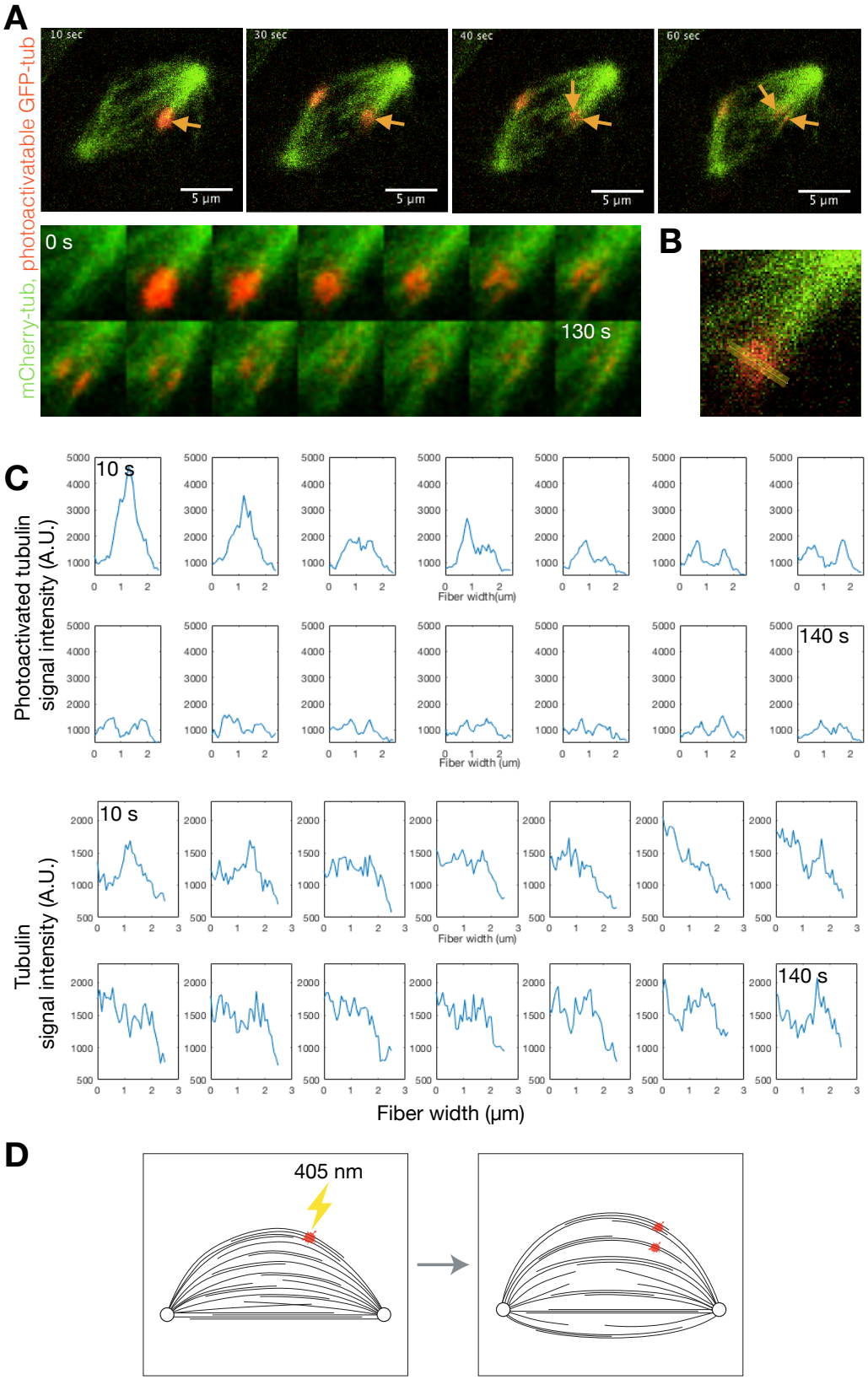

Figure 24. Prometaphase spindles undergo dynamic rearrangements of microtubules. A) Selected frames of U2OS cell line expressing mCherry-tubulin (green) and photoactivatable GFP-tubulin (red) imaged live during prometaphase (top). Arrow indicates the position of the

photoactivated tubulin aria. Bottom: enlarged area of the upper spindle with photoactivated tubulin where lateral splitting of the microtubule bundles over time can be seen. B) Example how the tubulin and photoactivated tubulin signal intensities were obtained using a line perpendicular to the tubulin bundle (yellow line). C) Photoactivated tubulin intensity profiles (top) and tubulin intensity profiles (bottom) taken from the spindle in A, every 10 s with the method as in B. D) Schematic representation of lateral splitting of photoactivated tubulin signal (red dots; lightning bolt represents photoactivation).

4.1.3. Inhibition of kinesin-5/Eg5 by STLC doesn't impact poleward flux of prometaphase bipolar spindles

To study the involvement of kinesins in prometaphase poleward flux, I used chemical inhibitors with the microtubule photoactivation assay to inspect the prometaphase poleward flux velocities and spindle architecture. The experiments were carried out on kinesin-5 that has the potential to slide the antiparallel overlaps and thus to potentially power the prometaphase poleward flux, on kinesin-12 that acts redundantly with Eg5, and kinesin-14 which has opposite directionality from Eg5.

The first kinesin studied here is kinesin-5/Eg5, one of the kinesins that is best known as the antiparallel microtubule slider throughout mitosis (Mann & Wadsworth, 2019). To explore the impact of kinesin-5/Eg5 on the microtubule poleward flux, I have treated U2OS cells expressing mCherry-tubulin and photoactivatable GFP-tubulin with S-trityl-L-cysteine (STLC) (Skoufias et al., 2006). This is a selective allosteric inhibitor of Eg5 which by inhibiting Eg5 prevents the formation of bipolar spindles causing the spindles to collapse into monopole (Gayek & Ohi, 2014). Indeed, after the addition of 40 μM STLC during NEBD, monopolar spindles formed. I have photoactivated the tubulin in the monopolar spindle in circular pattern around the pole and continued the imaging every ten s (**Figure 25, A**). I have tracked the movement of photoactivated intensity maxima along the line of the photoactivated tubulin fibers towards the pole (**Figure 25, B**) and calculated microtubule poleward flux velocity (**Figure 25, C, D, E**). In monopolar spindles the microtubule poleward flux is 0.739 ± 0.07 μm/min (23 fibers from 11 cells), slower than prometaphase ($p < 0.0001$), but not different from metaphase poleward flux velocity ($p = 0.07$) (**Figure 25, E**).

Intriguingly, when I photoactivated the tubulin closer to the microtubule fiber plus end, in some fibers the photoactivated spot divided in two. One part of the signal slid very fast towards the cell cortex and the other fluxed towards the spindle pole. I added the DNA dye to mark the position of the chromosomes in monopolar spindles to inspect whether the chromosomes are located on the microtubule fibers that show rapid sliding towards the cell cortex (**Figure 25, F**). The photoactivated spot moved towards the cortex beside the chromosomes meaning that there are no chromosomes attached end-on to those fibers (**Figure 25, F**). The photoactivated spots moved away from each other with the velocity of 2.69 ± 0.363 μm/min, and the divided stub separated from the pole with the velocity of 1.92 ± 0.363 μm/min (9 events from 8 spindles, **Figure 25, G-I**). The fibers with splitting events fluxed with the velocity of 0.768 ± 0.124 μm/min (9 fibers from 8 spindles), and the other 0.716 ± 0.08 μm/min (13 fibers from 9 spindles) giving no difference in poleward flux velocities between those fibers ($p = 0.715$, **Figure 25, I**). Taken all together, this fast sliding implies that the photoactivated microtubule is antiparallel non-kinetochore fiber that has probably detached from the rest of the spindle after the addition of STLC and remained the fast antiparallel sliding.

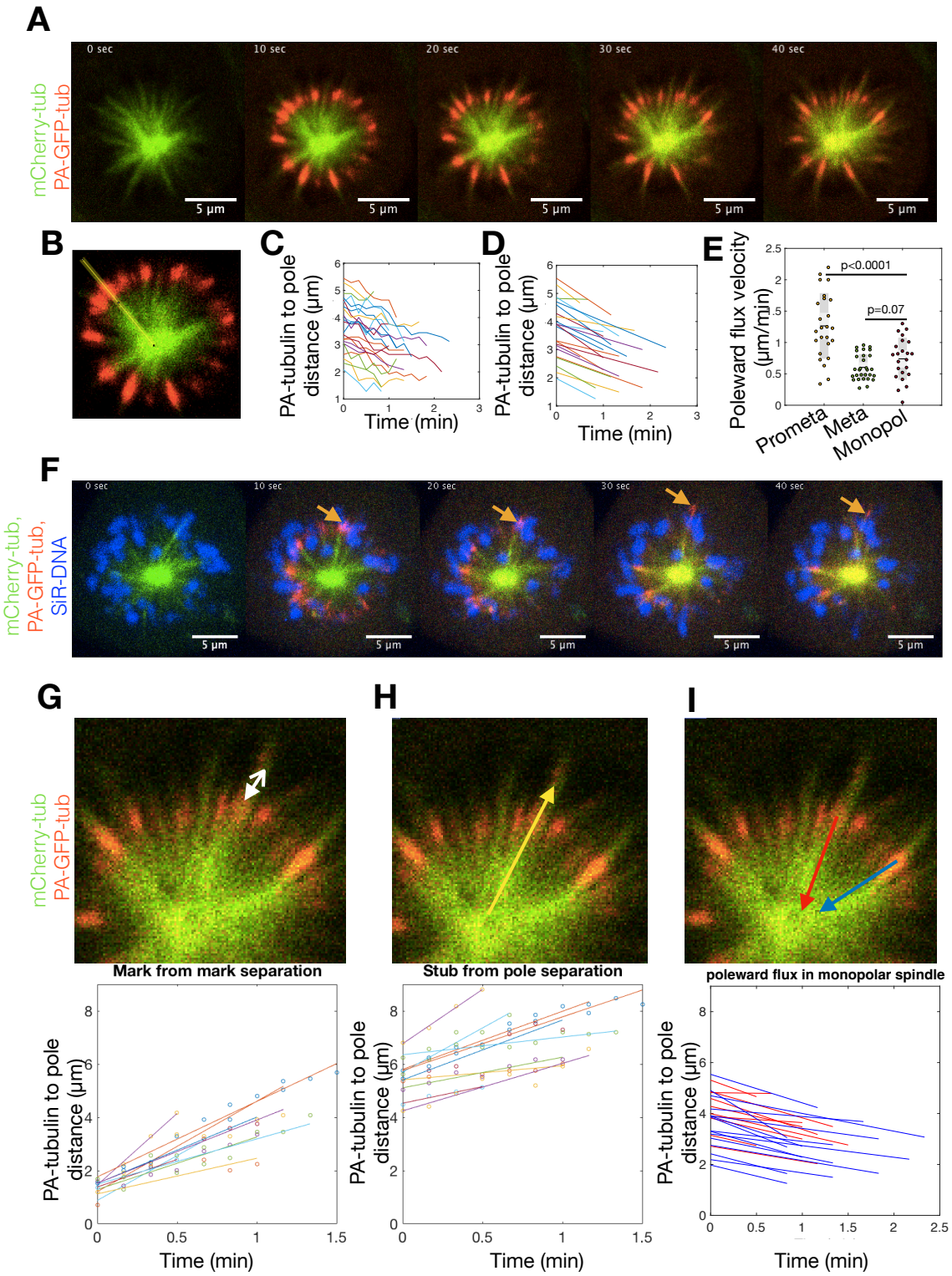

Figure 25. STLC treated monopolar spindles flux with same rate as metaphase spindles. A) Monopolar spindle of U2OS cell expressing mCherry-tubulin (green) and photoactivatable GFP-tubulin (red) imaged live after the addition of STLC and photoactivated in circular pattern (red). The movement of photoactivated tubulin towards the pole can be seen. B) Demonstration how the tracking of the photoactivated spot was made on the spindle in A). C)

The trajectories of the movement of the photoactivated tubulin towards the spindle pole. D) The linear fit on tracks from C. E) Poleward flux velocities in untreated prometaphase, monopolar and metaphase spindles. F) STLC treated U2OS cell as in A) with the addition of SiR-DNA dye (blue) to visualize the chromosomes and the movement of the photoactivated spot (orange arrow). G-I)) The detail from the spindle in A) representing the splitting of the photoactivated tubulin spot (white arrow in G) and mark from mark separation velocity (graph); stub from pole separation (yellow arrow in H) and their velocity (graph); poleward flux of fibers with splitting events (red) and without them (blue) with the corresponding distances from photoactivated marks to pole.

Occasionally, the addition of STLC didn't cause the spindle to collapse into monopole (**Figure 26, A**). Those spindles were shorter than the untreated (10.703 ± 0.257 μm in STLC treatment, 16.249 ± 0.423 μm in untreated, $p < 0.0001$), but remained bipolar (**Figure 26, B**). In those bipolar spindles the average poleward flux velocity during prometaphase was 1.348 ± 0.219 μm/min (10 photoactivated fibers from 10 cells), meaning that the kinesin-5 inhibition did not impact the prometaphase poleward flux velocity ($p = 0.718$) (**Figure 26, C-E**), suggesting that other motors in the overlap remain functional after Eg5 inhibition in bipolar spindles, consistent with (Steblyanko et al., 2020).

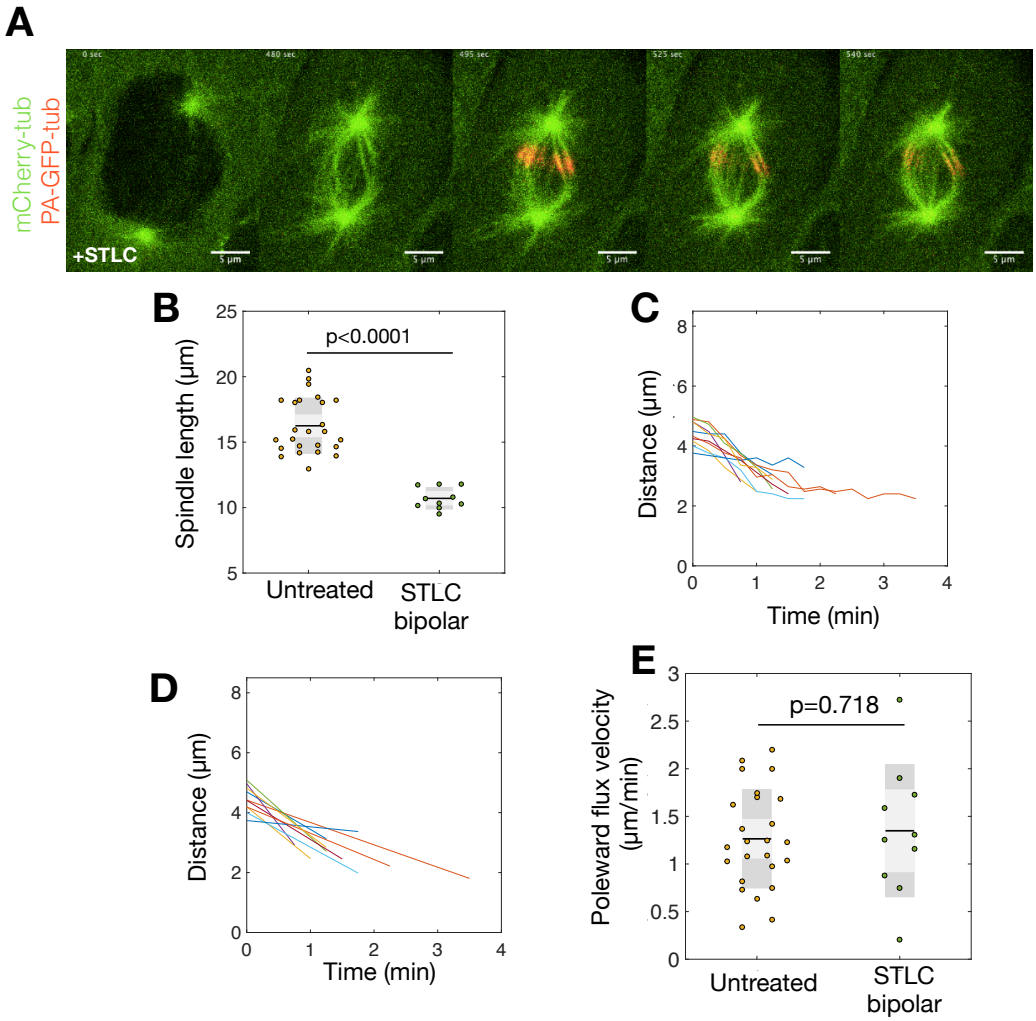

Figure 26. Inhibition of Eg5 by STLC doesn't impact poleward flux of prometaphase bipolar spindles. A) Bipolar spindle of U2OS cell expressing mCherry-tubulin (green) and photoactivatable GFP-tubulin (red) imaged live after the addition of STLC during NEBD, with photoactivated tubulin spot (red). B) The pole to pole contour length of the untreated and STLC-treated bipolar spindles. C) The trajectories of the photoactivated tubulin spot approaching the spindle pole. D) Linear fit on trajectories from C. E) Poleward flux velocity in the untreated and STLC treated bipolar prometaphase cells.

4.1.4. Inhibition of Eg5 with FCPT strongly affects microtubule poleward flux velocity

To further inspect the impact of Eg5 on prometaphase, I have treated the U2OS cells with 2-(1-(4-fluorophenyl)cyclopropyl)-4-(pyridin-4-yl) thiazole (FCPT) (Groen et al., 2008). This is an ATP competitive inhibitor of Eg5. Unlike STLC which traps it in low friction mode, it induces tight binding of Eg5 onto the microtubules. I have used U2OS cells expressing

mCherry-tubulin, photoactivatable GFP-tubulin and CENP-A-GFP to visualize the microtubules and kinetochores (**Figure 27, A**). I have titrated the concentration of FCPT added to the spindles during NEBD, and it showed that poleward flux velocity depends on the FCPT dosage (**Figure 27, B-E**).

With lower doses of FCPT (5 μM), the spindle morphology was normal, including the poleward flux velocity of 0.986 ± 0.154 μm/min (13 fibers from 13 cells, $p = 0.132$) and normal kinetochore congression pattern. With higher doses, the poleward flux velocity slowed down. With 6 μM FCPT the poleward flux was slower (0.323 ± 0.086 μm/min; 7 fibers in 7 cells, $p < 0.0001$) and the kinetochores congressed slowly towards the metaphase plate. With 7 μM FCPT the poleward flux was notably reduced (0.193 ± 0.086 μm/min; 4 fibers in 4 cells, $p < 0.0001$) and the congression was impacted as some kinetochores remained behind the pole and were unable to attach to the spindle body. With higher doses of FCPT (50 μM) the entire spindle was in rigor and appeared completely frozen. The spindles were bipolar but the inhibited Eg5 in antiparallel overlaps was unable to separate the poles completely. Also, the microtubule bundles were unable to split laterally and remained very thick, probably because of the Eg5 linking also the k-fibers (Vladimirou et al., 2013). The kinetochores levitated around the spindle and they couldn't be attracted towards the spindle body. There was no poleward flux.

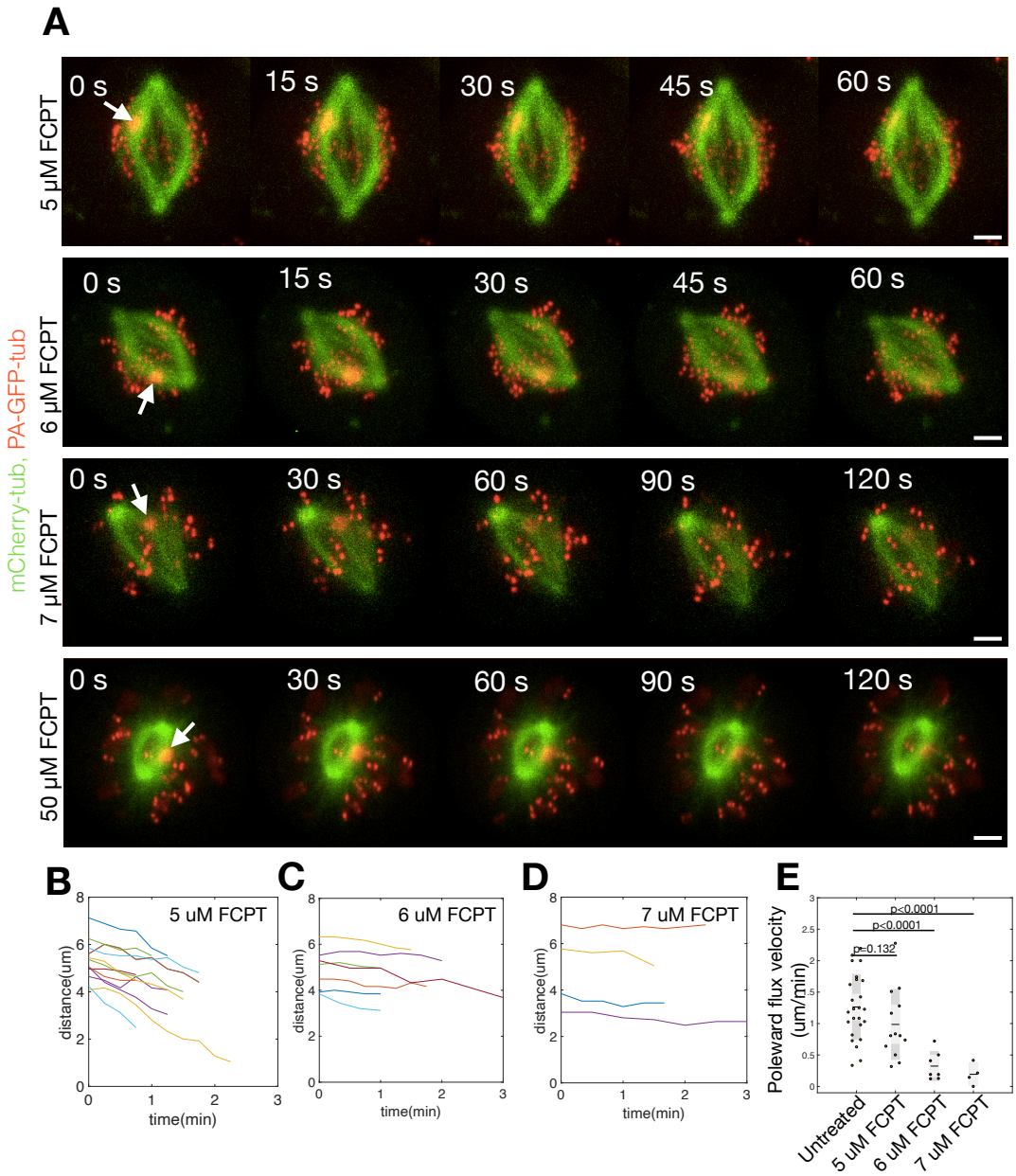

Figure 27. Inhibition of Eg5 with FCPT strongly affects microtubule poleward flux velocity and spindle morphology. A) Prometaphase U2OS cell expressing mCherry-tubulin (green) and photoactivatable GFP-tubulin (red) imaged live after the addition of FCPT, with photoactivated tubulin marks (red). The cells are treated during NEBD with FCPT in following concentrations: 5 µM (first row), 6 µM (second row), 7 µM (third row) and 50 µM (fourth row); scalebar represents 2 µm. B-D) The trajectories of the photoactivated tubulin spot approaching the spindle pole after the treatment with 5 µM, 6 µM, 7 µM FCPT respectively. E) Poleward flux velocity in untreated and FCPT treated prometaphase cells.

4.1.5. Kinesin-12 inhibition doesn't impact the prometaphase poleward flux velocity

Kinesin-12 Kif15 has a redundant role with Eg5 in maintaining spindle polarity, probably by targeting k-fiber bundles (Drechsler et al., 2014; Sturgill et al., 2014; Tanenbaum et al., 2009). To investigate the impact of kinesin-12 (Kif15) on microtubule poleward flux during prometaphase, I have treated the U2OS cells expressing mCherry-tubulin and photoactivatable GFP-tubulin with Kif15-IN-1, inhibitor of Kif15. I have added 20 μM Kif15-IN-1 on the cells during NEBD, imaged the cells every ten s during the spindle formation and photoactivated microtubule fibers during prometaphase (**Figure 28, A, upper panel**). The average prometaphase poleward flux velocity after Kif15 inhibition was 1.065 ± 0.164 μm/min (9 fibers in 8 cells), not significantly different from prometaphase poleward flux in untreated cells ($p = 0.322$) (**Figure 28, B**).

I have conducted the same photoactivation experiments with Kif15 inhibition on metaphase spindles (**Figure 28, A, lower panel**). The average metaphase poleward flux velocity after Kif15 inhibition is 0.369 ± 0.084 μm/min (6 fibers in 6 cells), slower than in untreated metaphase spindles ($p = 0.0152$; **Figure 28, C**). Pole to pole spindle contour length in prometaphase (16.702 ± 0.791 μm, $p = 0.597$) and metaphase was as in untreated cells (16.659 ± 0.550 μm, $p = 0.427$). Thus, those results indicate that kinesin-12 is involved in the mechanism of poleward flux in metaphase, but not in prometaphase.

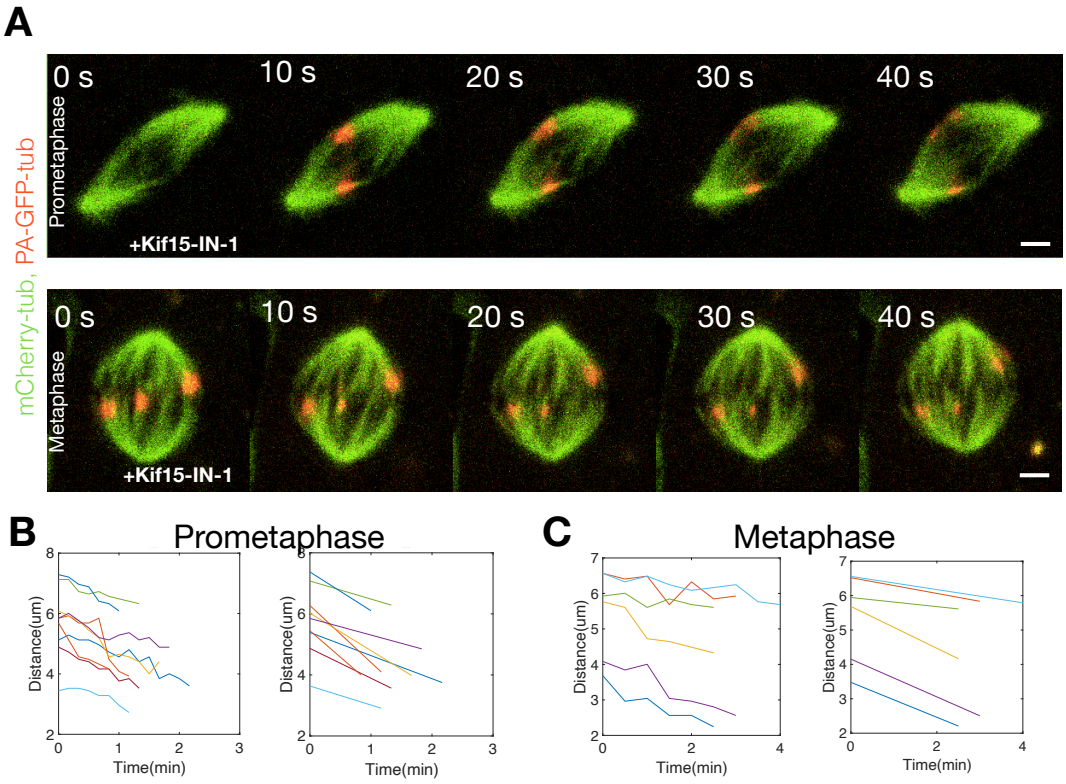

Figure 28. Inhibition of Kif15 doesn't impact poleward flux in prometaphase, but slightly contributes to metaphase flux. A) Prometaphase (upper panel) and metaphase (bottom panel) U2OS cell expressing mCherry-tubulin (green) and photoactivatable GFP-tubulin (red) imaged live after the addition of Kif15-IN-1, with photoactivated tubulin marks (red); scalebar represents 2 μm. B) The trajectories of the photoactivated tubulin spot approaching the spindle pole (left) and the linear fit on those trajectories (right) C) same as in B) but for metaphase cells.

4.1.6. Inhibition of HSET by CW069 slows down the prometaphase and metaphase poleward flux

The main antagonist of sliding the antiparallel microtubules apart is HSET (Mountain et al., 1999). It has opposite directionality because it pushes the plus ends apart, focusing the minus ends (reviewed in (She & Yang, 2017). To investigate the impact of HSET on microtubule poleward flux during prometaphase, I have treated the U2OS cells expressing mCherry-tubulin and photoactivatable GFP-tubulin with CW069, an allosteric inhibitor of HSET (Watts et al., 2013). I have added 200 μM CW069 on the cells during NEBD, imaged the cells

every ten s during the spindle formation and photoactivated microtubule fibers in prometaphase (**Figure 29, A, upper panel**). The average prometaphase poleward flux velocity after HSET inhibition is 0.878 ± 0.091 μm/min (23 fibers in 23 cells), suggesting that HSET contributes significantly to the poleward flux in prometaphase ($p = 0.0070$, **Figure 29, B, C, D**).

Also, I have conducted the same photoactivation experiments with HSET inhibition on metaphase spindles, imaging them every 30 s (**Figure 29, A, lower panel**). The average metaphase poleward flux velocity after HSET inhibition is 0.27 ± 0.055 μm/min (11 fibers in 10 cells), suggesting that HSET has also a role in the poleward flux in metaphase ($p < 0.0001$; **Figure 29, E,F,G**), as shown previously for metaphase cells (Steblyanko et al., 2020).

The HSET-inhibited spindles often formed tubulin asters near the poles and were unable to focus them into poles, confirming the role of HSET as pole focusing minus end directed kinesin (**Figure 29, H**). Intriguingly, during prometaphase the pole-to-pole contour length of the spindles was transiently longer, 18.005 ± 0.719 μm (23 spindles, $p = 0.0372$), but it shortened in metaphase more than in the untreated spindles (CW069 treated: 14.249 ± 0.359 μm, control: 15.959 ± 0.377 μm, $p = 0.0128$; **Figure 29, I**), as shown previously for metaphase spindles (Cai et al., 2009).

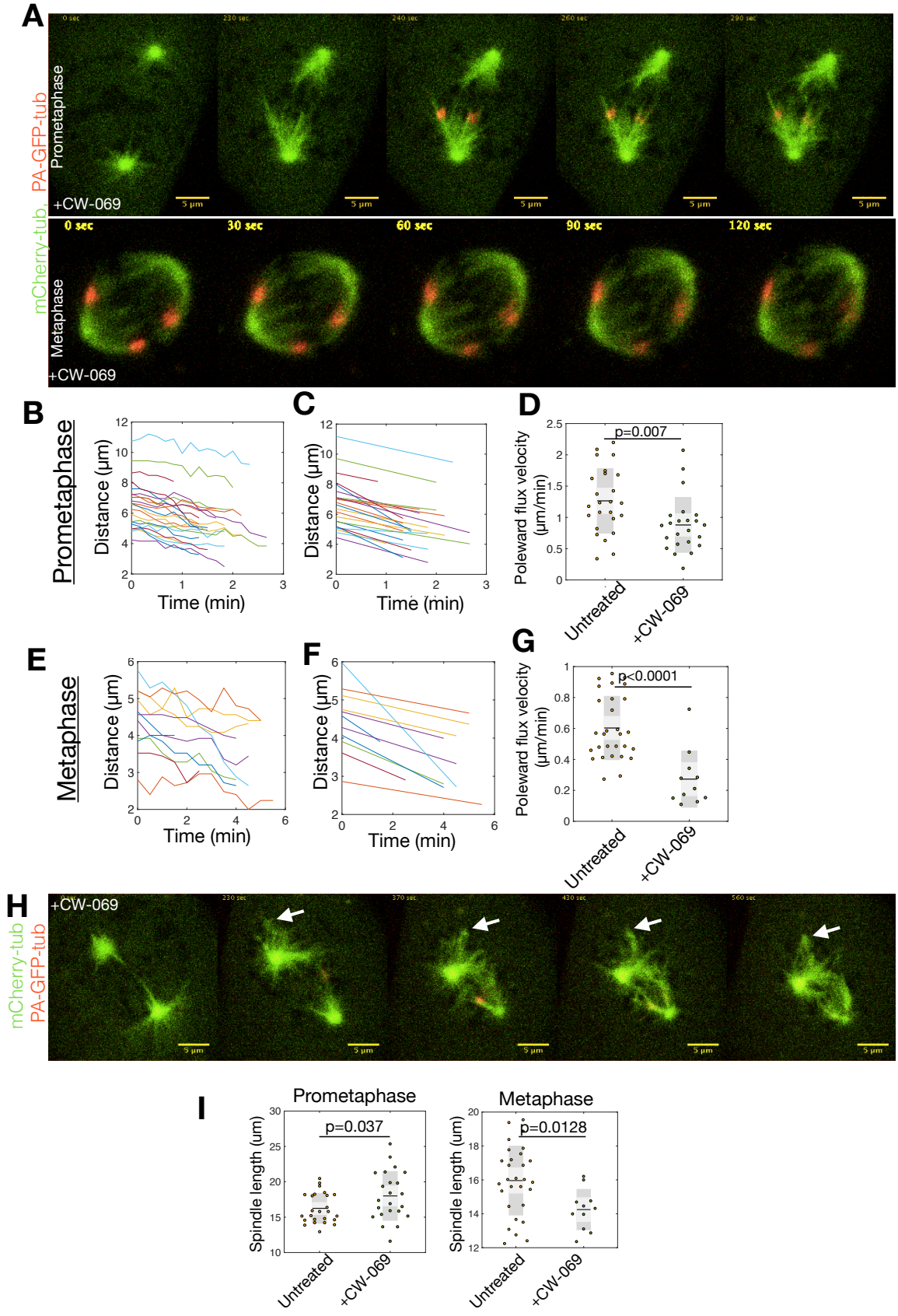

Figure 29. Inhibition of HSET strongly impacts poleward flux in prometaphase and metaphase. A) Prometaphase (upper panel) and metaphase (bottom panel) U2OS cell

expressing mCherry-tubulin (green) and photoactivatable GFP-tubulin (red) imaged live after the addition of CW069, with photoactivated tubulin marks (red). B) The trajectories of the photoactivated tubulin spot approaching the spindle pole. C) linear fit on trajectories from B. D) Poleward flux velocity in untreated and CW069 treated prometaphase cells. E-G) same as in B-D) but for metaphase cells. H) The U2OS cell as in A) with the tubulin asters (white arrow) unable to focus into the pole. I) Pole to pole microtubule contour length in prometaphase (left) and metaphase (right) spindles from untreated and CW069 treated spindles.

4.1.7. Photoactivation experiments indicate the existence of k-fibers and long antiparallel overlaps in prometaphase spindles

Besides for measurement of poleward flux speed, photoactivation assay can indicate the existence of different classes of microtubules. When I used the photoactivation assay near the equatorial plane, I often noticed the photoactivated spot splitting in two, as similarly shown in Steblyanko et al., 2020. They moved away from each other towards the opposite spindle poles (**Figure 30, A**) meaning that prometaphase spindles contain antiparallel microtubule overlaps. I have made signal intensity profiles along the photoactivated bundles and tracked the movement of intensity maxima of the photoactivated tubulin (**Figure 30, B**). I have marked the increasing distance between the separating signals (d1, d2 in **Figure 30, C**) and calculated the velocity of their separation. The photoactivated spots moved away from each other with the velocity of 3.47 ± 0.149 μm/min (22 separation events from 19 cells). This fast antiparallel sliding velocity reflects the fast poleward flux of non-kinetochore fibers in prometaphase (**Figure 30, D**).

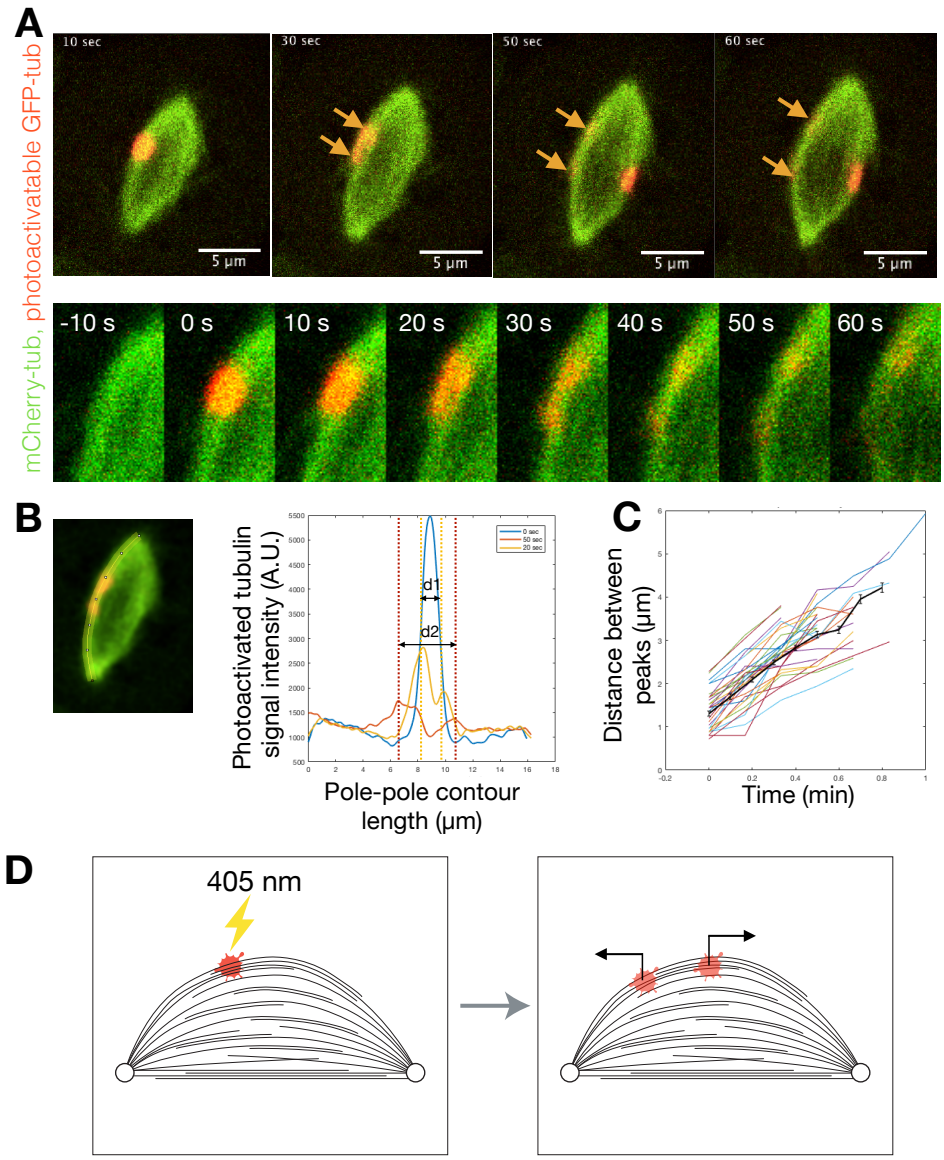

Figure 30. Prometaphase spindles have long antiparallel overlaps. A) Prometaphase spindle of U2OS cell expressing mCherry-tubulin (green) and photoactivatable GFP-tubulin (red) imaged live during prometaphase. The red dot represents the photoactivated tubulin on the prometaphase spindle with the arrows pointing to the moving spots (top). Enlarged area of the spindle from the top panel showing photoactivated signal separation and their movement towards the opposite poles. B) Demonstration how the tracking of the photoactivated spot was made on the spindle in A). The image was blurred to achieve the better definition of intensity maxima of the photoactivated spots. The intensity profile (yellow line) is taken every time frame from pole to pole across the photoactivated microtubule bundle (left). The distances between the intensity maxima are marked d1, d2, (right). C) The increasing distance between two photoactivated maxima over time. D) Schematic representation of antiparallel

microtubule sliding seen as the splitting of the photoactivated spot (red dots) towards the opposite spindle poles (black arrows). Lightning bolt represents photoactivation.

When I photoactivated the microtubules near the pole, I reason that the most of the signal consisted of k-fibers. Those fibers show length dependent poleward flux velocities, similarly as the k-fibers in metaphase (Risteski et al., 2022) (**Figure 31, A**). Photoactivation near the equator often resulted in splitting of the signal to opposite poles meaning that it consists mainly of antiparallel bridging fibers and their poleward flux velocity is not length dependent (**Figure 31, B**). Interestingly, the average poleward flux of the splitting fibers was faster than the flux of the non-splitting fibers (1.608 ± 0.11 and 1.26 ± 0.10, respectively; p = 0.0182). This suggests that in prometaphase there are two classes of microtubules, kinetochore and non-kinetochore, whose flux velocities differ. To study the prometaphase poleward flux intensely, more precise method for the poleward flux measurement is needed.

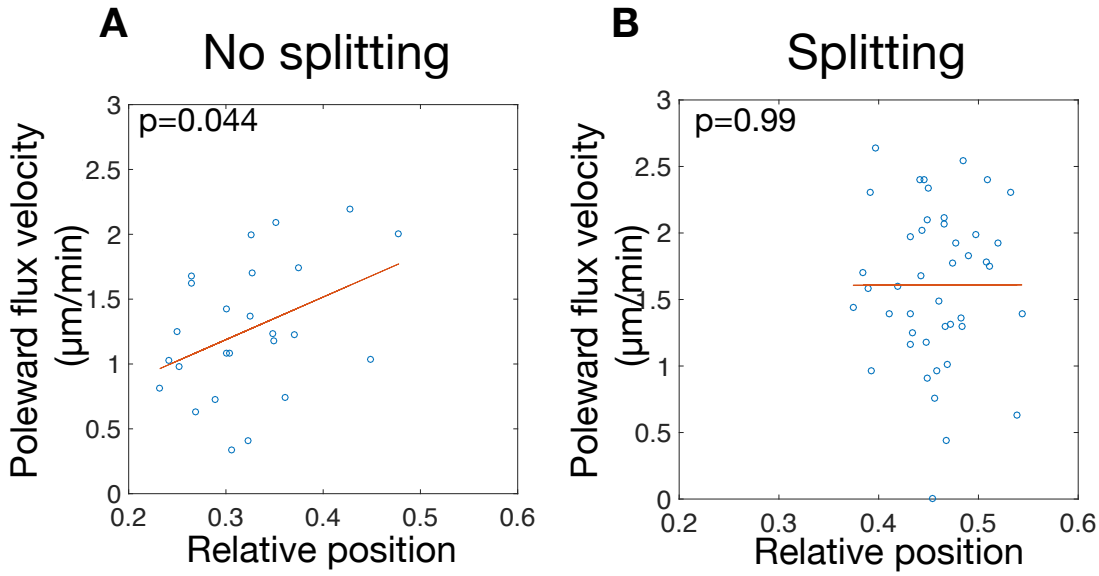

Figure 31. Photoactivation experiments indicate the existence of k-fibers and antiparallel non-kinetochore fibers. The poleward flux velocities plotted to the relative position of the photoactivated spot in the spindle. Zero on the x-axis represents the closer pole, and 0.5 represents the spindle equator. A) Data for the events when photoactivated tubulin didn't show antiparallel splitting; the flux velocities correlate with the relative position of the photoactivated spot. B) Data for the events when photoactivated tubulin showed antiparallel splitting; no correlation between flux velocities and relative position of the photoactivated spot.

4.2. Speckle microscopy assay to distinguish the prometaphase poleward flux of kinetochore fibers and bridging fibers

Tubulin photoactivation assay was so far the most commonly used method for studying poleward flux in mammalian cells. However, a limitation of this method is that all the microtubules inside the illuminated region are photoactivated and it is hard to discriminate the movement of individual microtubules. In order to achieve a deeper understanding of the influence of the spindle proteins on the prometaphase microtubule flux regulation, we must be able to differentiate the movement of individual microtubules within the prometaphase spindle.

I have used our previously developed speckle microscopy assay (Risteski, 2023; Risteski et al., 2022) which enabled me to distinguish between different classes of microtubules, kinetochore and bridging fibers, and to define their microtubule poleward flux movements within the prometaphase spindle (**Figure 32, Figure 33**). I have used human non-cancer immortalized epithelial cell line hTERT-RPE1 (from here on referred to as RPE1) with stable expression of CENP-A-GFP (to determine the sister kinetochore positions) and Centrin1-GFP (to determine spindle poles positions). With the addition of small concentration of fluorescently labelled tubulin dye, 1 nM SiR-tubulin (Lukinavičius et al., 2014), I was able to precisely investigate the existence and movement of speckle-like SiR-tubulin signal within the prometaphase spindles in five s intervals (**Figure 32, Figure 33**).

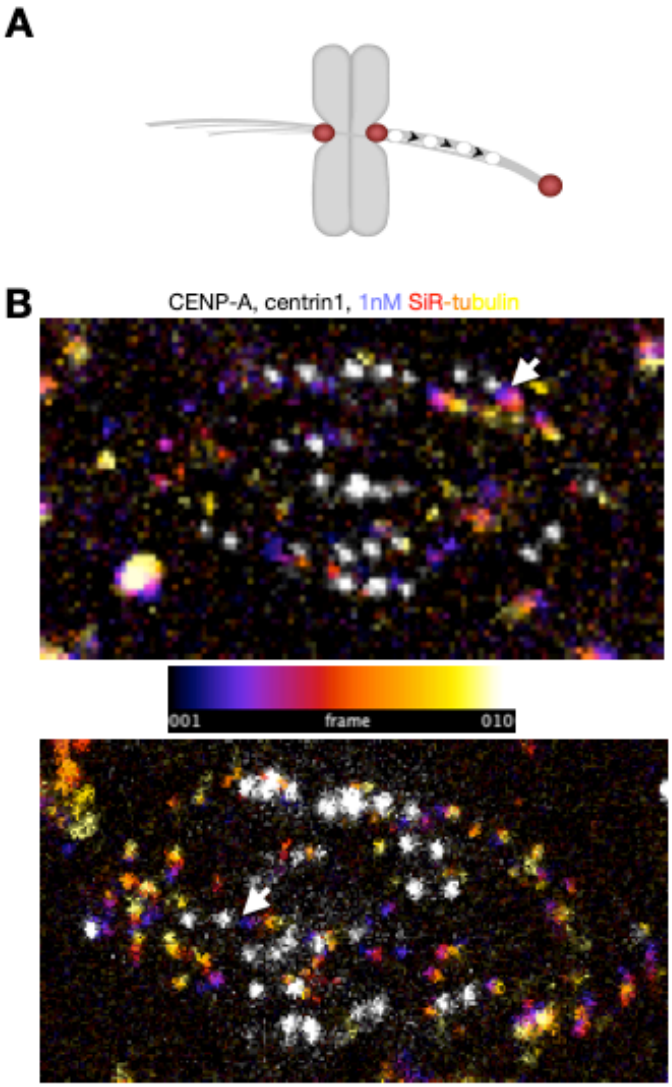

Figure 32. Appearance of prometaphase k-fiber speckles when using speckle microscopy assay. A) Schematic representation of k-fiber speckle (white circle) found on the congressing kinetochore (red circle) fluxing towards the closer pole (red circle right). B) Prometaphase spindle of RPE1 cell with stable expression of CENP-A-GFP (gray) and Centrin1-GFP (gray) with the tubulin speckles (colored) after the addition of 1 nM SiR-tubulin dye (colored). Legend represents temporal color code of ten time-frames; 50 s in total. Top: White arrow represents the k-fiber speckle found on the kinetochore facing the closer pole, fluxing towards that pole. Bottom: White arrow represents the k-fiber speckle found on the kinetochore facing the further pole, fluxing towards that pole.

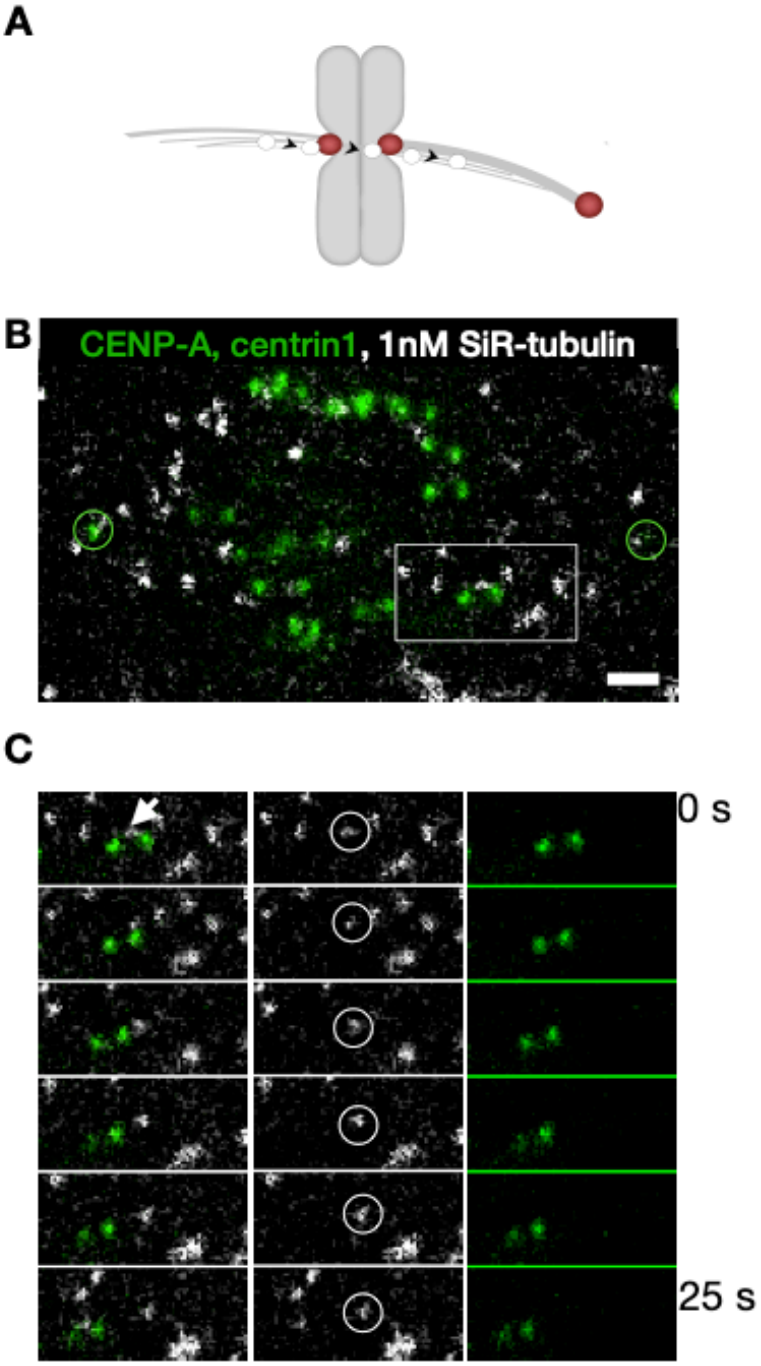

Figure 33. Appearance of prometaphase bridging fiber speckles when using speckle microscopy assay. A) Schematic representation of bridging fiber speckle (white circle) found on the one side of congressing sister kinetochores (red circle), passing the region between them and fluxing towards the closer pole (red circle right). B) Prometaphase spindle of RPE1 cell with stable expression of CENP-A-GFP (green spots) and Centrin1-GFP (green circles) with the tubulin speckles (gray) after the addition of 1 nM SiR-tubulin dye (gray). Scalebar represents 2 μm. C) Inset from B) demonstrating the existence of bridging fiber speckle followed within 25 s time interval.

4.2.1. Prometaphase spindles consist of kinetochore fibers and bridging fibers

With speckle microscopy assay I could observe kinetochore and bridging fiber speckles on both congressing kinetochores and evaluate their movement. The speckles that originate close to a kinetochore, at the pole-facing side, were defined as those on a kinetochore microtubule. The speckles that appear on one side of a pair of sister kinetochores, pass the region between them, and end up on the other side, were defined as those on a bridging microtubule (**Figure 22, Figure 33**). In prometaphase, with respect to the kinetochore pair in congression, I could observe the following speckle types: k-fiber and the bridging fiber that fluxes towards the closer pole; and k-fiber and the bridging fiber that fluxes towards the further pole, in the direction of the congressing chromosome. The fact that those microtubule speckles exist, indicates that prometaphase spindles consist of kinetochore fibers and bridging fibers. Moreover, the appearance of the speckles on both kinetochores of the congressing kinetochore pair implies that the k-fibers begin to form during the prometaphase congression. Also, the presence of the bridging fiber speckles confirmed the observations of splitting signal after photoactivation and the existence of antiparallel sliding in prometaphase.

4.2.2 Prometaphase poleward flux is similar as in metaphase

I tracked individual speckles together with the spindle poles and calculated poleward flux as the change of the speckle-to-pole distance over the first 15 s of their movement (**Figure 34, A, B**). During prometaphase, as in metaphase, k-fibers flux is slower than the bridging fiber flux ($p < 0.0001$; 67 k-fibers and 128 bridging fibers from 81 cells; **Figure 34, C**). Interestingly, I found that the poleward flux velocity is similar in prometaphase and metaphase both for k-fiber ($p = 0.5153$) and bridging fiber ($p = 0.449$). It suggests that prometaphase poleward flux could be generated in similar manner as in metaphase (**Figure 34, D**).

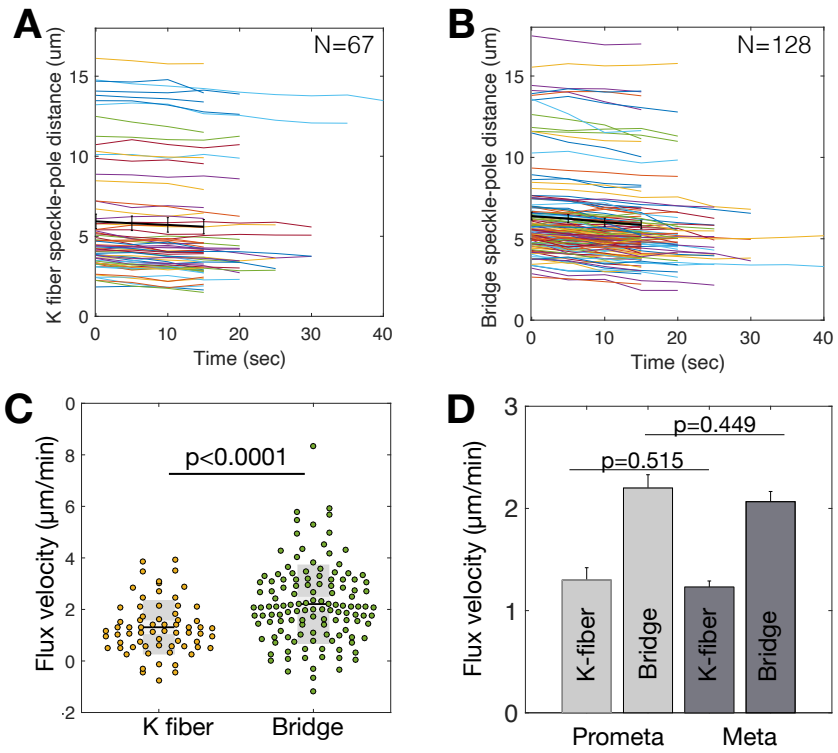

Figure 34. K-fiber and bridging fiber flux in prometaphase. A) Distance from the speckle to the pole in time for k-fiber. B) Same as A but for bridging fibers. Colored lines represent individual tracks; black lines represent mean and SEM. C) Univariate scatter plot of prometaphase k-fiber and bridging fiber speckle velocities corresponding to the poleward flux velocities. D) Poleward flux velocities of k-fibers and bridging fibers in prometaphase (light gray) and metaphase (dark gray).

4.3. The role of mitotic kinesins and crosslinkers in the prometaphase poleward flux

Currently, the newest model for poleward flux in metaphase says that the flux is produced in bridging fibers and transmitted to the kinetochore fibers via antiparallel and parallel crosslinkers (Matos et al., 2009; Risteski et al., 2022; Steblyanko et al., 2020). To test whether this theory stands also for prometaphase, although the evident difference in spindle architecture, I explore the relevance of different spindle proteins to prometaphase poleward flux regulation. I used speckle microscopy assay in prometaphase cells after a set of perturbations in which I depleted candidate microtubule-associated proteins by corresponding siRNA or by applying function inhibitors and inspected the poleward flux velocities of kinetochore- and bridging fibers.

To study the influence of passive crosslinkers on prometaphase poleward flux, I have chosen NuMA and PRC1. NuMA is a candidate because it is required for local load- bearing in the spindle (Elting et al., 2017) and for synchronous microtubule flux across the spindle (Steblyanko et al., 2020). PRC1 is a passive crosslinker which binds preferentially on bridging microtubules (Kajtez et al., 2016; Polak et al., 2017). Also, I have inspected the influence of microtubule nucleation on prometaphase poleward flux by inhibiting the important subunit of the augmin complex, HAUS6 (H6) (Kamasaki et al., 2013). Kinesin-13 members Kif2A and Kif2C were chosen because they are main microtubule minus end depolymerases at the spindle poles (Manning et al., 2007). As the major drivers of polar ejection forces (Drpic et al., 2015) and because of its proposed role in metaphase flux generation (Steblyanko et al., 2020), Kif4A and Kid are chosen to test the involvement of those forces on prometaphase poleward flux. Also, those kinesins are shown to influence the microtubule length which could impact the prometaphase flux velocities (Risteski et al., 2022; Zhu & Jiang, 2005). Protein CENP-E is proposed to be one of the main drivers of the prometaphase poleward flux in cancer cells (Steblyanko et al., 2020) so I chose to test its role on healthy untransformed cells in prometaphase by siRNA depletion and by chemical inhibition with GSK923295 (Bennett et al., 2015). HSET is a minus end directed kinesin which could help driving the poleward flux by focusing the microtubules towards the poles and/or by passively crosslink the parallel microtubules (Cai et al., 2009; She & Yang, 2017). I have demonstrated its role in prometaphase and metaphase poleward flux by photoactivation experiments, but by speckle microscopy I can distinguish between its impact on k-fiber and bridging fiber flux velocities separately.

After the addition of siRNA, I have immunolabelled the prometaphase spindles for the corresponding proteins to confirm the depletion efficiency. All of the protein candidates were visible on prometaphase spindles and the depletion efficiency was mostly sufficient (**Figure 35**). Also, I confirmed the effectiveness of chemical inhibitors by the appearance of phenotypes that are known from the literature (**Figure 36**). After the application of CENP-E inhibitor GSK923295, the CENP-E protein was on the prometaphase spindle, but in different distribution than in untreated prometaphase cells. Less protein signal was detected on the kinetochores and the majority of the protein enriched the area around the spindle poles. It confirms that the inhibitor works as a static inhibitor, preventing the CENP-E protein to slide towards the plus ends of the microtubules. Also, some kinetochores were stacked behind the pole, giving the expected phenotype (Bennett et al., 2015). HSET inhibitor CW069 caused the

protein to accumulate at the area around the poles and a slight defocusing of the pole area could be observed (Watts et al., 2013) (**Figure 36**).

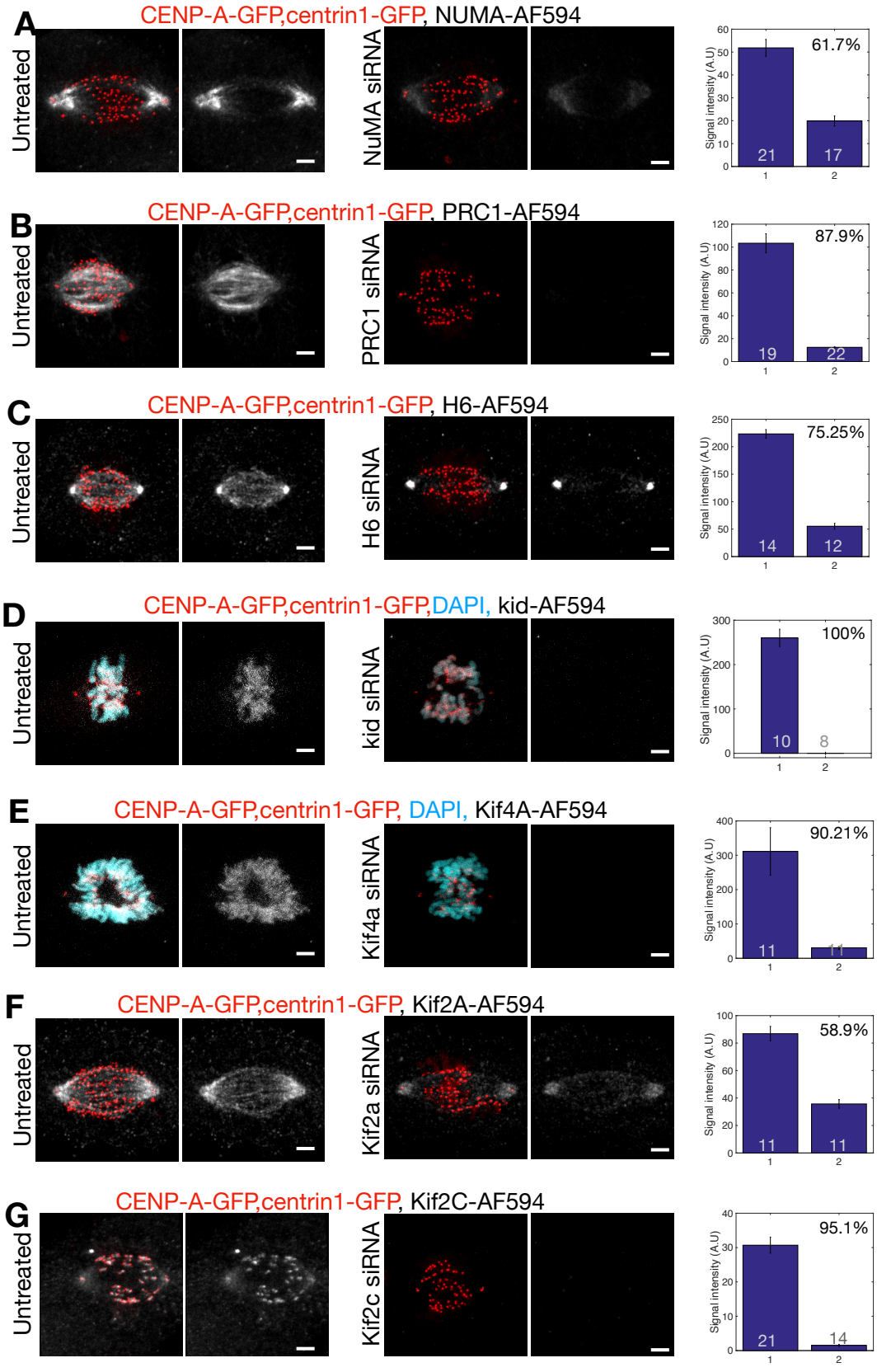

Figure 35. Depletion efficiency of siRNA treatments targeting spindle proteins. A)-G) Fixed spindles in RPE1 cell line stably expressing CENP-A-GFP (red) and centrin1-GFP (red) in cells immunostained for A) NuMA (AF-594, gray), B) PRC1 (AF-594, gray), C) H6 (AF-594, gray), D) kid (AF-594, gray), E) Kif4A (AF-594, gray), F) Kif2A (AF-594, gray) and G) Kif2C (AF-594, gray) in untreated (left) and corresponding siRNA-treated cells (right), with DNA stained with DAPI (blue) in D) and E). Left: merge; right: protein of interest (gray). Graphs showing intensities of indicated proteins in untreated and siRNA treated cells are given on the right. The number in the upper right corner denotes depletion percentage. Legend: 1-untreated, 2-siRNA treated prometaphase cells. All treatments include at least two independent experiments. Gray numbers in the bars represent number of cells. Scale bars; 2 μm. All images are maximum intensity projections of five z-planes. The intensities of the proteins of interest are adjusted to be the same in untreated and siRNA-treated cells.

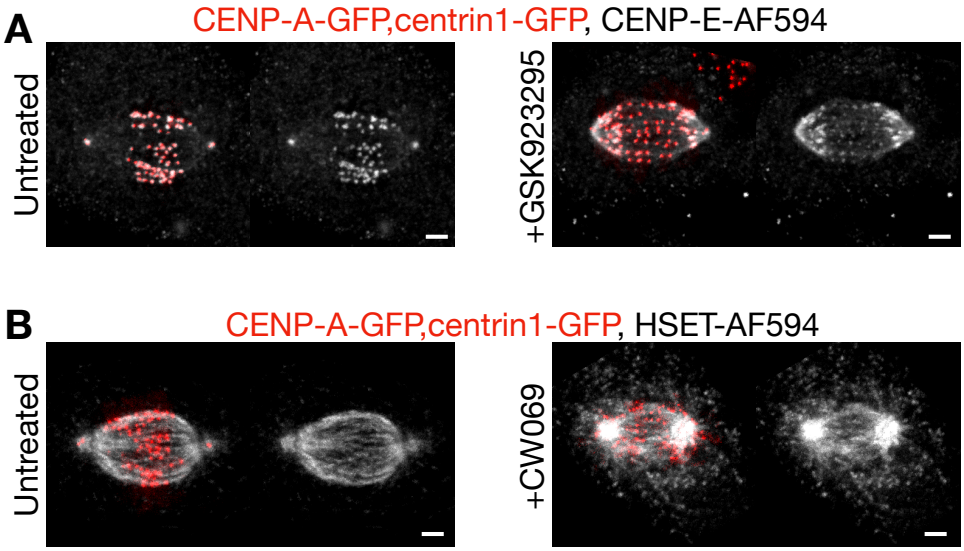

Figure 36. Localization of spindle proteins after chemical inhibition. A) and B) Fixed spindles in RPE1 cell line stably expressing CENP-A-GFP (red) and centrin1-GFP (red) in cells immunostained for A) CENP-E (AF-594, gray) and B) HSET (AF-594, gray) in untreated (left) and A) GSK923295 or B) CW069 treated cells (right). Left: merge; right: protein of interest (gray). Scale bars; 2 μm. All images are maximum intensity projections of five z-planes. The intensities of the proteins of interest are adjusted to be the same in untreated cells or cells treated with chemical inhibitors.

4.3.1. Influence of kinesins and passive crosslinkers on bridging fiber flux in prometaphase

With speckle microscopy assay, as in untreated cells, in all treatments both k-fiber and bridging fiber speckles could be observed (**Figures, 37-40**). The impact on bridging fiber flux velocities was observed for kinesins CENP-E and HSET, and for H6 (**Figure 37; Figure 38**). The CENPE effect on bridging fibers poleward flux was confirmed both after RNAi ($p = 0.0262$) and chemical inhibitor application ($p = 0.023$). The lowest bridging fiber velocities were observed after inhibiting the function of HSET ($p = 0.0061$). H6 depletion perturbed the nucleation of the bridging fibers which caused the fibers to flux slower ($p = 0.0075$), probably because they were thinner (Štimac et al., 2022) with insufficient motor proteins to slide in antiparallel overlaps. Depletion of passive crosslinkers NuMA and PRC1 showed no altered bridging fiber velocities ($p = 0.705$; $p = 0.989$, respectively). PRC1 depletion by siRNA perturbs the number of microtubules in the bridging fibers by approximately 50 % (Jagrić et al., 2021), that is to a lesser extent than H6 depletion (Štimac et al., 2022). This means that there are still enough microtubules in the fibers which are sufficient for the motor proteins to still produce enough force to power bridging fiber flux. Notably, neither Kif4A nor Kid or the kinesins from the kinesin-13 family showed any alterations in bridging fiber flux (**Figure 37; Figure 38**).

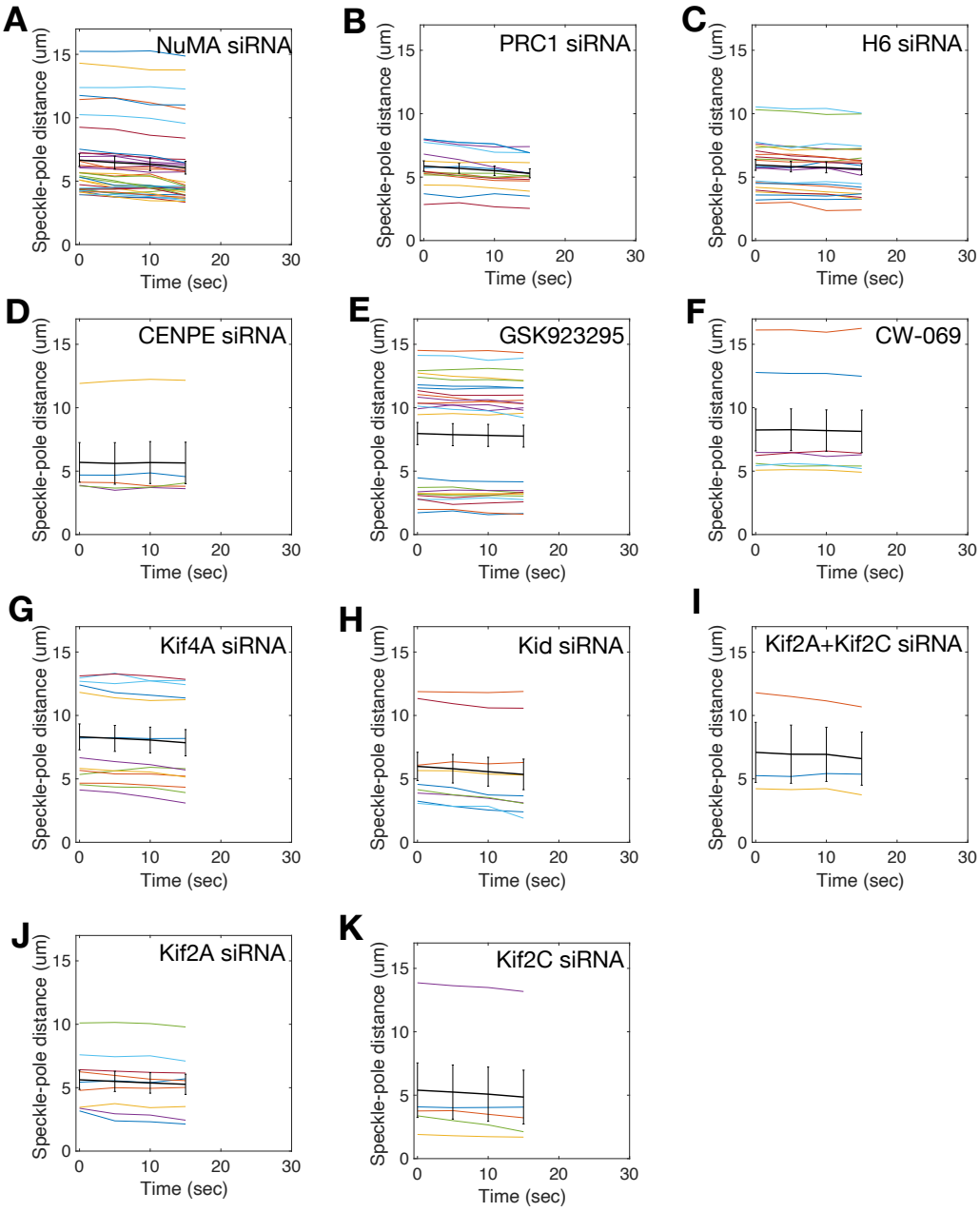

Figure 37. Tracks of bridging fiber speckles after various treatments in prometaphase spindles. A-K) Graphs showing the distance between prometaphase bridging fiber speckles and pole in time. Colored lines represent individual tracks; black lines represent mean and SEM. Various treatments are indicated in the upper right corner of the graphs.

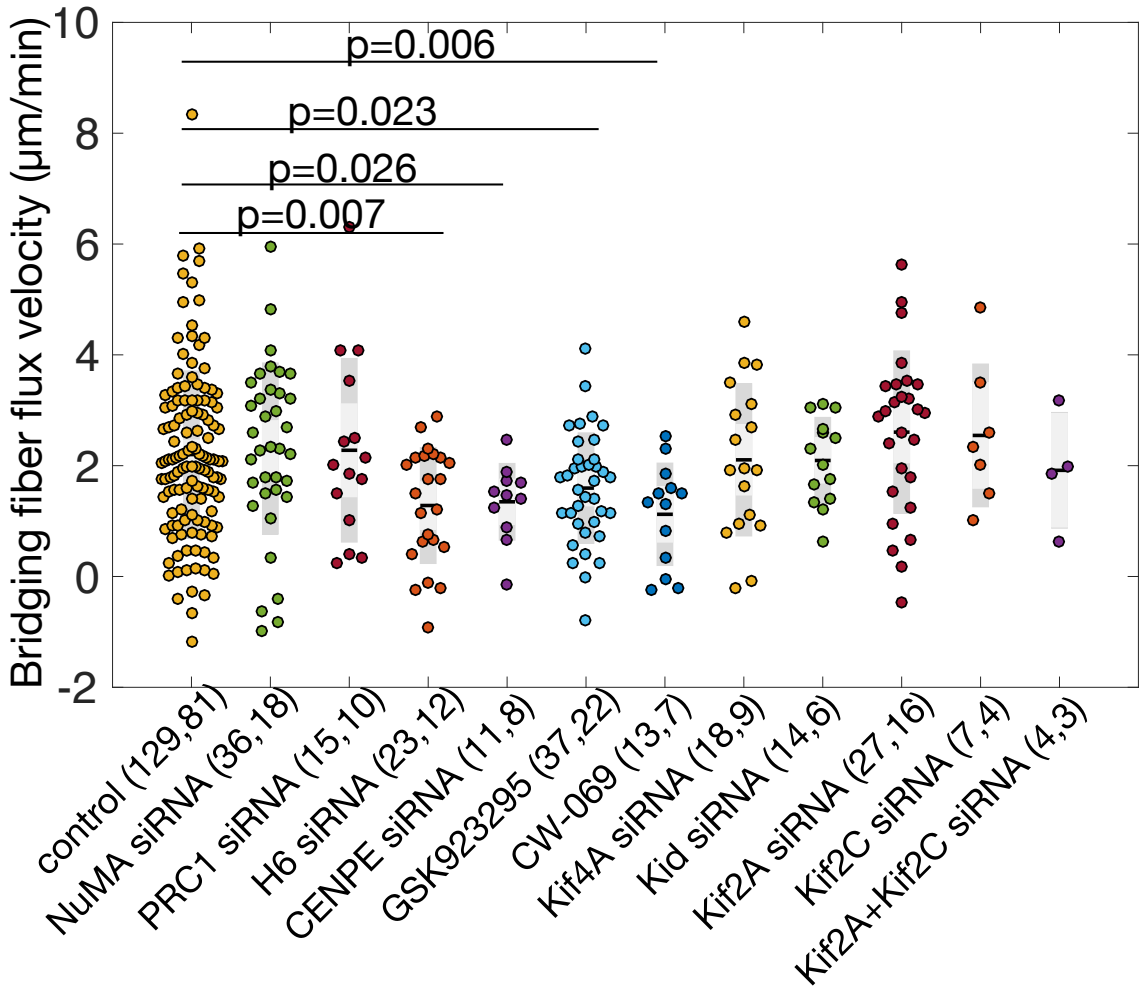

Figure 38. CENP-E, HSET and H6 impact the bridging fiber velocity in prometaphase RPE1 cells. Univariate scatter plot of bridging fiber velocities after different siRNA depletion or chemical inhibition of various spindle proteins. Boxes represent standard deviation (dark grey), 95% standard error of the mean (light grey) and mean value (black) for indicated conditions. Numbers in the brackets correspond to the number of speckles and cells, respectively. Statistics: t test.

4.3.2. Influence of kinesins and passive crosslinkers on k-fiber flux in prometaphase

I used the same assay to inspect the kinesins and passive crosslinkers in prometaphase k-fiber involvement (**Figure 39; Figure 40**). In treatments with slower bridging fiber flux due to H6, CENP-E or HSET depletion, k-fiber flux velocities were also reduced (H6 depletion p = 0.034; CENP-E depletion p = 0.014; CENP-E inhibition p = 0.046; HSET inhibition p = 0.043), suggesting that these proteins affect antiparallel sliding and consequently k-fiber

sliding, consistent with the proposed model for metaphase poleward flux (Risteski et al., 2022). Additionally, Kif4A, Kid, and NuMA depletions showed also altered k-fiber flux.

The sliding forces from the bridging fiber are transmitted to the k-fibers not only through the antiparallel overlaps but also through the zones of parallel microtubule overlaps. The passive crosslinkers link together the bridging and kinetochore microtubules encompassing the same spindle half. Thus, reducing the number of passive crosslinkers should result in reduced force that is transmitted from the bridging to the k-fibers and consequently in a slower k-fiber flux, as proposed for metaphase spindles (Risteski et al., 2022). Indeed, after the depletion of NuMA, prometaphase k-fiber flux was reduced ($p = 0.0132$), as shown previously in metaphase cells. PRC1 didn't show any alterations of k-fiber flux probably because it is mainly localized in bridging fibers, but it doesn't impact the bridging fiber flux and thus no alterations in k-fiber flux couldn't be observed, similarly shown previously (Steblyanko et al., 2020).

Interestingly, Kif4a and Kid altered k-fiber flux in a way that it increased to the values of bridging fiber velocities ($p = 0.0176$; $p = 0.0034$). This is consistent with the effects observed in metaphase (Risteski et al., 2022). Those proteins impact the microtubule length, and its depletion causes longer antiparallel overlaps so more bridging fiber force is being transmitted to k-fibers, making them fast as the bridging fibers. As for bridging fiber flux, neither of the major depolymerases showed an impact on k-fiber flux.

Taken all together, the flux of bridging fibers was faster than or equal to the flux of k-fibers across the treatments, suggesting that the bridging fiber flux drives the k-fiber flux, as proposed for the spindles in metaphase (**Figure 41**).

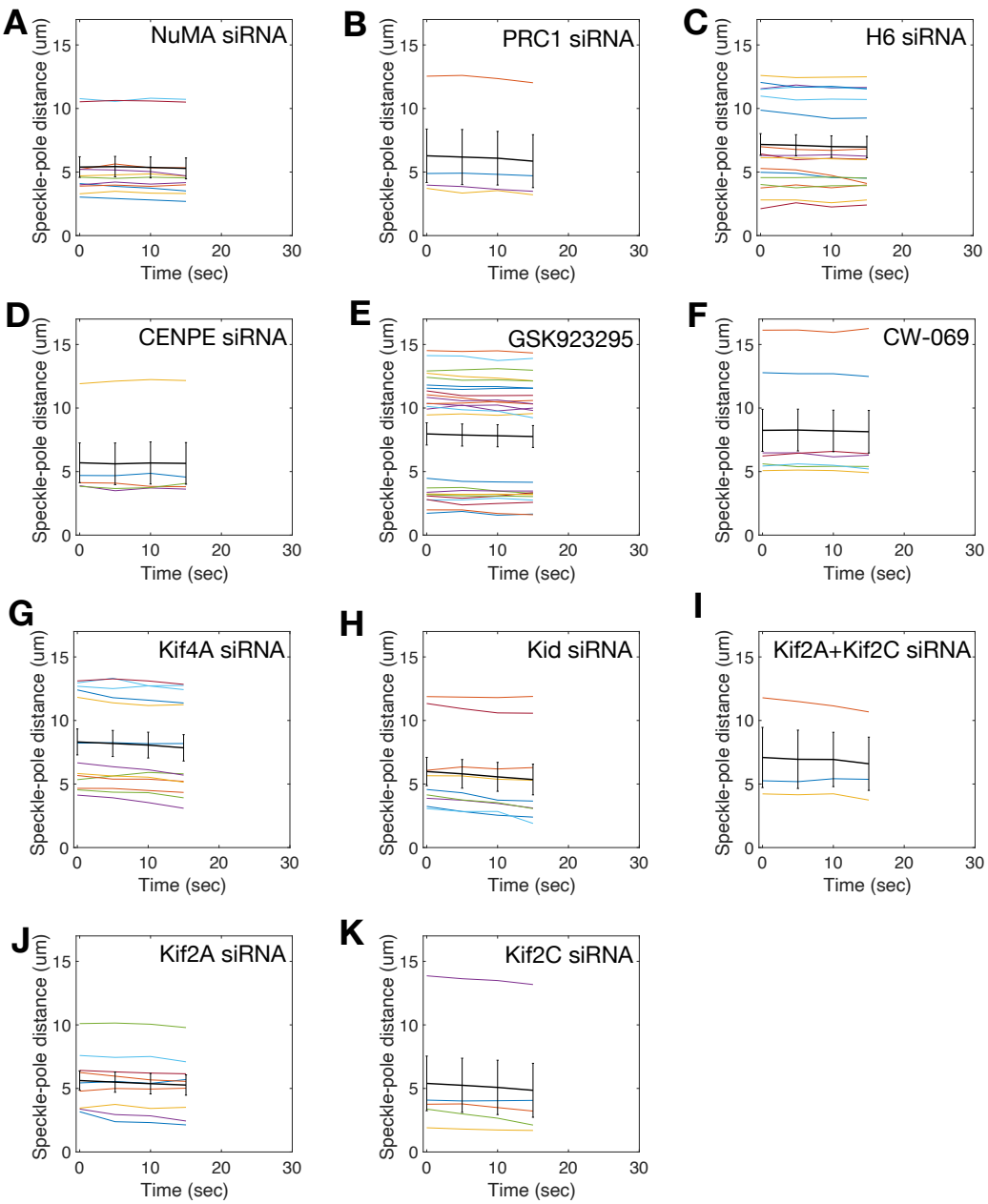

Figure 39. Tracks of kinetochore fiber speckles after various treatments in prometaphase spindles. A-K) Graphs showing the distance between prometaphase kinetochore fiber speckles and pole in time. Colored lines represent individual tracks; black lines represent mean and SEM. Various treatments are indicated in the upper right corner of the graphs.

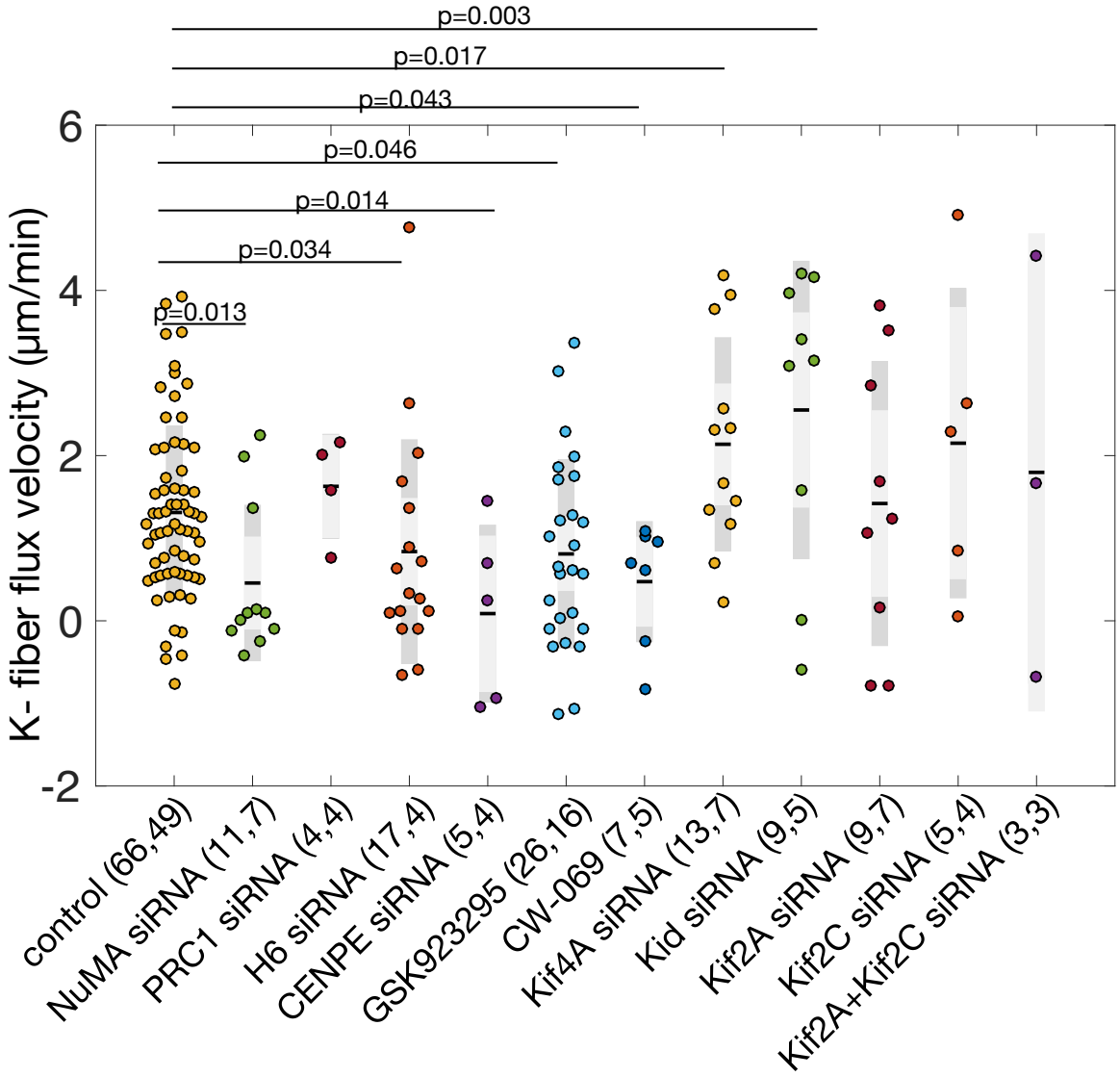

Figure 40. NuMA, CENP-E, HSET, H6 and chromokinesins impact the kinetochore fiber flux velocity in prometaphase RPE1 cells. Univariate scatter plot of kinetochore fiber velocities after different siRNA depletion or chemical inhibition of various spindle proteins. Boxes represent standard deviation (dark grey), 95% standard error of the mean (light grey) and mean value (black) for indicated conditions. Numbers in the brackets correspond to the number of speckles and cells, respectively. Statistics: t test.

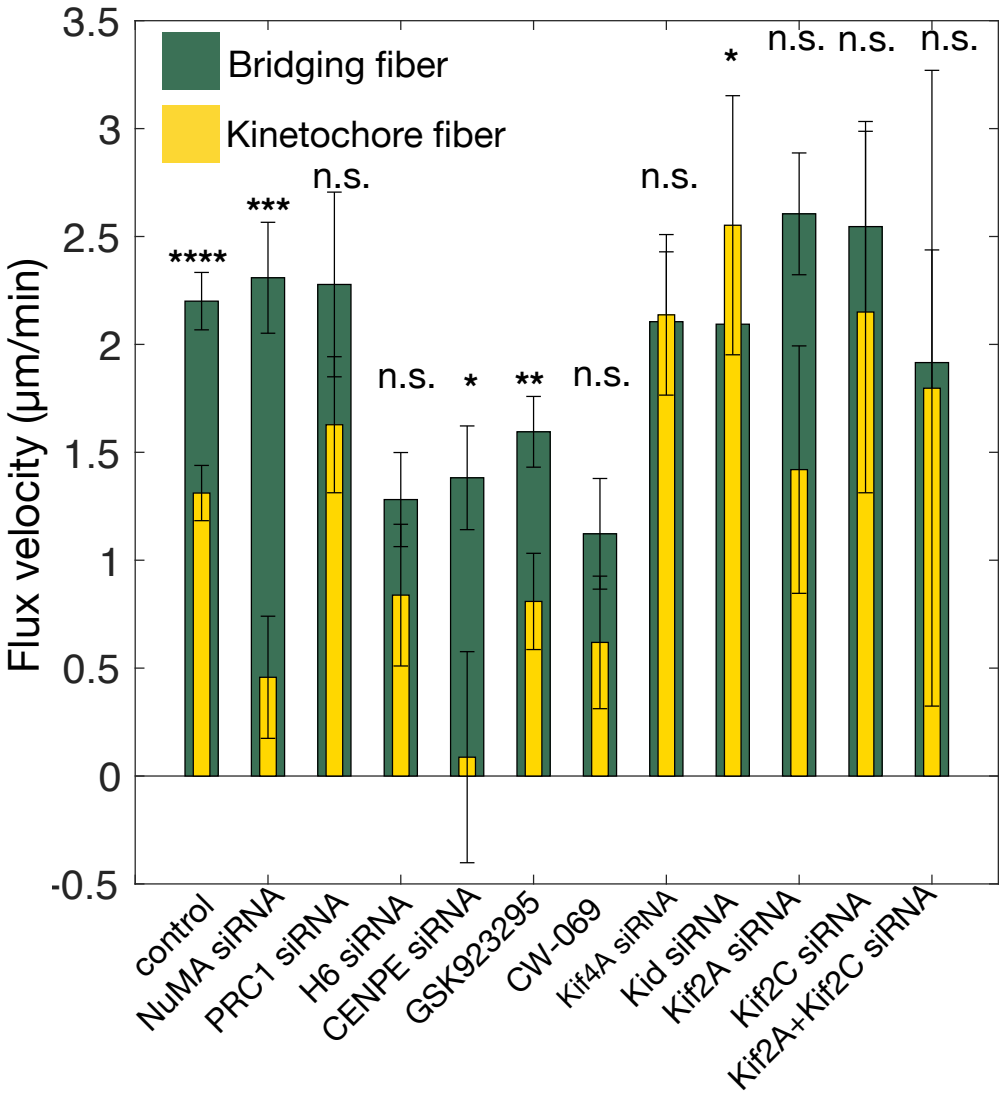

Figure 41. Flux of bridging fibers is faster than or equal to the flux of k-fibers across various treatments. Bar graph showing k-fiber (yellow) and bridging fiber (green) poleward flux velocities after individual treatments of spindle proteins in prometaphase.

4.4. Congressing kinetochores are asymmetrically bioriented

4.4.1. Mad2 is present on both kinetochores but decreases firstly from the closer kinetochore

The main goal of prometaphase is to congress the kinetochores to the spindle midplane to ensure proper alignment and segregation. To analyze the impact of poleward flux on the congressing kinetochores, I have firstly inspected the prometaphase spindle architecture and the nature of kinetochore attachments during the kinetochore congression. I have focused on

the kinetochores that are on the mitotic spindle in the region between the centrosomes and the spindle equator.

To investigate the nature of microtubule-kinetochore attachments of congressing kinetochores, I inspected the presence of Mad2 signal on those kinetochores. Mad2 is a part of spindle assembly checkpoint (SAC) machinery whose task is to prevent anaphase onset before all the kinetochores are attached properly to the spindle microtubules (Maldonado & Kapoor, 2011). It is enriched on the kinetochores in early mitosis, and dissociates from them as the proper microtubule end-on attachments appear (Kuhn & Dumont, 2019).

I immunostained RPE-1 cells stably expressing Ruby-Mad2 and CENP-A-Cerulean with anti-tubulin antibody and imaged prometaphase spindles (**Figure 42, A**). I measured Mad2 signal intensity at both sister kinetochores, and tracked their position within the spindle. Mad2 signal was present on both kinetochores, and it decreased gradually with respect to the relative position of the kinetochore pairs in the spindle as the kinetochores approached the spindle equatorial plane ($n = 50$ kinetochore pairs in 17 cells, $p = 0.0071$ for closer kinetochore; $p = 0.0212$ for further kinetochore), but firstly from the kinetochore facing the closer pole ($p = 0.0149$) (**Figure 42, B and C**). Also, as Mad2 signal decreased, interkinetochore distance increased ($p = 6.584 \times 10^{-5}$, $R^2 = 0.2848$; **Figure 42, D**). Mad2 signal intensity did not depend on the spindle length ($p = 0.625$, $R^2 = 0.0050$; **Figure 42, E**) or the position of the kinetochores with respect to the spindle long axis ($p = 0.556$, $R^2 = 0.007$; **Figure 42, F**). To summarize, the presence of Mad2 signal on the congressing kinetochores indicates that they don't have completely mature end-on attachments, but they do appear gradually and firstly on the kinetochore facing the closer pole.

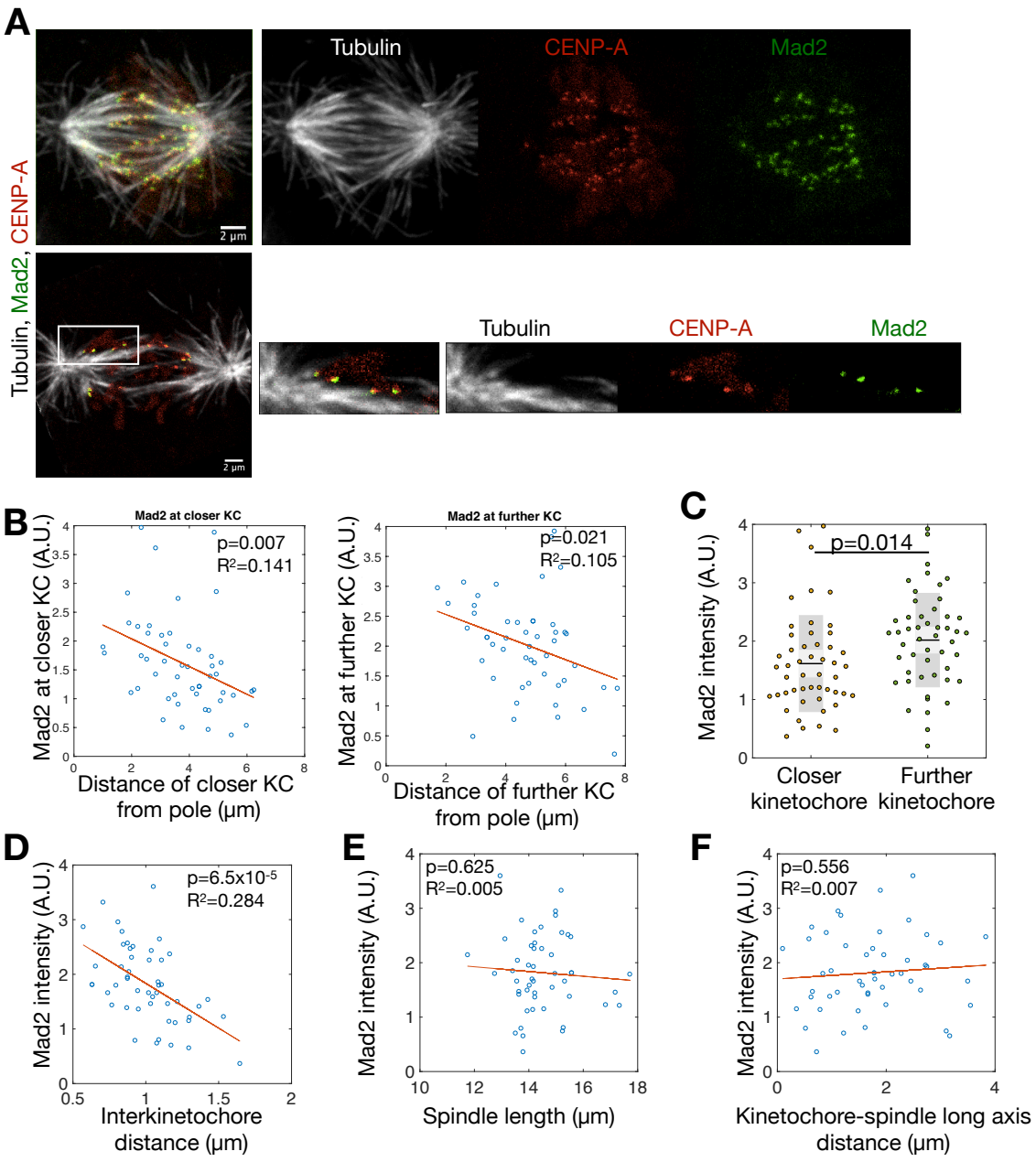

Figure 42. Mad2 is present on both kinetochores but decreases firstly from the closer kinetochore. A) Two prometaphase spindles (top and bottom) of RPE1 cells stably expressing Ruby-Mad2 (green) and CENP-A-Cerulean (red) immunostained with anti-tubulin antibody (grey). Insets (bottom) show slightly lower Mad2 intensities on the kinetochore facing the closer pole; B) Mad2 signal intensity on closer (left) and further (right) congressing kinetochore with respect to their distance from the closer pole. C) Average Mad2 signal intensity on closer and further prometaphase kinetochores. D) Mad2 signal intensity on congressing kinetochore pairs with respect to their interkinetochore distance. E) Mad2 signal intensity on congressing kinetochore pairs with respect to spindle length. F) Mad2 signal

intensity on congressing kinetochore pairs with respect to their distance from the spindle long axis.

4.4.2. Microtubules reach to both congressing kinetochores in 3:1 ratio

To further explore the probability of microtubule end-on attachments on the kinetochores during the congression, I used RPE1 cells with stable expression of CENP-A-GFP and imaged the immunostained tubulin fibers in prometaphase spindles with superresolution STED microscopy (**Figure 43, A**). I focused on the kinetochores that are on the mitotic spindle in the region between the centrosomes and the spindle equator. I revealed that both sister kinetochores have microtubules that end at the outer part of the kinetochore and thus I conclude that those are the k-fibers. Also, there are microtubule bundles that span between sister kinetochores and I speculate that those are the bridging fibers. To inspect the k-fibers in more detail, I have measured tubulin signal intensity in a small square region at the pole-site of sister kinetochore (see Methods, **Figure 43, B**). The tubulin signal intensity of the fibers connected to the sister kinetochore facing the closer pole was three times higher than the intensity of the fibers from the kinetochore facing the further pole (30 kinetochore pairs from four cells, $p < 0.0001$).

To study the microtubule end-on attachments during live prometaphase, I have used U2OS cells with stable expression of GFP-EB3 and mCherry-CENP-A (**Figure 43, C**). EB3 is a protein that tracks growing microtubule plus-ends, and can recruit various proteins responsible for microtubule plus-end stability, reviewed in (Akhmanova & Steinmetz, 2008). I have inspected if EB3 comets can reach from both poles (closer and further) to both kinetochores (facing the closer or further pole) during the congression. First, I have made one image of the whole spindle to see that it is in prometaphase, and then I used fast live cell imaging of the small area of the spindle to precisely track EB3 comets and congressing kinetochores (**Figure 43, C**). During the imaging I could track the EB3 comets on average for 2.478 ± 0.162 μm (15 kinetochore pairs from 11 cells) and they were always coming from the direction of the pole meaning that those microtubules are not short nor generated on the kinetochore.

By tracking the EB3 comets, I observed that they can reach to both kinetochores. I have counted 2.04 ± 0.041 EB3 comets per minute reaching the closer kinetochore from the closer

pole, and 0.62 ± 0.076 EB3 comets per minute reaching the further kinetochore from the further pole giving the 3:1 ratio favouring the closer kinetochore (15 kinetochore pairs from 11 cells, $p < 0.0001$, **Figure 43, D and E**). For comparison, during metaphase, I have counted 2.75 ± 0.054 EB3 comets per minute reaching the closer kinetochore from the closer pole, and 2.37 ± 0.058 EB3 comets per minute reaching the further kinetochore from the further pole (12 kinetochore pairs from 9 cells) giving roughly equal microtubule ratio on both kinetochores.

Interestingly, as the comets approached the congressing kinetochores, they didn't disappear immediately, but stayed on the kinetochore for a few seconds. I have tracked the kinetochore position in time to calculate their velocity. I have compared average control kinetochore velocity calculated every ten timeframes and the kinetochore velocity during the EB3 comet hit (**Figure 43, F**). Average congression velocity was 1.09 ± 0.34 μm/min, and it increased during the EB3-kinetochore hit to 2.92 ± 0.79 μm/min ($p = 0.0033$). This could imply that the microtubule polymerization on the kinetochore facing the closer pole could to some extent help the kinetochores to move towards the spindle equator.

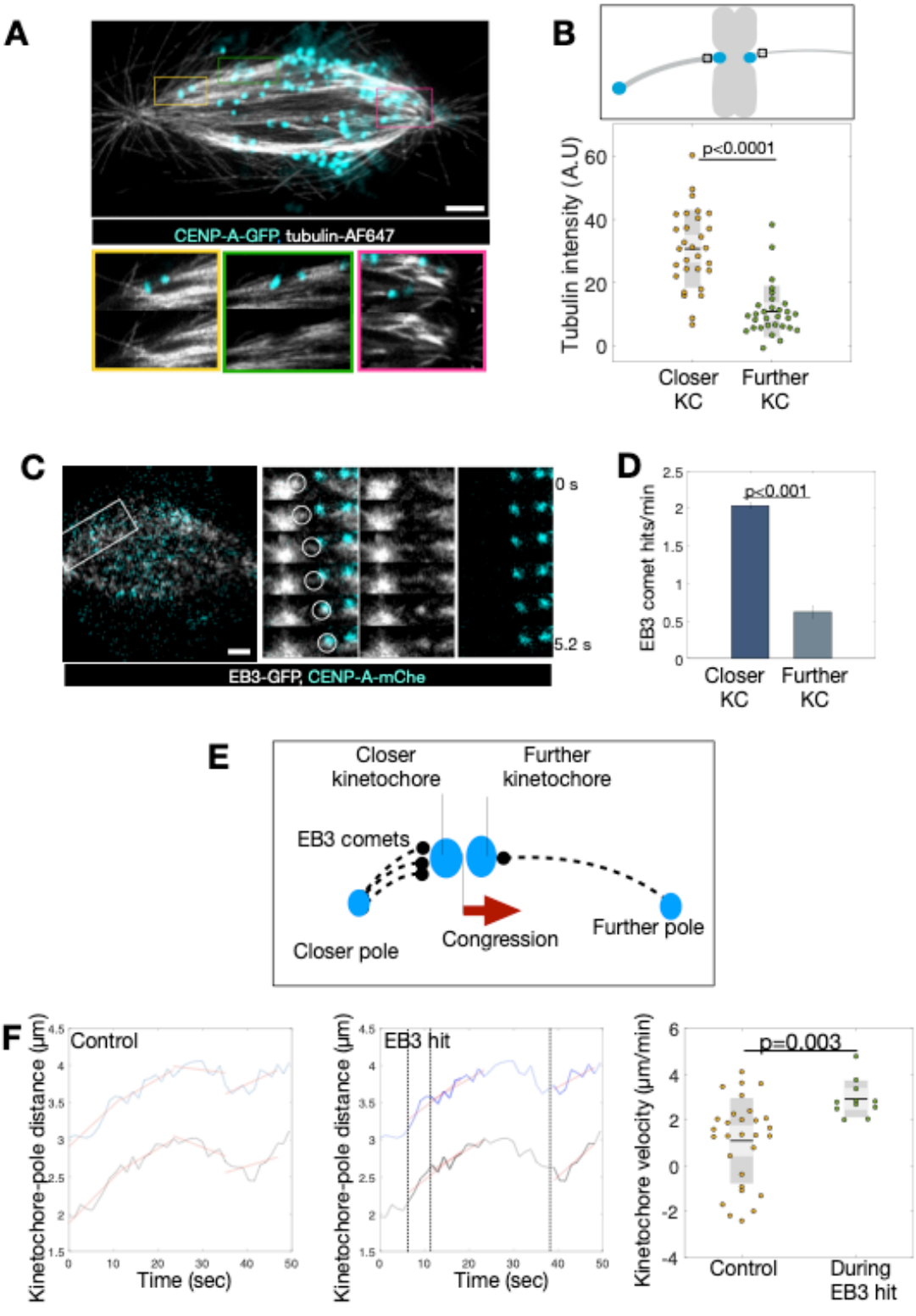

Figure 43. Microtubules reach to both kinetochores in 3:1 ratio. A) STED image of prometaphase spindle in RPE-1 cell with stable expression of CENP-A-GFP (cyan) and immunostained tubulin (gray) with enlarged areas (colored squares) showing microtubules at the sister kinetochores. B) Tubulin intensity measurement at the fibers from the pole site of

sister kinetochores. C) Prometaphase spindle of U2OS cell with stable expression of GFP-EB3 (grey) and mCherry-CENP-A (cyan), montage of enlarged area showing EB3 comet from the closer pole (white circle) approaching the closer kinetochore. D) Frequency of EB3 comet hit on closer (dark gray) or further (light gray) congressing kinetochore per minute. E) Schematic representation of EB3 comets reaching both congressing kinetochores in 3:1 ratio. F) Left and middle: kinetochore- pole distance in time for closer (black line) and further (blue line) kinetochore with the trajectory linear fit (red). Dashed lines represent the time of EB3 hit on the closer kinetochore. Right: average velocity of closer kinetochore during control movement and during EB3 hit.

4.4.3. Large interkinetochore distance indicates biorientation of congressing kinetochores

To analyze the congression parameters in high temporal resolution, RPE1 cells with stable expression of CENP-A-GFP and Centrin1-GFP were imaged live in 5 s intervals during the congression in prometaphase. I have followed the movements of the kinetochores that are on the mitotic spindle in the region between the centrosomes and the spindle equator. They started the congression on average 4.201 ± 0.12 μm from the pole and 4.254 ± 0.12 μm from the spindle equator (112 kinetochore pairs from 46 cells, **Figure 44**). They moved away from the closer pole with the average velocity of 0.77 ± 0.049 μm/min, and towards the spindle equator at 0.694 ± 0.051 μm/min.

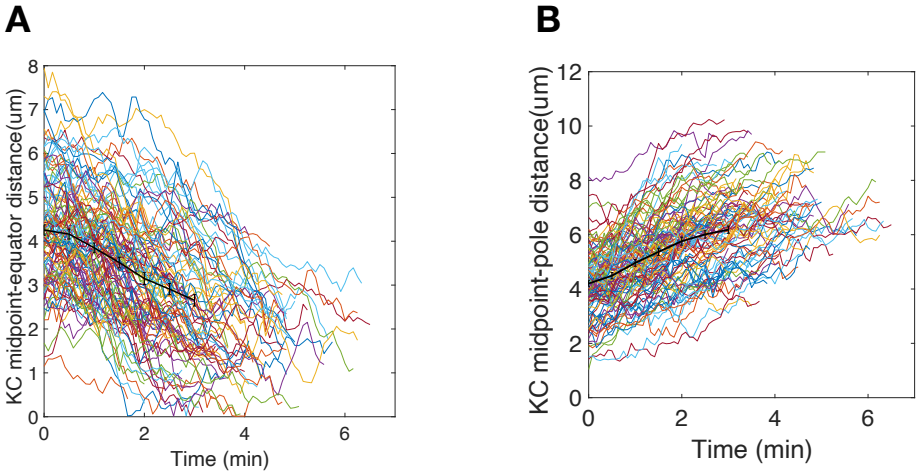

Figure 44. In prometaphase kinetochores move away from the closer pole towards the spindle equator. Graphs showing the movements of sister kinetochore midpoint (KC midpoint) in RPE1 cells during the prometaphase congression. Distance between sister

kinetochore midpoint and spindle equator (A) or closer pole (B) in time. Colored lines represent individual tracks; black lines represent mean and SEM.

Two direct effects of amphitelic attachments are a decrease in the angle between the line connecting sister kinetochores and the line connecting the spindle poles (i.e., spindle long axis; KC tilt), as well as an increase in the distance between sister kinetochores. Consistent with previous reports (Magidson et al., 2011; Renda et al., 2022), I have observed that the mean value of KC tilt decreases, whereas the mean interkinetochore distance increases during the congression (**Figure 45**). The average interkinetochore distance at the average beginning of the congression (4 μm from the closer pole) was 1.036 ± 0.018 μm, large as the distance in metaphase (1 ± 0.007 μm, (Renda et al., 2022)) and much greater than the distance at NEBD (0.65 μm, (Renda et al., 2022) implicating that the kinetochore- microtubule attachments were sufficient to produce the force on the congressing kinetochores. The average KC tilt is 21.759 ± 1.160° at the beginning of the congression. The KC tilt close to the values obtained previously for the bioriented kinetochores (~22.5°, (Renda et al., 2022)) and high interkinetochore distance favour the interpretation that the kinetochores can be to some extent bioriented during the congression. Similar pattern of interkinetochore distance and KC tilt can be observed after the depletion of various spindle proteins (**Figure 46 and Figure 47**).

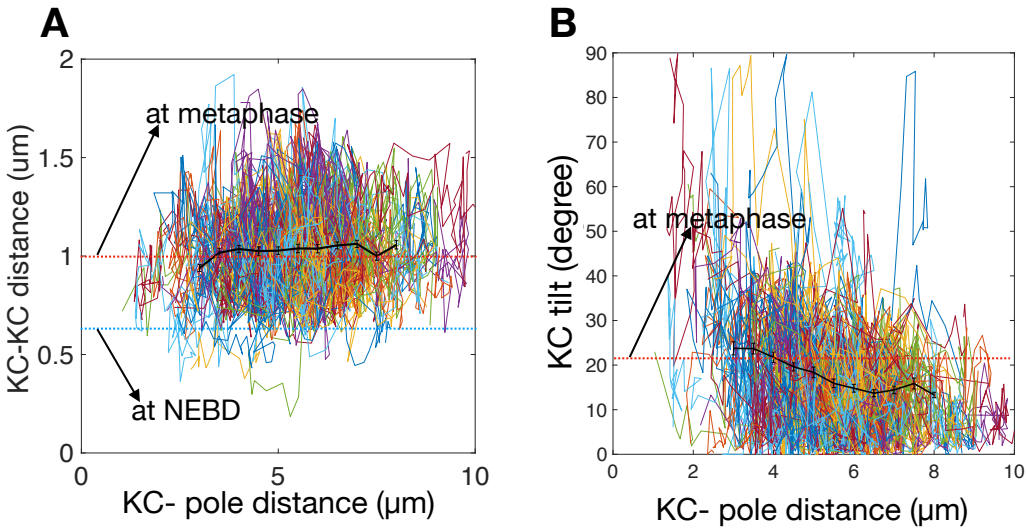

Figure 45. Interkinetochore distance and KC tilt imply congressing kinetochore biorientation. Graphs showing the movements of sister kinetochore midpoint (KC midpoint) in RPE1 cells during the prometaphase congression. Colored lines represent individual tracks; black lines represent mean and SEM. A) Distance between sister kinetochores (interkinetochore distance; KC-KC distance) at different positions of the kinetochore pairs

during the congression. Red dashed line represents the interkinetochore distance at metaphase; blue dashed line represents interkinetochore distance at NEBD. B) the angle between the line connecting sister kinetochores and the line connecting spindle poles (KC tilt) at different positions of the kinetochore pairs during the congression. Red dashed line represents the interkinetochore distance at metaphase.

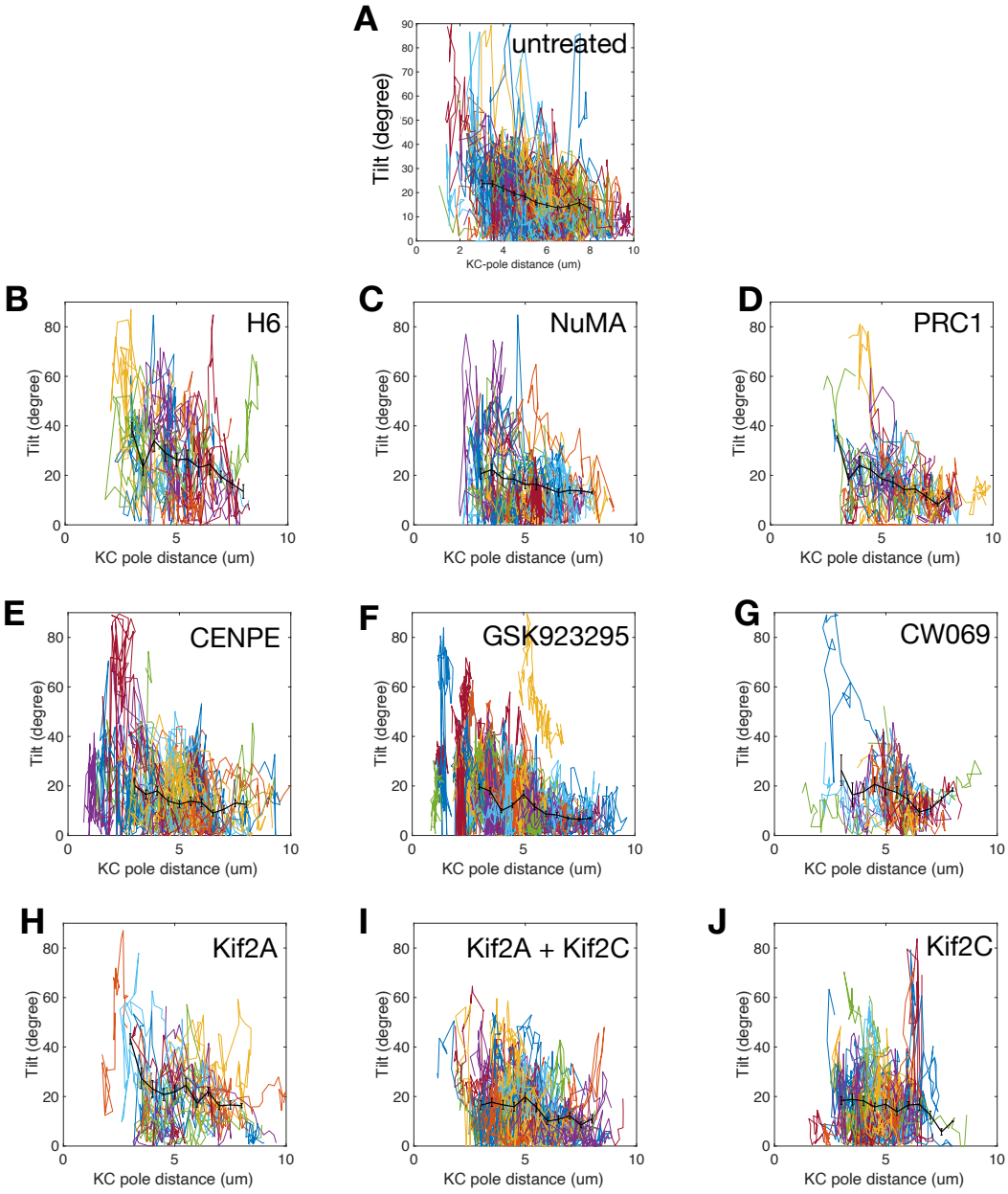

Figure 46. KC tilt after various spindle protein depletions implies congressing kinetochore biorientation. Graphs showing the movements of sister kinetochore midpoint (KC midpoint) in RPE1 cells during the prometaphase congression. Colored lines represent individual tracks; black lines represent mean and SEM. The angle between the line connecting sister kinetochores and the line connecting spindle poles (KC tilt) at different positions of the

kinetochore pairs during the congression after the depletion of various spindle proteins. The defined siRNA treatment or chemical inhibition is indicated at the upper right corners inside the graph.

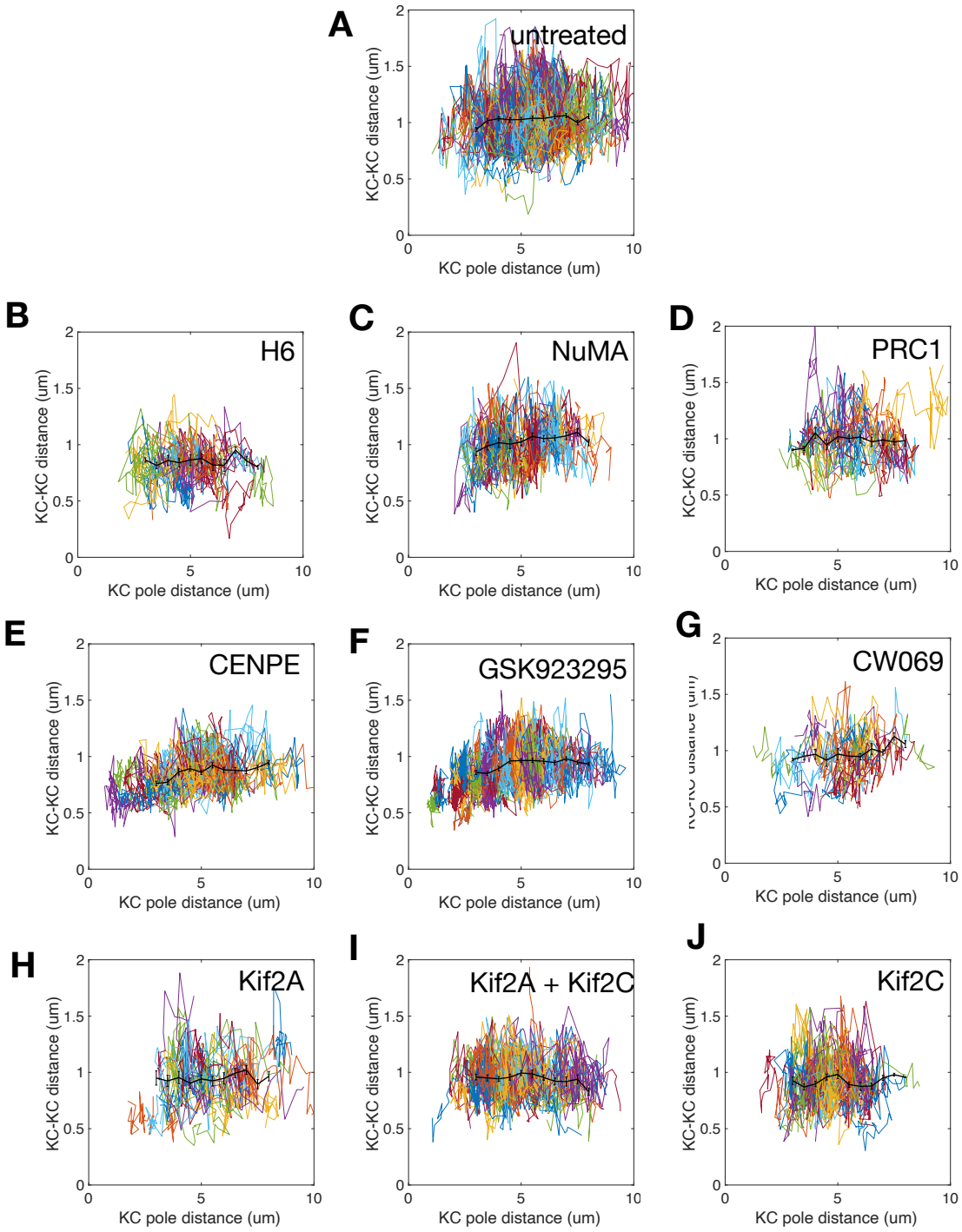

Figure 47. Interkinetochore distance after various spindle protein depletions implies congressing kinetochore biorientation. Graphs showing the movements of sister kinetochore midpoint (KC midpoint) in RPE1 cells during the prometaphase congression.

Colored lines represent individual tracks; black lines represent mean and SEM. Distance between sister kinetochores (interkinetochore distance; KC-KC distance) at different positions of the kinetochore pairs during the congression after the depletion of various spindle proteins. The defined siRNA treatment or chemical inhibition is indicated at the upper right corners inside the graph.

4.5. Antiparallel overlaps are longer in prometaphase than in metaphase

I have demonstrated the existence of antiparallel overlaps in prometaphase spindles via photoactivation experiments and the presence of bridging fiber speckles. Antiparallel overlapping non-kinetochore fibers could have an impact in chromosome congression, so it is necessary to determine their length in prometaphase.

To define prometaphase and metaphase antiparallel overlap length, I used live imaging of RPE1 cells expressing EB3-GFP and H2B-mCherry. First, I have made one image of the whole spindle to verify the phase of mitosis, and then I used fast live cell imaging of the small area of the spindle to precisely track EB3 comets (**Figure 48 A and B**). I have tracked their position from the appearance on the spindle equator until the furthest visible point. In that way I have tracked how far do the EB3 comets reach from one side of the spindle to the other, passing the equatorial plane, giving the half overlap length (**Figure 48 C and D**). In prometaphase they reached further than in metaphase confirming that the prometaphase antiparallel overlaps are longer than the metaphase ones. Half overlap length in prometaphase spindles was 4.697 ± 0.187 μm (55 EB3 comets from 11 cells), and in metaphase 3.160 ± 0.115 μm (55 EB3 comets from 11 cells; $p = 2.292x10^{-10}$). Also, the prometaphase spindles were longer than in metaphase. The average length of prometaphase spindle is 16.643 ± 0.795 μm, and in metaphase (14.333 ± 0.338 μm; p = 0.0147; **Figure 48, D**).

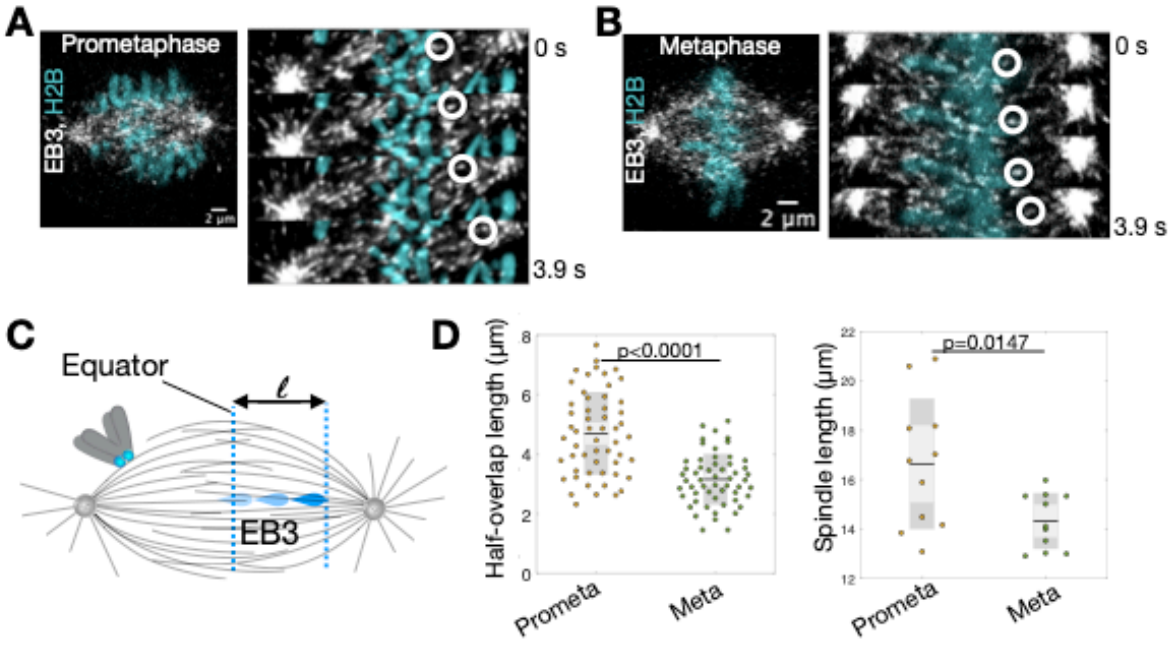

Figure 48. EB3 comets reach further in prometaphase than in metaphase. A) RPE1 cells expressing EB3-GFP (grey) and H2B-mCherry (cyan) in prometaphase (A) and metaphase (B). Left: whole spindle; Right: enlarged area of the left spindle with white circles tracking the EB3 comets. C) Schematic representation of the method how the EB3 comets (blue drops) were tracked. Their position was tracked from the appearance on the spindle equator (blue dotted line left) until the furthest visible point (blue dotted line right) and the average half overlap length (l) was calculated as the distance between those points. D) half overlap length (left) and spindle length (right) obtained for prometaphase and metaphase spindles.

To further investigate the spindle architecture during the kinetochore congression, I have inspected the average length of the antiparallel microtubule overlaps and the spindle length of prometaphase and metaphase spindles with another method. PRC1 is a rational candidate to verify the length of the antiparallel zone because it passively crosslinks antiparallel microtubules throughout mitosis, including prometaphase (Matković et al., 2022; Renda et al., 2022).

I have labelled RPE1 cells with stable expression of CENP-A-GFP and centrin1-GFP with anti-PRC1 antibody and imaged multiple z- stacks (**Figure 49, A**). To determine the antiparallel overlap length in those cells, I tracked the pole-to-pole contour of individual PRC1- labelled overlap regions and obtained the PRC1 intensity profile (**Figure 49, B, C**). The overlap length of individual PRC1-labeled overlap regions was determined as the width of the peak of the signal intensity in the central part of the contour. This method is another

line of evidence that prometaphase spindles have longer PRC1 labelled overlaps (11.084 ± 0.259 μm; 58 fibers from 19 cells) than in metaphase (7.144 ± 0.296 μm; 33 fibers from 11 cells, $p = 2.06x10^{-15}$; **Figure 49, D**). The average prometaphase pole- pole distance was not longer (14.59 ± 0.537 μm) than in metaphase (13.75 ± 0.433 μm; p = 0.289), but the antiparallel overlap to spindle length ratio vas greater in prometaphase (0.764 ± 0.012) than in metaphase (0.524 ± 0.022; $p = 2.34x10^{-6}$; **Figure 49, E, F**).

Thus, taken all together, I demonatrated that the congressing kinetochores are asymmetrically bioriented, with large interkinetochore distance and kinetochore fibers on both kinetochores in 3:1 ratio favouring the kinetochore facing the closer pole. Also, during the congression the kinetochores move on the long antiparallel overlaps that could help the congression.

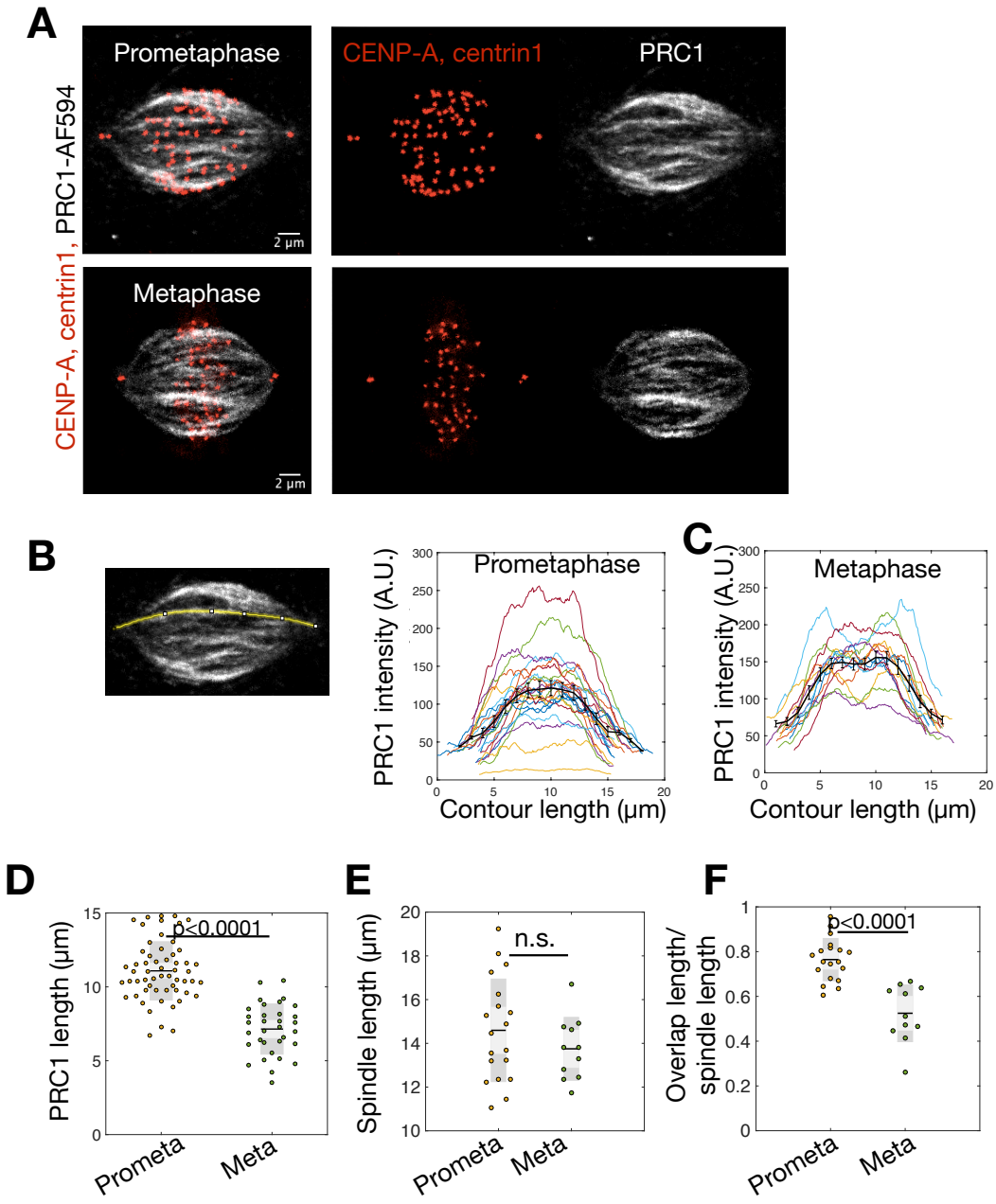

Figure 49. Antiparallel overlaps are longer in prometaphase than in metaphase. A) maximal projection of mitotic spindle in RPE1 cell with stable expression of CENP-A-GFP (red) and centrin1-GFP (red) immunolabelled with anti-PRC1 antibody (grey) in prometaphase (top) and metaphase (bottom). Left: merged image; middle and right: individual channels, B-C) Example how a 5-pixel-thick segmented line was used to track the pole-to-pole contour of individual PRC1- labelled overlap regions. Graphs showing PRC1 intensity profiles in prometaphase and metaphase (C) spindles. Colored lines represent individual tracks; black lines represent mean and SEM. D) Length of PRC1 labelled overlaps in prometaphase and metaphase cells. E) Spindle length and F) ratio of overlap and spindle length of prometaphase and metaphase spindles.

4.6. Poleward flux is producing forces that help the congression

To analyze the impact of poleward flux on the congressing kinetochores, I have tracked the movement of the speckles together with the position of the kinetochores on whose fibers those speckles appear. To emphasize, I have found in prometaphase spindles of RPE1 cells the k-fiber and bridging fiber speckles on both congressing kinetochores of the kinetochore pair. The existence of k-fiber speckles on both kinetochores further indicates that both kinetochores can be to some extent end-on attached during the congression.

In prometaphase, with respect to the kinetochore pair in congression, I could observe the following speckle types: k-fiber and the bridging fiber that fluxes towards the closer pole ("short" fibers); and k-fiber and the bridging fiber that fluxes towards the further pole ("long" fibers), i.e. in the direction of the congressing chromosome (**Figure 50**). For all speckle types, a strong impact of the flux on kinetochore movement velocity can be seen (**Figure 51**). The "normal" direction of the congression, that is towards the spindle equator (towards the further pole) is shown as the positive value in the graphs (**Figure 51**). For the fibers that flux in the same direction as the congression ("long" k-fiber and bridge), a correlation to kinetochore congression velocity can be seen (**Figure 51, C and D**). For the fibers that flux towards the closer pole ("short" k-fiber and bridge), i.e. in the opposite direction of congression, the anticorrelation to kinetochore congression velocity can be observed (**Figure 51, A and B**).

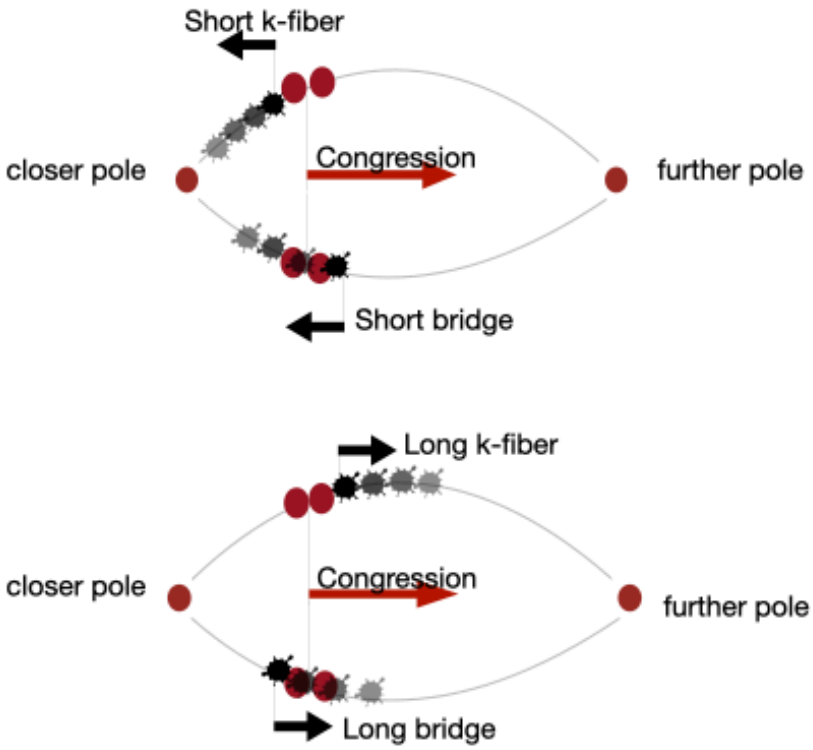

Figure 50. Different speckle types exist in prometaphase spindle. Scheme showing speckle types (gray blots) that can be found on the prometaphase spindle with respect to the congressing kinetochores (red spots). For clarity, two separate schemes are shown, but all four speckle types can be found on the same sister kinetochore. Red arrow represents the congression direction towards the spindle equator. Short k-fiber and short bridge are found on the kinetochore facing the closer pole and they flux towards that pole. Long k-fiber and long bridge are found on the kinetochore facing the further pole and they flux towards that pole.

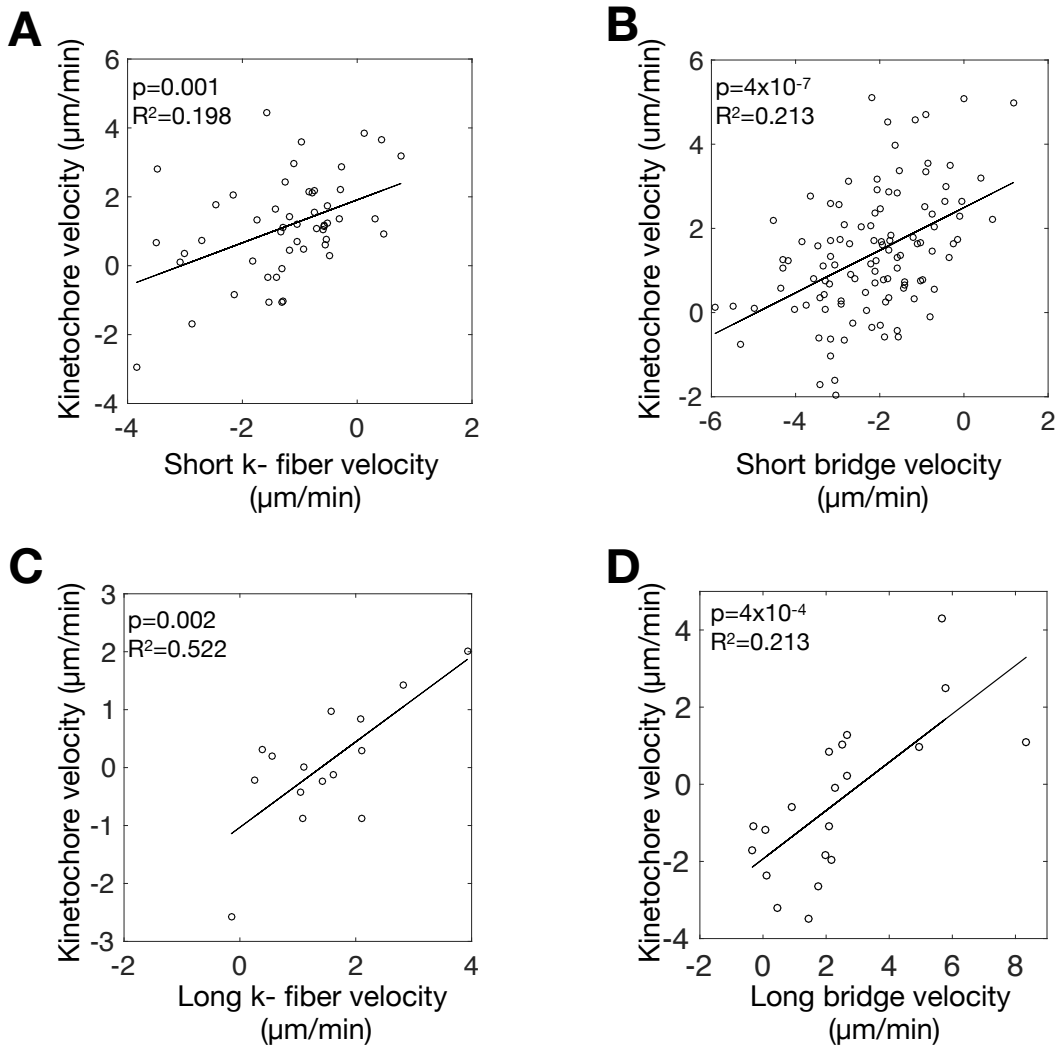

Figure 51. Poleward flux is dragging the kinetochores in the flux direction. Scatter plot of the kinetochore velocity versus poleward flux velocities of various microtubule fibers. The movement in the "normal" direction of the congression, i.e. towards the spindle equator (towards the further pole) is shown as the positive value. A)-D) Each dot represents the velocity of the speckle and corresponding kinetochore which is on the fiber where those speckles are found. Black line represents linear regression fit. Short k-fiber (A) and short bridge (B) are found on the side facing the closer pole; long k-fiber (C) and long bridge (D) are the speckles found on the fibers facing the further pole.

Furthermore, the impact of k-fiber poleward flux on the congression can be demonstrated after plotting the mean kinetochore velocity versus the mean flux velocities of all k-fibers. (**Figure 52**). Here I show that the kinetochore velocity and the direction of their movement depends on the k-fiber flux (**Figure 52**, see caption).

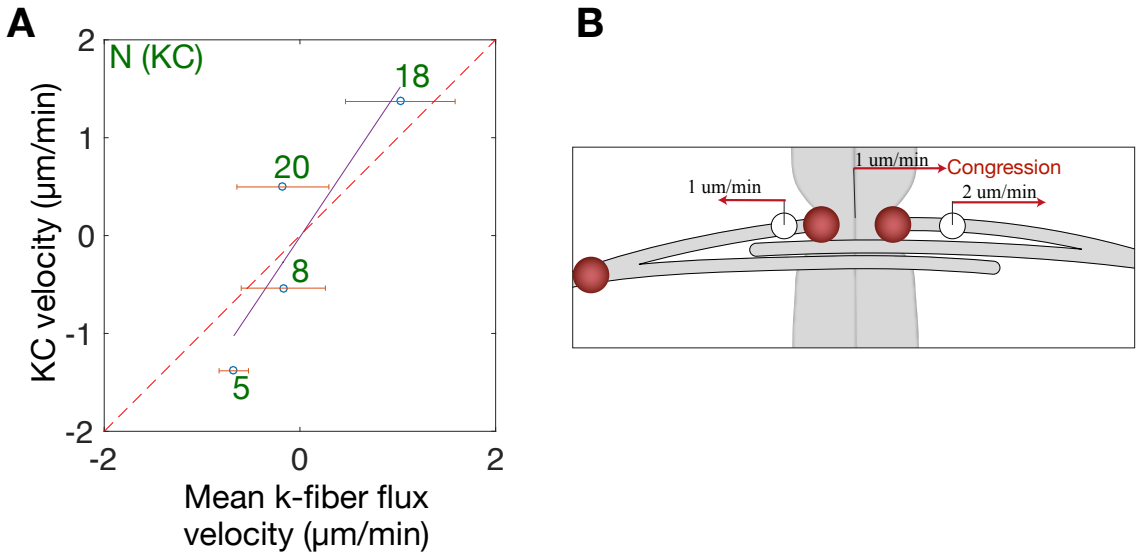

Figure 52. Kinetochore velocity and direction depends on the k-fiber flux. A) Scatter plot showing average kinetochore velocity versus average k-fiber flux velocities. The movement in the "normal" direction of the congression, i.e. towards the spindle equator (towards the further pole) is shown as the positive value in the graph. Kinetochore velocities are categorized in four groups considering their velocity (-2 to -1, -1 to 0, 0 to 1 and 1 to 2 µm/min). Those velocities are plotted against their k-fiber flux velocities (blue dots with SEM). Purple line represents linear regression fit; green numbers represent the number of kinetochores in individual category; red dashed line represents the identity line. B) Schematic representation of average velocities on k-fiber facing the closer pole (1 µm/min) and k-fiber facing the further pole (2 µm/min) and the average kinetochore congression velocity. Red arrows represent the direction of movement.

Speckle microscopy is a powerful and informative method because many speckles appear on various microtubules during the imaging (see **Figure 32**), but unfortunately almost never at the same time on the k-fibers of the same sister kinetochore pair. It means that I wasn't able to compare the flux of the long and short k-fiber at the kinetochore pair at the exact same moment, but I measured their average velocities. I compared the flux velocities of short and long k-fibers (**Figure 53**, see caption), and they anticorrelate. Thus, on average, the longer k-fiber flux shows greater flux velocities than the shorter ones, and I propose that it could help the kinetochores to congress (**Figure 53**).

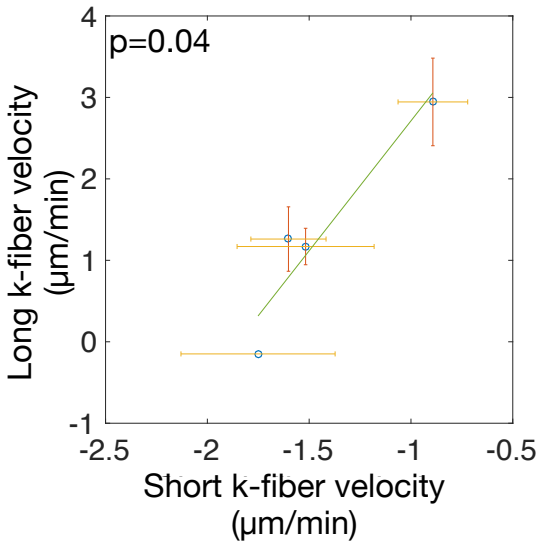

Figure 53. Long and short kinetochore fiber flux velocities anticorrelate. Scatter plot showing the relationship of long and short k-fiber flux velocities. The movement of the kinetochore flux in the "normal" direction of the congression, i.e. towards the spindle equator (towards the further pole) is taken as the positive value. The flux of long and short k-fibers (blue dots with SEM) is compared inside four categories made across the velocities of their corresponding kinetochores (-2 to -1, -1 to 0, 0 to 1 and 1 to 2 µm/min). Green line represents linear regression fit.

To test this hypothesis, I have tracked the movement of the kinetochores during the congresion across various treatments and calculated their congression velocities (**Figure 54**). NuMA depletion, Kif2C depletion and Kif2A+Kif2C codepletion showed significantly slower congression velocities ($p = 0.021$; $p < 0.0001$ and $p = 0.037$, respectively). As Kif2C localizes at the centromere and regulates k-fiber dynamics, its depletion probably reflected as the slower congression velocities (Kline-Smith et al., 2004). Notably, NuMA depletion showed slower k-fiber flux (**Figure 40**) and concurrently significant reduction of congression velocity. NuMA is not localized at the kinetochore but acts as a passive crosslinker that transmits the flux force from the bridging fibers to the k-fibers which in turn helps the congression.

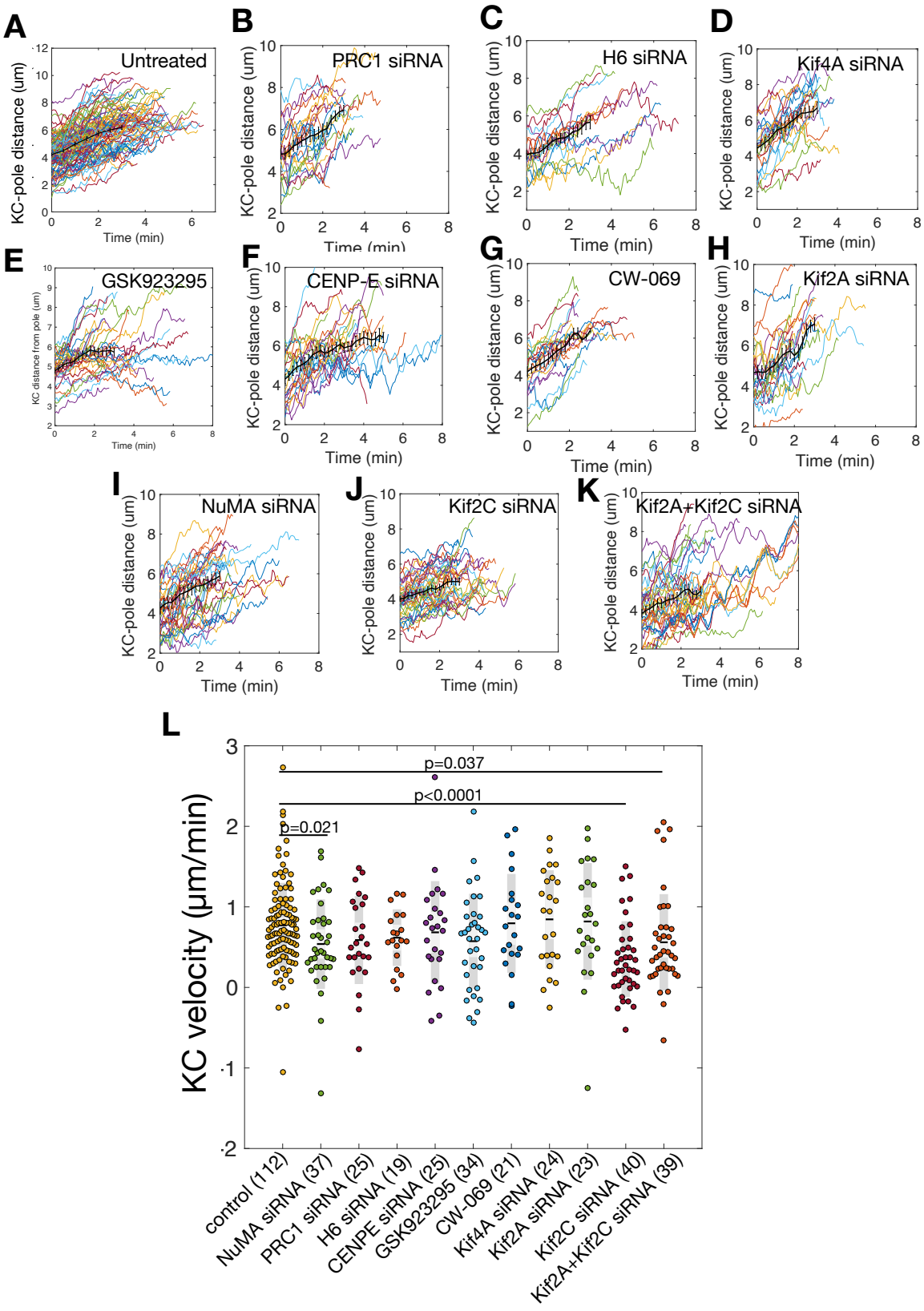

Figure 54. NuMA depletion shows altered congression velocity. A-K) Plots of kinetochore positions with respect to the pole. L) Kinetochore velocities during the congression after different siRNA depletion or chemical inhibition of various spindle proteins. Boxes represent

standard deviation (dark grey), 95% standard error of the mean (light grey) and mean value (black) for indicated conditions. Numbers in the brackets represent number of kinetochore pairs. Statistics: t test.

5. DISCUSSION

Prometaphase and metaphase poleward flux velocities are similar

In this thesis, I have utilized two microscopy methods to get the deeper insight into prometaphase poleward flux dynamics. Photoactivation experiments indicated that the prometaphase flux is faster than in metaphase, as shown previously with the same method (Cimini et al., 2006; Steblyanko et al., 2020). Surprisingly, speckle microscopy experiments revealed that both the k-fiber and bridging fiber velocities are in fact similar as in metaphase (Risteski et al., 2022). This discrepancy can be explained by different spindle architecture between prometaphase and metaphase. K-fibers in prometaphase spindles are not abundant as in metaphase so the majority of the spindle consists of the non-kinetochore microtubules (Cimini et al., 2006). As shown for Ptk1 cells, prometaphase spindles consist of about 75 % non-kinetochore fibers (Cimini et al., 2006). Thus, it is reasonable to imagine that the photoactivated signal in prometaphase arises mainly from the tubulin in non-kinetochore fibers. Those fibers flux faster, and thus give faster average flux velocities in prometaphase. Similar flux velocities in prometaphase and metaphase imply that the flux-driving mechanism may be similar.

Two classes of microtubules exist in prometaphase

Speckle microscopy approach in previous studies showed different dynamics in different classes of microtubules on various organisms (LaFountain et al., 2004; Maddox et al., 2003; Matos et al., 2009; Waterman-Storer et al., 1998). Correspondingly, with the speckle microscopy assay, I revealed that prometaphase spindles in healthy human cells consist of two classes of microtubules, and that they differ in microtubule dynamics. This was also indicative from my tubulin photoactivation experiments. The microtubule class that was photoactivated in the spindle middle often split to the opposite poles, similarly shown earlier (Steblyanko et al., 2020). It suggests the existence of the non-kinetochore antiparallel overlap with the flux velocity significantly higher than in the fibers closer to the pole.

Kinesins and passive crosslinkers are important players of prometaphase poleward flux

With photoactivation experiments I examined the importance of mitotic kinesins located in the antiparallel regions on the prometaphase flux regulation. Experiments with FCPT confirmed the importance of antiparallel overlap sliding in prometaphase, but Kinesin-5 inhibition with STLC didn't suggest this kinesin alone as the main driver of the prometaphase poleward flux. Flux in monopolar spindles was slower than in prometaphase, probably because it consisted mainly of k-fibers which flux slower. Monopolar spindles fluxed at the same speed as metaphase spindles. This suggests that other kinesins remained at the antiparallel overlap and powered the flux. Chemical inhibition of kinesin-12 didn't show any effect on flux in prometaphase, but reduced the metaphase flux. Similar results were obtained previously for prometaphase-like cells codepleted for NDC80 and Kif15 (Steblyanko et al., 2020). Kif15 is probably responsible for crosslinking and sliding of k-fibers (Sturgill et al., 2014; Tanenbaum et al., 2009), so I can speculate that it has a greater impact on metaphase spindles, because of more stable and mature k-fibers than in prometaphase.

Photoactivation experiments indicated, and speckle microscopy confirmed, the importance of HSET in prometaphase and metaphase flux regulation. It was shown previously that in metaphase it serves as the crosslinker which transmits the flux from antiparallel overlaps to the k-fibers (Steblyanko et al., 2020). I showed that HSET chemical inhibition reduced the flux velocity in prometaphase and metaphase. Importantly, in prometaphase it reduced the flux of k-fibers, but surprisingly also of the bridging fibers. It indicates that the crosslinking role of HSET is also important for the flux generation in the bridging fibers, possibly by parallel crosslinking of the bridging fiber minus-ends, and/or crosslinking in the antiparallel region (She & Yang, 2017).

Also, PRC1 has an indirect influence on flux regulation. It serves as a scaffold to recruit the proteins important for microtubule dynamics and also provides mechanical stability for antiparallel overlaps. Experiments with PRC1 depletion didn't demonstrate the impact of PRC1 on flux, as shown earlier (Risteski et al., 2022; Steblyanko et al., 2020; Vukušić et al., 2017), probably because the architecture of the bridging fibers wasn't influenced enough. Certainly, it was shown that the depletion of PRC1 reduces the bridge thickness to about 50% (Jagrić et al., 2021), suggesting that the remained antiparallel overlap is sufficient to drive the flux. Greater bridging fiber reduction can be obtained by inhibiting the H6 or H8, subunits of

the augmin complex (Štimac et al., 2022). Indeed, my depletion of H6 showed reduced bridging fiber and k-fiber prometaphase flux velocities. Similar effect on H8 depletion was shown previously on metaphase spindles (Risteski et al., 2022).

Thus, my mechanism for prometaphase flux fits the "coupled spindle" model (Matos et al., 2009; Risteski et al., 2022; Steblyanko et al., 2020), stating that the poleward flux is generated in the antiparallel region at the spindle middle and transferred to the k-fibers via the passive crosslinkers. CENP-E depletion and chemical inhibition reduced the bridging fiber flux, as shown previously (Risteski et al., 2022; Steblyanko et al., 2020). It was shown that CENP-E localization on the bridging fibers is PRC1-dependent, but PRC1 depletion didn't reduce flux velocities. Thus, CENP-E could help to power the prometaphase flux probably from the kinetochores by sliding the microtubules depending on their polarity, as proposed for cancer cell line (Steblyanko et al., 2020). HSET helps to power the flux in the bridging fibers. The flux force produced in bridging fibers is transmitted to the k-fibers via HSET and NuMA by their roles as passive crosslinkers. All treatments that reduced the bridging fiber flux, also reflected to the reduction of the k-fibers, further supporting the "coupled spindle" model for prometaphase flux generation.

Congressing kinetochores are asymmetrically bioriented

In this thesis, I have further inspected the prometaphase spindle architecture and conditions of chromosome congression. Mad2 signal was present on both sister kinetochores, indicating that they don't have mature end-on attachments. The existence of Mad2 signal was expected, as shown previously (Kuhn & Dumont, 2017, 2019; Sikirzhytski et al., 2018). It was shown earlier in Ptk1 cells that the sister kinetochores can sense the end-on occupancy separately (Kuhn & Dumont, 2017), and that the first end-on attachments occur at the kinetochore facing the closer pole. Here I showed that the same stands for the healthy human cells. Also, those results were corroborated by the live cell imaging of EB3 comets. I demonstrated that the kinetochore facing the closer pole has on average three times more microtubules that its sister, also, both kinetochores can to some extent be end-on attached. Interkinetochore distance and KC tilt were close to the values obtained earlier (Renda et al., 2022). Thus, my results support the idea that the chromosomes can rapidly biorient while congressing on the antiparallel overlaps (Renda et al., 2022).

As shown for the human cancer cells, my experiments confirmed that passive crosslinker PRC1 is present at the antiparallel overlap microtubule bundles in early mitosis (Matković et al., 2022; Steblyanko et al., 2020). Moreover, I provided two lines of evidence that the antiparallel overlaps are longer in prometaphase than in metaphase. To precisely immunolabel the PRC1, I have used the fixation with ice-cold methanol which occasionally can disturb some aspects of microtubule organization (Kellogg et al., 1988), and may have caused slight shrinkage of mitotic spindles. I think that the results regarding the spindle length from my live imaging experiments are therefore more trustworthy. Anyway, I propose that those long antiparallel overlaps could help kinetochores to congress, as proposed earlier in the same cells (Renda et al., 2022). Also, I speculate that those overlaps are important for the flux transmission to the kinetochore fibers.

Poleward flux is producing forces that help the congression

Although same classes of microtubules were found in prometaphase spindles as in metaphase, the spindle architecture between those two phases differ. I showed that k-fibers are present on both sister kinetochores during the chromosome congression, but, certainly, they are not as ripe as in metaphase. I found a strong correlation of k-fiber flux movement and the direction of the chromosome congression, so I conclude that the microtubule poleward flux is producing forces on the congressing kinetochores that help the congression. I speculate that the long bridging and k-fibers can produce forces that can assist the congression. During the congression the kinetochores move on long antiparallel overlaps, and the congressing kinetochore has approximately three times more microtubules on the kinetochore facing the closer pole. But, those fibers are short, and they probably produce less force than those on the other side because the overlap with the bridging fibers is much shorter than on the side facing the spindle equator.

If we compare the flux velocities of short and long k-fibers, we can see that it anticorrelates. It means that on average, inside the one pole-to-pole spindle entity which is made of the congressing kinetochore and their corresponding fibers, the faster the flux on the one side, the slower will be the flux on the other side. Finally, on average, the longer k-fiber flux shows greater flux velocities than the shorter ones, and I propose that it could help the kinetochores to congress. Indeed, NuMA depleted cells showed altered congression velocities concurrently

with lower k-fiber flux velocity. Certainly, impact on flux dynamics followed by the chromosome congression defects was observed earlier after NuMA depletion (Sun et al., 2021; van Toorn et al., 2023).

It would be interesting to test my predictions that kinesins and passive crosslinkers impact prometaphase flux, and thus chromosome congression, with physical model and to test the parameters from metaphase flux model for kinetochore centering (Risteski et al., 2022). It would be important to implement the difference in spindle architecture, as 3:1 microtubule ratio favouring the fiber on the kinetochore facing the closer pole, and longer antiparallel overlap. I predict that, for instance, the deficiency in passive crosslinkers would show less effective congression due to less efficient flux force transmission from the bridge to the k-fibers.

6. CONCLUSION

In my thesis I have inspected the complicated nature of microtubule flux regulation in prometaphase. I have used various microscopy techniques to get the deeper insight into the prometaphase spindle architecture. I demonstrated that the prometaphase spindle consists of k-fibers and bridging fibers, with latter fluxing twice faster as the k-fibers. Surprisingly, I found that the prometaphase flux velocities are similar as in metaphase. Thus, I suggest that the mechanisms governing the poleward flux are alike in those two phases of mitosis. The results of my experiments fitted into the coupled spindle model where the poleward flux is produced in the antiparallel regions of the spindle and the force is transmitted to the k-fibers via the passive crosslinkers. The main players in my mechanism are CENP-E on the kinetochores and HSET as the main generators of the flux in the long antiparallel overlaps. This force is spread to the k-fibers via the role of HSET and NuMA as the passive crosslinkers. Moreover, I demonstrated that during the congression between the pole and the midplane, the kinetochores are asymmetrically bioriented, confirmed by counting the EB3 comets that hit the congressing kinetochores. On average, three times more microtubules reach the kinetochore facing the closer pole. The detailed examination of tubulin signal near the sister kinetochores in superresolution images confirmed the live-cell experiments. In agreement, Mad2 signal decreases during the congression firstly from the kinetochore facing the closer pole. The interkinetochore distance and the angle between the kinetochores and the spindle long axis are as in metaphase, further confirming that the congressing kinetochores can to some extent be bioriented. I found that kinetochore movement is correlated with poleward flux of their associated k-fibers and bridging fibers. Thus, microtubule poleward flux is producing forces on the congressing kinetochores which drag the kinetochore in the flux direction, promoting their movement towards the midplane.

7. REFERENCES

Akhmanova, A., & Steinmetz, M. O. (2008). Tracking the ends: A dynamic protein network controls the fate of microtubule tips. *Nature Reviews Molecular Cell Biology*, *9*(4), Article 4. https://doi.org/10.1038/nrm2369

Alberts, B., Johnson, A., Lewis, J., Morgan, D., Raff, M., Roberts, K., Walter, P., & Hunt, T. (2014). *Molecular Biology of the cell* (Sixth edition). Garland Science.

Alfaro-Aco, R., & Petry, S. (2015). Building the Microtubule Cytoskeleton Piece by Piece. *The Journal of Biological Chemistry*, *290*(28), 17154–17162. https://doi.org/10.1074/jbc.R115.638452

Andrews, P. D., Ovechkina, Y., Morrice, N., Wagenbach, M., Duncan, K., Wordeman, L., & Swedlow, J. R. (2004). Aurora B regulates MCAK at the mitotic centromere. *Developmental Cell*, *6*(2), 253–268. https://doi.org/10.1016/s1534-5807(04)00025-5

Barford, D. (2020). Structural interconversions of the anaphase-promoting complex/cyclosome (APC/C) regulate cell cycle transitions. *Current Opinion in Structural Biology*, *61*, 86–97. https://doi.org/10.1016/j.sbi.2019.11.010

Barisic, M., Aguiar, P., Geley, S., & Maiato, H. (2014). Kinetochore motors drive congression of peripheral polar chromosomes by overcoming random arm-ejection forces. *Nature Cell Biology*, *16*(12), 1249–1256. https://doi.org/10.1038/ncb3060

Barisic, M., & Maiato, H. (2016). The tubulin code: A navigation system for chromosomes during mitosis. *Trends in Cell Biology*, *26*(10), 766–775. https://doi.org/10.1016/j.tcb.2016.06.001

Barisic, M., Rajendraprasad, G., & Steblyanko, Y. (2021). The metaphase spindle at steady state—Mechanism and functions of microtubule poleward flux. *Seminars in Cell & Developmental Biology*, *117*, 99–117. https://doi.org/10.1016/j.semcdb.2021.05.016

Barisic, M., Silva e Sousa, R., Tripathy, S. K., Magiera, M. M., Zaytsev, A. V., Pereira, A. L., Janke, C., Grishchuk, E. L., & Maiato, H. (2015). Mitosis. Microtubule detyrosination guides

chromosomes during mitosis. *Science (New York, N.Y.)*, *348*(6236), 799–803. https://doi.org/10.1126/science.aaa5175

Bennett, A., Bechi, B., Tighe, A., Thompson, S., Procter, D. J., & Taylor, S. S. (2015). Cenp-E inhibitor GSK923295: Novel synthetic route and use as a tool to generate aneuploidy. *Oncotarget*, *6*(25), 20921–20932.

Bringmann, H., Skiniotis, G., Spilker, A., Kandels-Lewis, S., Vernos, I., & Surrey, T. (2004). A Kinesin-like Motor Inhibits Microtubule Dynamic Instability. *Science*, *303*(5663), 1519–1522. https://doi.org/10.1126/science.1094838

Brinkley, B. R., & Cartwright Jr., J. (1975). Cold-Labile and Cold-Stable Microtubules in the Mitotic Spindle of Mammalian Cells*. *Annals of the New York Academy of Sciences*, *253*(1), 428–439. https://doi.org/10.1111/j.1749-6632.1975.tb19218.x

Brust-Mascher, I., Sommi, P., Cheerambathur, D. K., & Scholey, J. M. (2009). Kinesin-5–dependent Poleward Flux and Spindle Length Control in Drosophila Embryo Mitosis. *Molecular Biology of the Cell*, *20*(6), 1749–1762. https://doi.org/10.1091/mbc.E08-10-1033

Burbank, K. S., Mitchison, T. J., & Fisher, D. S. (2007). Slide-and-Cluster Models for Spindle Assembly. *Current Biology*, *17*(16), 1373–1383. https://doi.org/10.1016/j.cub.2007.07.058

Cai, S., Weaver, L. N., Ems-McClung, S. C., & Walczak, C. E. (2009). Kinesin-14 Family Proteins HSET/XCTK2 Control Spindle Length by Cross-Linking and Sliding Microtubules. *Molecular Biology of the Cell*, *20*(5), 1348–1359. https://doi.org/10.1091/mbc.e08-09-0971

Cameron, L. A., Yang, G., Cimini, D., Canman, J. C., Kisurina-Evgenieva, O., Khodjakov, A., Danuser, G., & Salmon, E. D. (2006). Kinesin 5–independent poleward flux of kinetochore microtubules in PtK1 cells. *The Journal of Cell Biology*, *173*(2), 173–179. https://doi.org/10.1083/jcb.200601075

Carazo-Salas, R. E., Guarguaglini, G., Gruss, O. J., Segref, A., Karsenti, E., & Mattaj, I. W. (1999). Generation of GTP-bound Ran by RCC1 is required for chromatin-induced mitotic spindle formation. *Nature*, *400*(6740), Article 6740. https://doi.org/10.1038/22133

Cheeseman, I. M., Chappie, J. S., Wilson-Kubalek, E. M., & Desai, A. (2006). The Conserved KMN Network Constitutes the Core Microtubule-Binding Site of the Kinetochore. *Cell*, *127*(5), 983–997. https://doi.org/10.1016/j.cell.2006.09.039

Cimini, D., Howell, B., Maddox, P., Khodjakov, A., Degrassi, F., & Salmon, E. D. (2001). Merotelic kinetochore orientation is a major mechanism of aneuploidy in mitotic mammalian tissue cells. *The Journal of Cell Biology*, *153*(3), 517–527. https://doi.org/10.1083/jcb.153.3.517

Cimini, D., Wan, X., Hirel, C. B., & Salmon, E. D. (2006). Aurora kinase promotes turnover of kinetochore microtubules to reduce chromosome segregation errors. *Current Biology: CB*, *16*(17), 1711–1718. https://doi.org/10.1016/j.cub.2006.07.022

Civelekoglu-Scholey, G., & Scholey, J. M. (2010). Mitotic force generators and chromosome segregation. *Cellular and Molecular Life Sciences*, *67*(13), 2231–2250. https://doi.org/10.1007/s00018-010-0326-6

Cross, R. A., & McAinsh, A. (2014). Prime movers: The mechanochemistry of mitotic kinesins. *Nature Reviews. Molecular Cell Biology*, *15*(4), 257–271. https://doi.org/10.1038/nrm3768

David, A. F., Roudot, P., Legant, W. R., Betzig, E., Danuser, G., & Gerlich, D. W. (2019). Augmin accumulation on long-lived microtubules drives amplification and kinetochore-directed growth. *Journal of Cell Biology*, *218*(7), 2150–2168. https://doi.org/10.1083/jcb.201805044

Desai, A., Verma, S., Mitchison, T. J., & Walczak, C. E. (1999). Kin I Kinesins Are Microtubule-Destabilizing Enzymes. *Cell*, *96*(1), 69–78. https://doi.org/10.1016/S0092-8674(00)80960-5

Drechsler, H., McHugh, T., Singleton, M. R., Carter, N. J., & McAinsh, A. D. (2014). The Kinesin-12 Kif15 is a processive track-switching tetramer. *eLife*, *3*, e01724. https://doi.org/10.7554/eLife.01724

Drpic, D., Pereira, A. J., Barisic, M., Maresca, T. J., & Maiato, H. (2015). Polar Ejection Forces Promote the Conversion from Lateral to End-on Kinetochore-Microtubule Attachments on Mono-oriented Chromosomes. *Cell Reports*, *13*(3), 460–468. https://doi.org/10.1016/j.celrep.2015.08.008

Du, Q., & Macara, I. G. (2004). Mammalian Pins is a conformational switch that links NuMA to heterotrimeric G proteins. *Cell*, *119*(4), 503–516. https://doi.org/10.1016/j.cell.2004.10.028

Dumont, S., & Mitchison, T. J. (2009). Force and length in the mitotic spindle. *Current Biology: CB*, *19*(17), R749-761. https://doi.org/10.1016/j.cub.2009.07.028

Elting, M. W., Prakash, M., Udy, D. B., & Dumont, S. (2017). Mapping Load-Bearing in the Mammalian Spindle Reveals Local Kinetochore Fiber Anchorage that Provides Mechanical Isolation and Redundancy. *Current Biology: CB*, *27*(14), 2112-2122.e5. https://doi.org/10.1016/j.cub.2017.06.018

Fang, G. (2002). Checkpoint Protein BubR1 Acts Synergistically with Mad2 to Inhibit Anaphase-promoting Complex. *Molecular Biology of the Cell*, *13*(3), 755–766. https://doi.org/10.1091/mbc.01-09-0437

Ferreira, L. T., & Maiato, H. (2021). Prometaphase. *Seminars in Cell & Developmental Biology*, *117*, 52–61. https://doi.org/10.1016/j.semcdb.2021.06.004

Forer, A. (1965). LOCAL REDUCTION OF SPINDLE FIBER BIREFRINGENCE IN LIVING NEPHROTOMA SUTURALIS (LOEW) SPERMATOCYTES INDUCED BY ULTRAVIOLET MICROBEAM IRRADIATION. *The Journal of Cell Biology*, *25*(1), 95–117.

Gadde, S., & Heald, R. (2004). Mechanisms and Molecules of the Mitotic Spindle. *Current Biology*, *14*(18), R797–R805. https://doi.org/10.1016/j.cub.2004.09.021

Ganem, N. J., & Compton, D. A. (2004). The KinI kinesin Kif2a is required for bipolar spindle assembly through a functional relationship with MCAK. *Journal of Cell Biology*, *166*(4), 473–478. https://doi.org/10.1083/jcb.200404012

Ganem, N. J., Upton, K., & Compton, D. A. (2005). Efficient mitosis in human cells lacking poleward microtubule flux. *Current Biology: CB*, *15*(20), 1827–1832. https://doi.org/10.1016/j.cub.2005.08.065

Gayek, A. S., & Ohi, R. (2014). Kinetochore-microtubule stability governs the metaphase requirement for Eg5. *Molecular Biology of the Cell*, *25*(13), 2051–2060. https://doi.org/10.1091/mbc.e14-03-0785

Godek, K. M., Kabeche, L., & Compton, D. A. (2015). Regulation of kinetochore–microtubule attachments through homeostatic control during mitosis. *Nature Reviews. Molecular Cell Biology*, *16*(1), 57–64. https://doi.org/10.1038/nrm3916

Goshima, G., Mayer, M., Zhang, N., Stuurman, N., & Vale, R. D. (2008). Augmin: A protein complex required for centrosome-independent microtubule generation within the spindle. *Journal of Cell Biology*, *181*(3), 421–429. https://doi.org/10.1083/jcb.200711053

Goshima, G., & Scholey, J. M. (2010). Control of Mitotic Spindle Length. *Annual Review of Cell and Developmental Biology*, *26*(1), 21–57. https://doi.org/10.1146/annurev-cellbio-100109-104006

Griffis, E. R., Stuurman, N., & Vale, R. D. (2007). Spindly, a novel protein essential for silencing the spindle assembly checkpoint, recruits dynein to the kinetochore. *The Journal of Cell Biology*, *177*(6), 1005–1015. https://doi.org/10.1083/jcb.200702062

Groen, A. C., Needleman, D., Brangwynne, C., Gradinaru, C., Fowler, B., Mazitschek, R., & Mitchison, T. J. (2008). A novel small-molecule inhibitor reveals a possible role of kinesin-5 in anastral spindle-pole assembly. *Journal of Cell Science*, *121*(14), 2293–2300. https://doi.org/10.1242/jcs.024018

Hardwick, K. G., Johnston, R. C., Smith, D. L., & Murray, A. W. (2000). MAD3 encodes a novel component of the spindle checkpoint which interacts with Bub3p, Cdc20p, and Mad2p. *The Journal of Cell Biology*, *148*(5), 871–882. https://doi.org/10.1083/jcb.148.5.871

He, B., & Cimini, D. (2016). Using Photoactivatable GFP to Study Microtubule Dynamics and Chromosome Segregation. In P. Chang & R. Ohi (Eds.), *The Mitotic Spindle: Methods and Protocols* (pp. 15–31). Springer. https://doi.org/10.1007/978-1-4939-3542-0_2

Hiramoto, Y., & Izutsu, K. (1977). Poleward Movement of “Markers” Existing in Mitotic Spindles of Grasshopper Spermatocytes. *Cell Structure and Function*, *2*(3), 257–259. https://doi.org/10.1247/csf.2.257

Hirokawa, N., Noda, Y., Tanaka, Y., & Niwa, S. (2009). Kinesin superfamily motor proteins and intracellular transport. *Nature Reviews Molecular Cell Biology*, *10*(10), Article 10. https://doi.org/10.1038/nrm2774

Hiruma, Y., Sacristan, C., Pachis, S. T., Adamopoulos, A., Kuijt, T., Ubbink, M., von Castelmur, E., Perrakis, A., & Kops, G. J. P. L. (2015). CELL DIVISION CYCLE. Competition between MPS1 and microtubules at kinetochores regulates spindle checkpoint signaling. *Science (New York, N.Y.)*, *348*(6240), 1264–1267. https://doi.org/10.1126/science.aaa4055

Howell, B. J., McEwen, B. F., Canman, J. C., Hoffman, D. B., Farrar, E. M., Rieder, C. L., & Salmon, E. D. (2001). Cytoplasmic dynein/dynactin drives kinetochore protein transport to the spindle poles and has a role in mitotic spindle checkpoint inactivation. *The Journal of Cell Biology*, *155*(7), 1159–1172. https://doi.org/10.1083/jcb.200105093

Hueschen, C. L., Kenny, S. J., Xu, K., & Dumont, S. (2017). NuMA recruits dynein activity to microtubule minus-ends at mitosis. *eLife*, *6*, e29328. https://doi.org/10.7554/eLife.29328

Inoué, S., & Sato, H. (1967). Cell Motility by Labile Association of Molecules. *The Journal of General Physiology*, *50*(6), 259–292.

Jagrić, M., Risteski, P., Martinčić, J., Milas, A., & Tolić, I. M. (2021). Optogenetic control of PRC1 reveals its role in chromosome alignment on the spindle by overlap length-dependent forces. *eLife*, *10*, e61170. https://doi.org/10.7554/eLife.61170

Ji, Z., Gao, H., & Yu, H. (2015). Kinetochore attachment sensed by competitive Mps1 and microtubule binding to Ndc80C. *Science*, *348*(6240), 1260–1264. https://doi.org/10.1126/science.aaa4029

Kajtez, J., Solomatina, A., Novak, M., Polak, B., Vukušić, K., Rüdiger, J., Cojoc, G., Milas, A., Šumanovac Šestak, I., Risteski, P., Tavano, F., Klemm, A. H., Roscioli, E., Welburn, J., Cimini, D., Glunčić, M., Pavin, N., & Tolić, I. M. (2016). Overlap microtubules link sister k-fibres and balance the

forces on bi-oriented kinetochores. *Nature Communications*, *7*(1), Article 1. https://doi.org/10.1038/ncomms10298

Kamasaki, T., O'Toole, E., Kita, S., Osumi, M., Usukura, J., McIntosh, J. R., & Goshima, G. (2013). Augmin-dependent microtubule nucleation at microtubule walls in the spindle. *The Journal of Cell Biology*, *202*(1), 25–33. https://doi.org/10.1083/jcb.201304031

Kapitein, L. C., Peterman, E. J. G., Kwok, B. H., Kim, J. H., Kapoor, T. M., & Schmidt, C. F. (2005). The bipolar mitotic kinesin Eg5 moves on both microtubules that it crosslinks. *Nature*, *435*(7038), Article 7038. https://doi.org/10.1038/nature03503

Kapoor, T. M., Lampson, M. A., Hergert, P., Cameron, L., Cimini, D., Salmon, E. D., McEwen, B. F., & Khodjakov, A. (2006). Chromosomes can congress to the metaphase plate before biorientation. *Science (New York, N.Y.)*, *311*(5759), 388–391. https://doi.org/10.1126/science.1122142

Kapoor, T. M., Mayer, T. U., Coughlin, M. L., & Mitchison, T. J. (2000). Probing spindle assembly mechanisms with monastrol, a small molecule inhibitor of the mitotic kinesin, Eg5. *The Journal of Cell Biology*, *150*(5), 975–988. https://doi.org/10.1083/jcb.150.5.975

Kellogg, D. R., Mitchison, T. J., & Alberts, B. M. (1988). Behaviour of microtubules and actin filaments in living Drosophila embryos. *Development*, *103*(4), 675–686. https://doi.org/10.1242/dev.103.4.675

Kim, Y., Holland, A. J., Lan, W., & Cleveland, D. W. (2010). Aurora Kinases and Protein Phosphatase 1 Mediate Chromosome Congression through Regulation of CENP-E. *Cell*, *142*(3), 444–455. https://doi.org/10.1016/j.cell.2010.06.039

Kirschner, M., & Mitchison, T. (1986). Beyond self-assembly: From microtubules to morphogenesis. *Cell*, *45*(3), 329–342. https://doi.org/10.1016/0092-8674(86)90318-1

Klein, U. R., Nigg, E. A., & Gruneberg, U. (2006). Centromere Targeting of the Chromosomal Passenger Complex Requires a Ternary Subcomplex of Borealin, Survivin, and the N-Terminal

Domain of INCENP. *Molecular Biology of the Cell*, *17*(6), 2547–2558. https://doi.org/10.1091/mbc.e05-12-1133

Kline-Smith, S. L., Khodjakov, A., Hergert, P., & Walczak, C. E. (2004). Depletion of centromeric MCAK leads to chromosome congression and segregation defects due to improper kinetochore attachments. *Molecular Biology of the Cell*, *15*(3), 1146–1159. https://doi.org/10.1091/mbc.e03-08-0581

Knowlton, A. L., Lan, W., & Stukenberg, P. T. (2006). Aurora B Is Enriched at Merotelic Attachment Sites, Where It Regulates MCAK. *Current Biology*, *16*(17), 1705–1710. https://doi.org/10.1016/j.cub.2006.07.057

Kuhn, J., & Dumont, S. (2017). Spindle assembly checkpoint satisfaction occurs via end-on but not lateral attachments under tension. *Journal of Cell Biology*, *216*(6), 1533–1542. https://doi.org/10.1083/jcb.201611104

Kuhn, J., & Dumont, S. (2019). Mammalian kinetochores count attached microtubules in a sensitive and switch-like manner. *The Journal of Cell Biology*, *218*(11), 3583–3596. https://doi.org/10.1083/jcb.201902105

Kuriyama, R., & Borisy, G. G. (1981). Microtubule-nucleating activity of centrosomes in Chinese hamster ovary cells is independent of the centriole cycle but coupled to the mitotic cycle. *Journal of Cell Biology*, *91*(3), 822–826. https://doi.org/10.1083/jcb.91.3.822

LaFountain, J. R., Cohan, C. S., Siegel, A. J., & LaFountain, D. J. (2004). Direct visualization of microtubule flux during metaphase and anaphase in crane-fly spermatocytes. *Molecular Biology of the Cell*, *15*(12), 5724–5732. https://doi.org/10.1091/mbc.e04-08-0750

Lara-Gonzalez, P., Pines, J., & Desai, A. (2021). Spindle assembly checkpoint activation and silencing at kinetochores. *Seminars in Cell & Developmental Biology*, *117*, 86–98. https://doi.org/10.1016/j.semcdb.2021.06.009

Lawrence, C. J., Dawe, R. K., Christie, K. R., Cleveland, D. W., Dawson, S. C., Endow, S. A., Goldstein, L. S. B., Goodson, H. V., Hirokawa, N., Howard, J., Malmberg, R. L., McIntosh, J. R., Miki, H.,

Mitchison, T. J., Okada, Y., Reddy, A. S. N., Saxton, W. M., Schliwa, M., Scholey, J. M., … Wordeman, L. (2004). A standardized kinesin nomenclature. *Journal of Cell Biology*, *167*(1), 19–22. https://doi.org/10.1083/jcb.200408113

Li, Y., Yu, W., Liang, Y., & Zhu, X. (2007). Kinetochore dynein generates a poleward pulling force to facilitate congression and full chromosome alignment. *Cell Research*, *17*(8), Article 8. https://doi.org/10.1038/cr.2007.65

Lodish, H. F., Berk, A., Kaiser, C., Krieger, M., Scott, M. P., Bretscher, A., Ploegh, H. L., & Matsudaira, P. T. (2008). *Molecular cell biology* (6th ed). W.H. Freeman. http://catdir.loc.gov/catdir/toc/ecip0710/2007006188.html

Lüders, J., Patel, U. K., & Stearns, T. (2006). GCP-WD is a γ-tubulin targeting factor required for centrosomal and chromatin-mediated microtubule nucleation. *Nature Cell Biology*, *8*(2), Article 2. https://doi.org/10.1038/ncb1349

Lukinavičius, G., Reymond, L., D'Este, E., Masharina, A., Göttfert, F., Ta, H., Güther, A., Fournier, M., Rizzo, S., Waldmann, H., Blaukopf, C., Sommer, C., Gerlich, D. W., Arndt, H.-D., Hell, S. W., & Johnsson, K. (2014). Fluorogenic probes for live-cell imaging of the cytoskeleton. *Nature Methods*, *11*(7), Article 7. https://doi.org/10.1038/nmeth.2972

Maddox, P., Bloom, K. S., & Salmon, E. D. (2000). The polarity and dynamics of microtubule assembly in the budding yeast Saccharomyces cerevisiae. *Nature Cell Biology*, *2*(1), 36–41. https://doi.org/10.1038/71357

Maddox, P., Chin, E., Mallavarapu, A., Yeh, E., Salmon, E. D., & Bloom, K. (1999). Microtubule Dynamics from Mating through the First Zygotic Division in the Budding Yeast Saccharomyces cerevisiae. *The Journal of Cell Biology*, *144*(5), 977–987.

Maddox, P., Straight, A., Coughlin, P., Mitchison, T. J., & Salmon, E. D. (2003). Direct observation of microtubule dynamics at kinetochores in Xenopus extract spindles: Implications for spindle mechanics. *Journal of Cell Biology*, *162*(3), 377–382. https://doi.org/10.1083/jcb.200301088

Magidson, V., O'Connell, C. B., Lončarek, J., Paul, R., Mogilner, A., & Khodjakov, A. (2011). The spatial arrangement of chromosomes during prometaphase facilitates spindle assembly. *Cell*, *146*(4), 555–567. https://doi.org/10.1016/j.cell.2011.07.012

Magidson, V., Paul, R., Yang, N., Ault, J. G., O'Connell, C. B., Tikhonenko, I., McEwen, B. F., Mogilner, A., & Khodjakov, A. (2015). Adaptive changes in the kinetochore architecture facilitate proper spindle assembly. *Nature Cell Biology*, *17*(9), Article 9. https://doi.org/10.1038/ncb3223

Maiato, H., Gomes, A. M., Sousa, F., & Barisic, M. (2017). Mechanisms of Chromosome Congression during Mitosis. *Biology*, *6*(1), 13. https://doi.org/10.3390/biology6010013

Maiato, H., Khodjakov, A., & Rieder, C. L. (2005). Drosophila CLASP is required for the incorporation of microtubule subunits into fluxing kinetochore fibres. *Nature Cell Biology*, *7*(1), 42–47. https://doi.org/10.1038/ncb1207

Maldonado, M., & Kapoor, T. M. (2011). Constitutive Mad1 targeting to kinetochores uncouples checkpoint signalling from chromosome biorientation. *Nature Cell Biology*, *13*(4), 475–482. https://doi.org/10.1038/ncb2223

Mann, B. J., & Wadsworth, P. (2019). Kinesin-5 Regulation and Function in Mitosis. *Trends in Cell Biology*, *29*(1), 66–79. https://doi.org/10.1016/j.tcb.2018.08.004

Manning, A. L., Ganem, N. J., Bakhoum, S. F., Wagenbach, M., Wordeman, L., & Compton, D. A. (2007). The Kinesin-13 Proteins Kif2a, Kif2b, and Kif2c/MCAK Have Distinct Roles during Mitosis in Human Cells. *Molecular Biology of the Cell*, *18*(8), 2970–2979. https://doi.org/10.1091/mbc.e07-02-0110

Maresca, T. J., Groen, A. C., Gatlin, J. C., Ohi, R., Mitchison, T. J., & Salmon, E. D. (2009). Spindle Assembly in the Absence of a RanGTP Gradient Requires Localized CPC Activity. *Current Biology*, *19*(14), 1210–1215. https://doi.org/10.1016/j.cub.2009.05.061

Maresca, T. J., & Salmon, E. D. (2009). Intrakinetochore stretch is associated with changes in kinetochore phosphorylation and spindle assembly checkpoint activity. *The Journal of Cell Biology*, *184*(3), 373–381. https://doi.org/10.1083/jcb.200808130

Mastronarde, D. N., McDonald, K. L., Ding, R., & McIntosh, J. R. (1993). Interpolar spindle microtubules in PTK cells. *The Journal of Cell Biology*, *123*(6 Pt 1), 1475–1489. https://doi.org/10.1083/jcb.123.6.1475

Matković, J., Ghosh, S., Ćosić, M., Eibes, S., Barišić, M., Pavin, N., & Tolić, I. M. (2022). Kinetochore- and chromosome-driven transition of microtubules into bundles promotes spindle assembly. *Nature Communications*, *13*(1), 7307. https://doi.org/10.1038/s41467-022-34957-4

Matos, I., Pereira, A. J., Lince-Faria, M., Cameron, L. A., Salmon, E. D., & Maiato, H. (2009). Synchronizing chromosome segregation by flux-dependent force equalization at kinetochores. *The Journal of Cell Biology*, *186*(1), 11–26. https://doi.org/10.1083/jcb.200904153

Maurer, S. P., Fourniol, F. J., Bohner, G., Moores, C. A., & Surrey, T. (2012). EBs recognize a nucleotide-dependent structural cap at growing microtubule ends. *Cell*, *149*(2), 371–382. https://doi.org/10.1016/j.cell.2012.02.049

Mayr, M. I., Hümmer, S., Bormann, J., Grüner, T., Adio, S., Woehlke, G., & Mayer, T. U. (2007). The Human Kinesin Kif18A Is a Motile Microtubule Depolymerase Essential for Chromosome Congression. *Current Biology*, *17*(6), 488–498. https://doi.org/10.1016/j.cub.2007.02.036

McDonald, K. L., O'Toole, E. T., Mastronarde, D. N., & McIntosh, J. R. (1992). Kinetochore microtubules in PTK cells. *The Journal of Cell Biology*, *118*(2), 369–383. https://doi.org/10.1083/jcb.118.2.369

McEwen, B. F., Chan, G. K., Zubrowski, B., Savoian, M. S., Sauer, M. T., & Yen, T. J. (2001). CENP-E is essential for reliable bioriented spindle attachment, but chromosome alignment can be achieved via redundant mechanisms in mammalian cells. *Molecular Biology of the Cell*, *12*(9), 2776–2789. https://doi.org/10.1091/mbc.12.9.2776

McEwen, B. F., Heagle, A. B., Cassels, G. O., Buttle, K. F., & Rieder, C. L. (1997). Kinetochore Fiber Maturation in PtK1 Cells and Its Implications for the Mechanisms of Chromosome

Congression and Anaphase Onset. *Journal of Cell Biology*, *137*(7), 1567–1580. https://doi.org/10.1083/jcb.137.7.1567

McIntosh, J. R., & Landis, S. C. (1971). The distribution of spindle microtubules during mitosis in cultured human cells. *The Journal of Cell Biology*, *49*(2), 468–497. https://doi.org/10.1083/jcb.49.2.468

McKenney, R. J., Huynh, W., Vale, R. D., & Sirajuddin, M. (2016). Tyrosination of α-tubulin controls the initiation of processive dynein–dynactin motility. *The EMBO Journal*, *35*(11), 1175–1185. https://doi.org/10.15252/embj.201593071

McKinley, K. L., Sekulic, N., Guo, L. Y., Tsinman, T., Black, B. E., & Cheeseman, I. M. (2015). The CENP-L-N Complex Forms a Critical Node in an Integrated Meshwork of Interactions at the Centromere-Kinetochore Interface. *Molecular Cell*, *60*(6), 886–898. https://doi.org/10.1016/j.molcel.2015.10.027

Mimori-Kiyosue, Y., Grigoriev, I., Lansbergen, G., Sasaki, H., Matsui, C., Severin, F., Galjart, N., Grosveld, F., Vorobjev, I., Tsukita, S., & Akhmanova, A. (2005). CLASP1 and CLASP2 bind to EB1 and regulate microtubule plus-end dynamics at the cell cortex. *The Journal of Cell Biology*, *168*(1), 141–153. https://doi.org/10.1083/jcb.200405094

Mitchison. (1989). Polewards microtubule flux in the mitotic spindle: Evidence from photoactivation of fluorescence. *The Journal of Cell Biology*, *109*(2), 637–652. https://doi.org/10.1083/jcb.109.2.637

Mitchison, T. J., Evans, L., Schulze, E., & Kirschner, M. (1986). Sites of microtubule assembly and disassembly in the mitotic spindle. *Cell*, *45*(4), 515–527. https://doi.org/10.1016/0092-8674(86)90283-7

Mitchison, T. J., Maddox, P., Groen, A., Cameron, L., Perlman, Z., Ohi, R., Desai, A., Salmon, E. D., & Kapoor, T. M. (2004). Bipolarization and poleward flux correlate during Xenopus extract spindle assembly. *Molecular Biology of the Cell*, *15*(12), 5603–5615. https://doi.org/10.1091/mbc.e04-05-0440

Miyamoto, D. T., Perlman, Z. E., Burbank, K. S., Groen, A. C., & Mitchison, T. J. (2004). The kinesin Eg5 drives poleward microtubule flux in Xenopus laevis egg extract spindles. *Journal of Cell Biology*, *167*(5), 813–818. https://doi.org/10.1083/jcb.200407126

Mollinari, C., Kleman, J.-P., Jiang, W., Schoehn, G., Hunter, T., & Margolis, R. L. (2002). PRC1 is a microtubule binding and bundling protein essential to maintain the mitotic spindle midzone. *The Journal of Cell Biology*, *157*(7), 1175–1186. https://doi.org/10.1083/jcb.200111052

Moore, A. T., Rankin, K. E., von Dassow, G., Peris, L., Wagenbach, M., Ovechkina, Y., Andrieux, A., Job, D., & Wordeman, L. (2005). MCAK associates with the tips of polymerizing microtubules. *The Journal of Cell Biology*, *169*(3), 391–397. https://doi.org/10.1083/jcb.200411089

Morrison, E. E., Wardleworth, B. N., Askham, J. M., Markham, A. F., & Meredith, D. M. (1998). EB1, a protein which interacts with the APC tumour suppressor, is associated with the microtubule cytoskeleton throughout the cell cycle. *Oncogene*, *17*(26), Article 26. https://doi.org/10.1038/sj.onc.1202247

Mountain, V., Simerly, C., Howard, L., Ando, A., Schatten, G., & Compton, D. A. (1999). The Kinesin-Related Protein, Hset, Opposes the Activity of Eg5 and Cross-Links Microtubules in the Mammalian Mitotic Spindle. *Journal of Cell Biology*, *147*(2), 351–366. https://doi.org/10.1083/jcb.147.2.351

Musacchio, A., & Desai, A. (2017). A Molecular View of Kinetochore Assembly and Function. *Biology*, *6*(1), 5. https://doi.org/10.3390/biology6010005

Nakamura, S., Grigoriev, I., Nogi, T., Hamaji, T., Cassimeris, L., & Mimori-Kiyosue, Y. (2012). Dissecting the Nanoscale Distributions and Functions of Microtubule-End-Binding Proteins EB1 and ch-TOG in Interphase HeLa Cells. *PLOS ONE*, *7*(12), e51442. https://doi.org/10.1371/journal.pone.0051442

Nicklas, R. B., & Arana, P. (1992). Evolution and the meaning of metaphase. *Journal of Cell Science*, *102 (Pt 4)*, 681–690. https://doi.org/10.1242/jcs.102.4.681

Nicklas, R. B., & Koch, C. A. (1972). Chromosome micromanipulation. IV. Polarized motions within the spindle and models for mitosis. *Chromosoma*, *39*(1), 1–26. https://doi.org/10.1007/BF00320586

Patterson, G. H., & Lippincott-Schwartz, J. (2002). A photoactivatable GFP for selective photolabeling of proteins and cells. *Science (New York, N.Y.)*, *297*(5588), 1873–1877. https://doi.org/10.1126/science.1074952

Pavin, N., & Tolić, I. M. (2016). Self-Organization and Forces in the Mitotic Spindle. *Annual Review of Biophysics*, *45*(1), 279–298. https://doi.org/10.1146/annurev-biophys-062215-010934

Polak, B., Risteski, P., Lesjak, S., & Tolić, I. M. (2017). PRC1-labeled microtubule bundles and kinetochore pairs show one-to-one association in metaphase. *EMBO Reports*, *18*(2), 217–230. https://doi.org/10.15252/embr.201642650

Prosser, S. L., & Pelletier, L. (2017). Mitotic spindle assembly in animal cells: A fine balancing act. *Nature Reviews Molecular Cell Biology*, *18*(3), Article 3. https://doi.org/10.1038/nrm.2016.162

Reinemann, D. N., Sturgill, E. G., Das, D. K., Degen, M. S., Vörös, Z., Hwang, W., Ohi, R., & Lang, M. J. (2017). Collective Force Regulation in Anti-parallel Microtubule Gliding by Dimeric Kif15 Kinesin Motors. *Current Biology*, *27*(18), 2810-2820.e6. https://doi.org/10.1016/j.cub.2017.08.018

Renda, F., Miles, C., Tikhonenko, I., Fisher, R., Carlini, L., Kapoor, T. M., Mogilner, A., & Khodjakov, A. (2022). Non-centrosomal microtubules at kinetochores promote rapid chromosome biorientation during mitosis in human cells. *Current Biology: CB*, *32*(5), 1049-1063.e4. https://doi.org/10.1016/j.cub.2022.01.013

Rieder, C. L. (1981). The structure of the cold-stable kinetochore fiber in metaphase PtK1 cells. *Chromosoma*, *84*(1), 145–158. https://doi.org/10.1007/BF00293368

Rieder, C. L. (2005). Kinetochore fiber formation in animal somatic cells: Dueling mechanisms come to a draw. *Chromosoma*, *114*(5), 310–318. https://doi.org/10.1007/s00412-005-0028-2

Rieder, C. L., Cole, R. W., Khodjakov, A., & Sluder, G. (1995). The checkpoint delaying anaphase in response to chromosome monoorientation is mediated by an inhibitory signal produced by unattached kinetochores. *Journal of Cell Biology*, *130*(4), 941–948. https://doi.org/10.1083/jcb.130.4.941

Risteski, P. (2023). Permeable dye-based fluorescent speckle microscopy for human cells. *Nature Reviews Molecular Cell Biology*, *24*(5), Article 5. https://doi.org/10.1038/s41580-023-00588-w

Risteski, P., Božan, D., Jagrić, M., Bosilj, A., Pavin, N., & Tolić, I. M. (2022). Length-dependent poleward flux of sister kinetochore fibers promotes chromosome alignment. *Cell Reports*, *40*(5), 111169. https://doi.org/10.1016/j.celrep.2022.111169

Rogers, G. C., Rogers, S. L., Schwimmer, T. A., Ems-McClung, S. C., Walczak, C. E., Vale, R. D., Scholey, J. M., & Sharp, D. J. (2004). Two mitotic kinesins cooperate to drive sister chromatid separation during anaphase. *Nature*, *427*(6972), 364–370. https://doi.org/10.1038/nature02256

Rogers, G. C., Rogers, S. L., & Sharp, D. J. (2005). Spindle microtubules in flux. *Journal of Cell Science*, *118*(Pt 6), 1105–1116. https://doi.org/10.1242/jcs.02284

Salmon, E. D. (1975). Spindle Microtubules: Thermodynamics of in Vivo Assembly and Role in Chromosome Movement*. *Annals of the New York Academy of Sciences*, *253*(1), 383–406. https://doi.org/10.1111/j.1749-6632.1975.tb19216.x

Salmon, E. D., Leslie, R. J., Saxton, W. M., Karow, M. L., & McIntosh, J. R. (1984). Spindle microtubule dynamics in sea urchin embryos: Analysis using a fluorescein-labeled tubulin and measurements of fluorescence redistribution after laser photobleaching. *Journal of Cell Biology*, *99*(6), 2165–2174. https://doi.org/10.1083/jcb.99.6.2165

Sampath, S. C., Ohi, R., Leismann, O., Salic, A., Pozniakovski, A., & Funabiki, H. (2004). The Chromosomal Passenger Complex Is Required for Chromatin-Induced Microtubule

Stabilization and Spindle Assembly. *Cell*, *118*(2), 187–202. https://doi.org/10.1016/j.cell.2004.06.026

Saxton, W. M., Stemple, D. L., Leslie, R. J., Salmon, E. D., Zavortink, M., & McIntosh, J. R. (1984). Tubulin dynamics in cultured mammalian cells. *Journal of Cell Biology*, *99*(6), 2175–2186. https://doi.org/10.1083/jcb.99.6.2175

Schaar, B. T., Chan, G. K. T., Maddox, P., Salmon, E. D., & Yen, T. J. (1997). CENP-E Function at Kinetochores Is Essential for Chromosome Alignment. *The Journal of Cell Biology*, *139*(6), 1373–1382.

She, Z.-Y., & Yang, W.-X. (2017). Molecular mechanisms of kinesin-14 motors in spindle assembly and chromosome segregation. *Journal of Cell Science*, *130*(13), 2097–2110. https://doi.org/10.1242/jcs.200261

Sikirzhytski, V., Renda, F., Tikhonenko, I., Magidson, V., McEwen, B. F., & Khodjakov, A. (2018). Microtubules assemble near most kinetochores during early prometaphase in human cells. *The Journal of Cell Biology*, *217*(8), 2647–2659. https://doi.org/10.1083/jcb.201710094

Skoufias, D. A., DeBonis, S., Saoudi, Y., Lebeau, L., Crevel, I., Cross, R., Wade, R. H., Hackney, D., & Kozielski, F. (2006). S-Trityl-L-cysteine Is a Reversible, Tight Binding Inhibitor of the Human Kinesin Eg5 That Specifically Blocks Mitotic Progression *. *Journal of Biological Chemistry*, *281*(26), 17559–17569. https://doi.org/10.1074/jbc.M511735200

Song, J.-G., King, M. R., Zhang, R., Kadzik, R. S., Thawani, A., & Petry, S. (2018). Mechanism of how augmin directly targets the γ-tubulin ring complex to microtubules. *The Journal of Cell Biology*, *217*(7), 2417–2428. https://doi.org/10.1083/jcb.201711090

Steblyanko, Y., Rajendraprasad, G., Osswald, M., Eibes, S., Jacome, A., Geley, S., Pereira, A. J., Maiato, H., & Barisic, M. (2020). Microtubule poleward flux in human cells is driven by the coordinated action of four kinesins. *The EMBO Journal*, *39*(23), e105432. https://doi.org/10.15252/embj.2020105432

Štimac, V., Koprivec, I., Manenica, M., Simunić, J., & Tolić, I. M. (2022). Augmin prevents merotelic attachments by promoting proper arrangement of bridging and kinetochore fibers. *eLife*, *11*, e83287. https://doi.org/10.7554/eLife.83287

Stumpff, J., von Dassow, G., Wagenbach, M., Asbury, C., & Wordeman, L. (2008). The kinesin-8 motor Kif18A suppresses kinetochore movements to control mitotic chromosome alignment. *Developmental Cell*, *14*(2), 252–262. https://doi.org/10.1016/j.devcel.2007.11.014

Stumpff, J., Wagenbach, M., Franck, A., Asbury, C. L., & Wordeman, L. (2012). Kif18A and chromokinesins confine centromere movements via microtubule growth suppression and spatial control of kinetochore tension. *Developmental Cell*, *22*(5), 1017–1029. https://doi.org/10.1016/j.devcel.2012.02.013

Sturgill, E. G., Das, D. K., Takizawa, Y., Shin, Y., Collier, S. E., Ohi, M. D., Hwang, W., Lang, M. J., & Ohi, R. (2014). Kinesin-12 Kif15 Targets Kinetochore Fibers through an Intrinsic Two-Step Mechanism. *Current Biology*, *24*(19), 2307–2313. https://doi.org/10.1016/j.cub.2014.08.022

Subramanian, R., Wilson-Kubalek, E. M., Arthur, C. P., Bick, M. J., Campbell, E. A., Darst, S. A., Milligan, R. A., & Kapoor, T. M. (2010). Insights into antiparallel microtubule crosslinking by PRC1, a conserved nonmotor microtubule binding protein. *Cell*, *142*(3), 433–443. https://doi.org/10.1016/j.cell.2010.07.012

Sudakin, V., Chan, G. K. T., & Yen, T. J. (2001). Checkpoint inhibition of the APC/C in HeLa cells is mediated by a complex of BUBR1, BUB3, CDC20, and MAD2. *The Journal of Cell Biology*, *154*(5), 925–936. https://doi.org/10.1083/jcb.200102093

Sun, M., Jia, M., Ren, H., Yang, B., Chi, W., Xin, G., Jiang, Q., & Zhang, C. (2021). NuMA regulates mitotic spindle assembly, structural dynamics and function via phase separation. *Nature Communications*, *12*(1), Article 1. https://doi.org/10.1038/s41467-021-27528-6

Tanenbaum, M. E., Macůrek, L., Janssen, A., Geers, E. F., Alvarez-Fernández, M., & Medema, R. H. (2009). Kif15 Cooperates with Eg5 to Promote Bipolar Spindle Assembly. *Current Biology*, *19*(20), 1703–1711. https://doi.org/10.1016/j.cub.2009.08.027

Telzer, B. R., Moses, M. J., & Rosenbaum, J. L. (1975). Assembly of microtubules onto kinetochores of isolated mitotic chromosomes of HeLa cells. *Proceedings of the National Academy of Sciences of the United States of America*, *72*(10), 4023–4027.

Tolić, I. M. (2018). Mitotic spindle: Kinetochore fibers hold on tight to interpolar bundles. *European Biophysics Journal: EBJ*, *47*(3), 191–203. https://doi.org/10.1007/s00249-017-1244-4

Trivedi, P., & Stukenberg, P. T. (2016). A Centromere-Signaling Network Underlies the Coordination among Mitotic Events. *Trends in Biochemical Sciences*, *41*(2), 160–174. https://doi.org/10.1016/j.tibs.2015.11.002

Tulu, U. S., Fagerstrom, C., Ferenz, N. P., & Wadsworth, P. (2006). Molecular Requirements for Kinetochore-Associated Microtubule Formation in Mammalian Cells. *Current Biology*, *16*(5), 536–541. https://doi.org/10.1016/j.cub.2006.01.060

Tulu, U. S., & Ferenz, N. P. (2010). Photoactivatable Green Fluorescent protein-Tubulin. *Methods in Cell Biology*, *97*, 81–90. https://doi.org/10.1016/S0091-679X(10)97005-2

Uchida, K. S. K., Takagaki, K., Kumada, K., Hirayama, Y., Noda, T., & Hirota, T. (2009). Kinetochore stretching inactivates the spindle assembly checkpoint. *The Journal of Cell Biology*, *184*(3), 383–390. https://doi.org/10.1083/jcb.200811028

Uehara, R., Nozawa, R., Tomioka, A., Petry, S., Vale, R. D., Obuse, C., & Goshima, G. (2009). The augmin complex plays a critical role in spindle microtubule generation for mitotic progression and cytokinesis in human cells. *Proceedings of the National Academy of Sciences*, *106*(17), 6998–7003. https://doi.org/10.1073/pnas.0901587106

van Toorn, M., Gooch, A., Boerner, S., & Kiyomitsu, T. (2023). NuMA deficiency causes micronuclei via checkpoint-insensitive k-fiber minus-end detachment from mitotic spindle poles. *Current Biology*, *33*(3), 572-580.e2. https://doi.org/10.1016/j.cub.2022.12.017

Vladimirou, E., Mchedlishvili, N., Gasic, I., Armond, J. W., Samora, C. P., Meraldi, P., & McAinsh, A. D. (2013). Nonautonomous Movement of Chromosomes in Mitosis. *Developmental Cell*, *27*(1), 60–71. https://doi.org/10.1016/j.devcel.2013.08.004

Vukušić, K., Buđa, R., Bosilj, A., Milas, A., Pavin, N., & Tolić, I. M. (2017). Microtubule Sliding within the Bridging Fiber Pushes Kinetochore Fibers Apart to Segregate Chromosomes. *Developmental Cell*, *43*(1), 11-23.e6. https://doi.org/10.1016/j.devcel.2017.09.010

Waitzman, J. S., & Rice, S. E. (2014). Mechanism and Regulation of Kinesin-5, an essential motor for the mitotic spindle. *Biology of the Cell / under the Auspices of the European Cell Biology Organization*, *106*(1), 1–12. https://doi.org/10.1111/boc.201300054

Walczak, C. E., Cai, S., & Khodjakov, A. (2010). Mechanisms of chromosome behaviour during mitosis. *Nature Reviews. Molecular Cell Biology*, *11*(2), 91–102. https://doi.org/10.1038/nrm2832

Wandke, C., Barisic, M., Sigl, R., Rauch, V., Wolf, F., Amaro, A. C., Tan, C. H., Pereira, A. J., Kutay, U., Maiato, H., Meraldi, P., & Geley, S. (2012). Human chromokinesins promote chromosome congression and spindle microtubule dynamics during mitosis. *The Journal of Cell Biology*, *198*(5), 847–863. https://doi.org/10.1083/jcb.201110060

Wang, H., Brust-Mascher, I., & Scholey, J. M. (2014). Sliding filaments and mitotic spindle organization. *Nature Cell Biology*, *16*(8), Article 8. https://doi.org/10.1038/ncb3019

Waterman-Storer, C. M., Desai, A., Chloe Bulinski, J., & Salmon, E. D. (1998). Fluorescent speckle microscopy, a method to visualize the dynamics of protein assemblies in living cells. *Current Biology*, *8*(22), 1227-S1. https://doi.org/10.1016/S0960-9822(07)00515-5

Watts, C. A., Richards, F. M., Bender, A., Bond, P. J., Korb, O., Kern, O., Riddick, M., Owen, P., Myers, R. M., Raff, J., Gergely, F., Jodrell, D. I., & Ley, S. V. (2013). Design, synthesis, and biological evaluation of an allosteric inhibitor of HSET that targets cancer cells with supernumerary centrosomes. *Chemistry & Biology*, *20*(11), 1399–1410. https://doi.org/10.1016/j.chembiol.2013.09.012

Wendell, K. L., Wilson, L., & Jordan, M. A. (1993). Mitotic block in HeLa cells by vinblastine: Ultrastructural changes in kinetochore-microtubule attachment and in centrosomes. *Journal of Cell Science*, *104*(2), 261–274. https://doi.org/10.1242/jcs.104.2.261

Whyte, J., Bader, J. R., Tauhata, S. B. F., Raycroft, M., Hornick, J., Pfister, K. K., Lane, W. S., Chan, G. K., Hinchcliffe, E. H., Vaughan, P. S., & Vaughan, K. T. (2008). Phosphorylation regulates targeting of cytoplasmic dynein to kinetochores during mitosis. *The Journal of Cell Biology*, *183*(5), 819–834. https://doi.org/10.1083/jcb.200804114

Wollman, R., Cytrynbaum, E. N., Jones, J. T., Meyer, T., Scholey, J. M., & Mogilner, A. (2005). Efficient Chromosome Capture Requires a Bias in the 'Search-and-Capture' Process during Mitotic-Spindle Assembly. *Current Biology*, *15*(9), 828–832. https://doi.org/10.1016/j.cub.2005.03.019

Wordeman, L., & Mitchison, T. J. (1995). Identification and partial characterization of mitotic centromere-associated kinesin, a kinesin-related protein that associates with centromeres during mitosis. *Journal of Cell Biology*, *128*(1), 95–104. https://doi.org/10.1083/jcb.128.1.95

Yamashita, N., Morita, M., Legant, W. R., Chen, B.-C., Betzig, E., Yokota, H., & Mimori-Kiyosue, Y. (2015). Three-dimensional tracking of plus-tips by lattice light-sheet microscopy permits the quantification of microtubule growth trajectories within the mitotic apparatus. *Journal of Biomedical Optics*, *20*(10), 101206. https://doi.org/10.1117/1.JBO.20.10.101206

Ye, A. A., Deretic, J., Hoel, C. M., Hinman, A. W., Cimini, D., Welburn, J. P., & Maresca, T. J. (2015). Aurora A kinase contributes to a pole-based error correction pathway. *Current Biology : CB*, *25*(14), 1842–1851. https://doi.org/10.1016/j.cub.2015.06.021

Zhu, C., & Jiang, W. (2005). Cell cycle-dependent translocation of PRC1 on the spindle by Kif4 is essential for midzone formation and cytokinesis. *Proceedings of the National Academy of Sciences of the United States of America*, *102*(2), 343–348. https://doi.org/10.1073/pnas.0408438102

8. AUTHOR BIOGRAPHY

Jelena Martinčić was born on September 20th 1987 in Koprivnica. She finished her elementary and high school education in Križevci. She graduated Molecular Biology in 2012 at the Faculty of Science, University of Zagreb. Her graduate thesis was awarded with the Annual award of the Croatian Association of Genetic Engineers for the best graduate thesis in which genetic engineering methods are applied. She worked as a research assistant at the Laboratory for chemical biology at the Ruđer Bošković Institute, Zagreb. Since 2016 she has been working at the Laboratory of Cell Biophysics under the mentorship of Prof Iva M. Tolić at the same institute. She continued her education at the Faculty of Science, University of Zagreb, where she enrolled in the Postgraduate Study of Biology. She was a research assistant on two European Research Council projects and European Structural and an Investment Funds project. She has published five scientific papers, two of them as the cofirst author. For one of the papers she was awarded with Annual award of the Ruđer Bošković Institute for the best scientific papers in 2022. She presented her research results at several international scientific conferences and workshops. Also, she participated in several science popularization events, such as “European Researchers’ Night” and “RBI open day”.